Soliton Steering and Switching Dynamics in $\mathscr{PT}$-Symmetric Nonlinear Directional Couplers

by

Dipti Kanika Mahato

Roll No.: 166121101

A thesis submitted
in Partial Fulfillment of the Requirements
for the Degree of
DOCTOR OF PHILOSOPHY

Supervisor: Prof. Amarendra Kumar Sarma

Department of Physics
Indian Institute of Technology Guwahati
Guwahati - 781039, Assam, India

April 2022

TH-2744_166121101

TH-2744_166121101

Soliton Steering and Switching Dynamics in $\mathscr{PT}$-Symmetric Nonlinear Directional Couplers

by

Dipti Kanika Mahato

Roll No.: 166121101

A thesis submitted
in Partial Fulfillment of the Requirements
for the Degree of
DOCTOR OF PHILOSOPHY

Supervisor: Prof. Amarendra Kumar Sarma

Department of Physics
Indian Institute of Technology Guwahati
Guwahati - 781039, Assam, India

April 2022

TH-2744_166121101

TH-2744_166121101

DECLARATION

Dipti Kanika Mahato
Roll no. 166121101
Department of Physics
Indian Institute of Technology Guwahati
Guwahati-781039, Assam, India.

The work in this thesis entitled "***Soliton Steering and Switching Dynamics in $\mathscr{PT}$-Symmetric Nonlinear Directional Couplers***" has been carried out by me under the supervision of Prof. Amarendra K. Sarma, Department of Physics, Indian Institute of Technology Guwahati, India. No part of this thesis has been submitted elsewhere for award of any other degree or qualification. Works presented in the thesis are all my own unless referenced to the contrary in the thesis.

Dipti Kanika Mahato

Dipti Kanika Mahato
Date: April 12, 2022

TH-2744_166121101

TH-2744_166121101

CERTIFICATE

Prof. Amarendra Kumar Sarma
Department of Physics
Indian Institute of Technology Guwahati
Guwahati-781039, Assam, India.
email: aksarma@iitg.ac.in

It is certified that the work contained in the thesis entitled "*Soliton Steering and Switching Dynamics in $\mathcal{PT}$-Symmetric Nonlinear Directional Couplers*" by Dipti Kanika Mahato, a student of the Department of Physics, IIT Guwahati was carried out under my supervision and has not been submitted elsewhere for award of any degree.

Prof. Amarendra Kumar Sarma

Date: April 12, 2022

TH-2744_166121101

TH-2744_166121101

DEDICATION

To my beloved grandfather 'Late Shitikantha Mahata'.

TH-2744_166121101

TH-2744_166121101

ACKNOWLEDGMENTS

At this stage, I believe that I am indebted to all individuals who have contributed to this thesis in their own way.

To begin with, I would like to express my earnest gratitude to my supervisor Prof. Amarendra Kumar Sarma, for allowing me to work under his guidance. His constant support, patience, and kindness over these five years have shaped and inspired me to strive for betterment every time I faced any difficulty. He has offered enough freedom to deal with the problems in the field of research and even beyond it. His unique strategies of guidance based on the strength of individual students have allowed me to learn and expand my knowledge freely. I am indeed grateful to him for his words of encouragement and effective feedback which continued to motivate me throughout my Ph.D. tenure.

I would like to express gratitude to my Doctoral Committee Chairman Dr. Gagan Kumar, Dr. Tapan Mishra, and Prof. Bhupen Deka for reviewing my progress and helping me improve the quality of my work with their useful suggestions and positive criticisms.

My sincere gratitude goes to all my collaborators and co-authors: Prof. M. Lakshmanan and Dr. A. Govindarajan for allowing me to work with them and gain experience. I am especially thankful to my senior and collaborator Dr. Ambaresh Sahoo for his immense support and thorough academic discussions whenever I needed any suggestion. His very humble and hard-working nature has taught me how to frame a problem, develop it bit by bit and think independently, for which I am grateful to him.

I would like to thank the current and former Heads of the Department of Physics, Prof. Perumal Alagarsamy, Prof. Subhradip Ghosh, and Prof. P. Poulose for providing me with all the necessary resources for my research, and other faculty members of the department for their various academic help. I would like to thank all the technical, administrative, and non-academic staff of the Department of Physics for their help, whenever it was needed. I am thankful to Mridupaban Patowary and Rupam Kalita for their help whenever I had any machine-related issues.

TH-2744_166121101

I am also grateful to IIT Guwahati and the Ministry of Human Resource and Development, Government of India, for the financial assistantship. I thank the people working in the IITG library, for providing an wonderful place for the students to study quietly and access a large collection of books at any hours, smoothly. I would like to thank my current group members, Sampreet, Roson, Puja, Alolika and Urmimala for their wonderful friendship and amusing discussions that we had about academic and non-academic stuffs. I am thankful to my former seniors Dr. Samit Kumar Gupta, Dr. Kaushik Paul, Dr. Bijita Sarma, Dr. Koijam Monika Devi, Dr. Jyoti Prasad Deka, Dr. Subhadeep Chakraborty, and Dr. Abdelsalam Hassan Muhammad Abdelaziz for their guidance during the initial period of my Ph.D. years and all the fun-filled interactions which we had during that time. I especially thank Kaushik Da and Jyoti Da for their strong support and affection which helped me to overcome my tough times. I would like to thank all my batchmates of 2016, all seniors and juniors for their company and positive interactions. A hearty thanks goes to SPIE IIT Guwahati student chapter and its members for providing me opportunities to get involved and organize various events in several schools, colleges and universities in Assam.

Also, I have been fortunate to make a few great friends in the campus, Geetanjali, Deepa, Papi, Munmi, Priyanka, Sneha and Basabendu Da. Back home, I have been blessed to have friends like Jayi and Sayani whose lovely and chirpy companionship made the journey more enjoyable. I am also indebted to my school friends Saswati, Sriparna, Sucharita and Subhrajit, for their years of faith and friendship.

Finally, the moment arrives to convey my very special thanks to my parents Mrs. Smritirekha Mahato and Dr. Gurucharan Mahato for their unconditional love, sacrifice and encouragement throughout my academic career. Without their continuous support, it would not have been possible to walk this journey. I can not thank my most beloved younger siblings Iti and Sayan enough for being my pillar of strengths and showing their affection and care, without them I would not have made it. I also want to express my special gratitude to three important persons, Masi, Dadu and Bishu Kaku, whose unconditional love since childhood made me achieve anything that I set my mind to. Lastly, I heartily thank my companion for lifetime, Sourav, for keeping his faith in me and for being the greatest emotional support throughout all these years.

TH-2744_166121101

ABSTRACT

The dynamical behavior of a classical or quantum mechanical system is described by a Hamiltonian H. The manifestation of Hermiticity of such Hamiltonian appears in form of physical observables through experimental demonstrations. After C.M. Bender put forward a very novel perspective on the quantum mechanical non-Hermitian Hamiltonians, Parity-time ($\mathscr{PT}$) symmetry, as a theoretical concept, got tremendous attention. The recent recognition that optical systems can provide a ground to realize the mathematical concepts of $\mathscr{PT}$ symmetry in the table-top experiments, $\mathscr{PT}$ symmetry in photonics systems has become a very active research area. In photonics, $\mathscr{PT}$ symmetry has been readily established by judiciously incorporating balanced gain and loss in coupled system so that the refractive index profile plays the role of the complex potential. In this thesis, we use coupled waveguides (nonlinear directional couplers) for exploiting the effect of $\mathscr{PT}$ symmetry for switching dynamics of optical signals. Considering the application of nonlinear directional couplers as an all-optical switching device, we have studied the steering and switching dynamics of different solitons inside $\mathscr{PT}$-symmetric coupler manoeuvring the dispersion and the nonlinearity of the system. All the investigated $\mathscr{PT}$-symmetric couplers evidently emerged to be a better choice as an optical switching device in contrast to their conventional counterparts showing unique $\mathscr{PT}$-symmetric features.

TH-2744_166121101

TH-2744_166121101

List of Publications

Publications included in the thesis

1. **Dipti Kanika Mahato**, A. Govindarajan and Amarendra K. Sarma, “Dark soliton steering in $\mathscr{PT}$-symmetric couplers with third-order and intermodal dispersions," *J. Opt. Soc. Am. B* **37**, 3443 (2020).

2. A. Sahoo, **Dipti Kanika Mahato**, A. Govindarajan and Amarendra K. Sarma, “Ultrafast all-optical femtosecond soliton steering in $\mathscr{PT}$-symmetric fiber couplers," arXiv:2111.10878 (Under review in Phys. Rev. A).

3. A. Sahoo, **Dipti Kanika Mahato**, A. Govindarajan and Amarendra K. Sarma, “Bistable soliton switching dynamics in a $\mathscr{PT}$-symmetric coupler with saturating nonlinearity," *Phys. Rev. A* **105**, 063503 (2022).

Other Publications

1. **Dipti Kanika Mahato**, A. Govindarajan, M. Laxmanan and Amarendra K. Sarma, “Dispersion Managed Generation of Peregrine Solitons and Kuznetsov-Ma Breather in an Optical Fiber,” *Phys. Lett. A* **392**, 127134 (2020).

TH-2744_166121101

Conferences/Schools attended

1. DST-SERB school on Frontiers in Quantum Optics, 1-19 December, 2017, IIT Guwahati (**Participation**).

2. The International Conference on Fiber Optics and Photonics, 'PHOTONICS-2018', 12-15 December, 2018, IIT Delhi, India (**Poster presentation**).

3. Nonlinear Systems and Dynamics (CNSD) 12-15 December, 2019, IIT Kanpur, Kanpur, India (**Oral presentation**).

4. Virtual Conference on Lasers and Electro-Optics, 'CLEO 2020', 10-15 May, 2020 (**Participation**).

TH-2744_166121101

List of Acronyms

CW Continuous Wave

DW Dispersive Wave

EP Exceptional Point

FOD Fourth-Order Dispersion

GVD Group Velocity Dispersion

HOD Higher-Order Dispersion

IMD Intermodal Dispersion

IRS Intrapulse Raman Scattering

ISTM Inverse Scattering Theorem Method

NLDC Nonlinear Directional Coupler

NLSE Nonlinear Scrödinger Equation

SN Saturable Nonlinearity

SNC Saturable Nonlinear Coupler

SPM Self-Phase Modulation

SRS Stimulated Raman Scattering

SS Self-Steepening

SSFM Split-Step Fourier Method

TOD Third-Order Dispersion

TH-2744_166121101

TH-2744_166121101

List of Figures

TH-2744_166121101

TH-2744_166121101

TH-2744_166121101

TH-2744_166121101

भारतीय प्रौद्योगिकी संस्थान गुवाहाटी • Indian Institute of Technology Guwahati •

TH-2744_166121101

TH-2744_166121101

List of Tables

TH-2744_166121101

TH-2744_166121101

Table of Contents

TH-2744_166121101

TH-2744_166121101

CHAPTER 1

INTRODUCTION

In the domain of quantum physics, the dynamics of systems which are isolated and therefore are considered to be in equilibrium with their surroundings, are expressed by a Hermitian Hamiltonian. In order to preserve the fundamental axioms of quantum theory, the energy eigenvalues of such Hermitian Hamiltonians are required to be real and positive. To the contrary, there also exist physical systems which interact with their surroundings by changing energies whose dynamical behaviors are described by a non-Hermitian Hamiltonian. The energy eigenvalues of such Hamiltonians are complex, they are not measurable. However, in 1998, the pioneering work by Bender and Boettcher showed that even a non-Hermitian Hamiltonian can possess real eigenvalues, provided it satisfies the physical condition for parity-time reversal symmetry ($\mathscr{PT}$ symmetry) [1]. In general, for a Hamiltonian with the form, $\hat{H} = \hat{p}^2/2m + V(\hat{x})$, a necessary condition for it to be $\mathscr{PT}$-symmetric is that the potential should satisfy the condition: $V(\hat{x}) = V^*(-\hat{x})$. In search for physical systems with such complex $\mathscr{PT}$-symmetric potential, based on the mathematical analogy between the quantum mechanical Schrödinger equation and the paraxial equation of light propagation, it was first theoretically suggested in 2007 that it is possible to treat a coupled waveguide structure with symmetric refractive index guiding ($n_R(x) = n_R(-x)$) and an antisymmetric gain/loss profile ($n_I(x) = -n_I(-x)$) as an optical $\mathscr{PT}$-symmetric system [2, 3, 4]. In 2009, following the theoretical predictions, there was experimental observation of onset of $\mathscr{PT}$ symmetry breaking in a 1-D planar waveguide by controlling loss in the system [5]. The loss-induced transparency was also

TH-2744_166121101

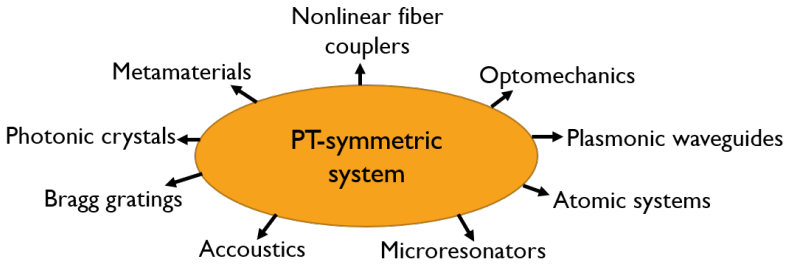

Figure 1.1: Application branch of $\mathscr{PT}$ symmetry in photonics

observed in this arrangement. In the following year in 2010, the first realizations of the optical $\mathscr{PT}$ symmetry in linear coupled waveguide system with balanced gain and loss in the two arms of the coupler [6] was demonstrated featuring the non-reciprocity nature of $\mathscr{PT}$ symmetry. Some interesting $\mathscr{PT}$-symmetric features such as unidirectional invisibility and Bloch oscillations were observed in different photonics structure [7]. This subsequently led to extend the $\mathscr{PT}$-symmetric theory in other branches of physics such as microresonators [8], photonic crystals [9], atomic systems [10] and atomic lattices [11, 12], optomechanics [13, 14, 15] and acoustics [16]. Further progress in understanding the $\mathscr{PT}$ symmetry was observed once the nonlinearity is included in the system. The interplay between the $\mathscr{PT}$ symmetry and the nonlinearity gave arise to the existence of localized modes [17, 18] and $\mathscr{PT}$-symmetric solitons [7, 19]. Several authors reported existence of bright [7, 19], dark [20], gap [21] and Bragg solitons as well as many other interesting phenomena [22, 23, 24, 25]. Such rapid growth of theoretical and experimental studies on $\mathscr{PT}$-symmetric photonic systems has made it a very active research area which is now expanding its boundary beyond photonics.

The operational domains of any $\mathscr{PT}$-symmetric system are generally categorized into three regimes: unbroken regime- where all the eigenvalues are real, broken regime- where all the eigenvalues are complex, and an Exceptional Point (EP)- where the symmetry-breaking transition happens and the eigenvalues coalesce. In the context of directional couplers, the interplay between gain, loss, and the coupling between them decides whether the eigenvalues will be real or complex. When the coupling is strong, the gain present in the system can help to compensate for the loss fully so that the system can operate in the unbroken $\mathscr{PT}$-symmetric regime with real eigenvalues; on the other hand, when the coupling is weak, gain becomes unable to compensate for the loss, resulting in the system to operate in the broken $\mathscr{PT}$-symmetric regime with complex

TH-2744_166121101

conjugate eigenvalues. In between these two unbroken and broken regimes, at the EP, a phase transition takes place from real-to-complex energy. One important aspect of such coupled $\mathscr{PT}$-symmetric system is that the incorporation of an equal amount of gain and loss is not sufficient to have real eigenvalues, a proper amount of coupling between them is also needed.

Thus, a nonlinear directional coupler can be considered the simplest design of a $\mathscr{PT}$-symmetric system which is efficient to display rich soliton physics and phenomena associated with the interaction between gain, loss, coupling, and nonlinearity. The applications of directional couplers, which are linear, are mostly observed as power-splitting, wavelength division multiplexing/demultiplexing devices. Very recently in 2019, the operation of $\mathscr{PT}$-symmetric nonlinear couplers showed huge improvement as an all-optical switching device by drastically reducing the critical power of switching while maintaining high efficiency [26, 27]. While soliton switching in $\mathscr{PT}$-symmetric nonlinear directional couplers have been explored quite recently, stability solitons in such systems have already been studied by Malomed and his collaborators [28, 29, 20]. Therefore, in search of an all-optical switching device with lower critical power, we have played with the system configurations and parameters under the effect of $\mathscr{PT}$ symmetry while keeping the basic structure as a nonlinear directional coupler.

1.1 The topics and aim of research

In this thesis, we report our studies on the steering and switching dynamics of solitons inside the $\mathscr{PT}$-symmetric nonlinear directional couplers that are briefly discussed below.

(a) ***Ultrashort Soliton:*** In the domains of high-speed signal processing and ultrafast communication, all-optical switching devices are considered to be key elements that have drawn significant attention over the past few decades [30]. In this context, a dual-core nonlinear directional coupler featuring power-dependent switching has been studied extensively [31, 32, 33]. The requirement of high critical power for optical solitons has been reduced sharply by introducing $\mathscr{PT}$ symmetry in a nonlinear directional coupler. However, in the domain of ultra-short bright solitons, ranging from few femtoseconds (fs) to 1 picosecond (ps), the practical application of any real fiber coupler requires incorporation of higher-order perturbative effects such as higher-order dispersions including

TH-2744_166121101

third-order dispersion and fourth-order dispersion, self-steepening, and intrapulse Raman scattering [34, 35] in the coupled nonlinear Schrödinger equation. Here, we explore the idea of $\mathscr{PT}$-symmetric fiber coupler for the fs pulse switching and observe the switching dynamics under the effect of balanced gain and loss in great detail.

(b) *Bistable Soliton:* The operation of $\mathscr{PT}$-symmetric couplers especially with the Kerr nonlinearity showed improvement as the critical power of switching reduces drastically while maintaining high efficiency. However, a conventional coupler with Kerr nonlinear medium has low nonlinear coefficient n_2 which requires high input power for switching. To overcome this hindrance, non-Kerr saturable nonlinear media, such as semiconductor doped glass and organic polymers have been employed due to their higher n_2 values compared to pure silica [36] and their relatively low saturable intensities [37, 38]. Therefore, for a $\mathscr{PT}$-symmetric couplers, if saturable nonlinearity is introduced, one can expect to achieve advantageous transmission characteristics over the Kerr one. However, any saturable media do not support Kerr solitons, instead there exist bistable solitons which are basically two solitons having the same pulse width but different energies and shapes [39]. The switching dynamics inside a conventional saturable nonlinear couplers by utilizing bistable soliton have been reported previously which had been found to be better alternatives for all-optical switching devices [40, 41, 42, 43]. Although, there have been several studies demonstrating the existence of stable fundamental soliton, gap soliton, and higher order solitons in different $\mathscr{PT}$-symmetric potentials [44, 45, 46, 47], there has not been any study on the existence of bistable solitons inside a $\mathscr{PT}$-symmetric saturating coupler. So, in connection with the all-optical switching devices, in this thesis, we concentrate on the steering dynamics of bistable solitons in a $\mathscr{PT}$-symmetric saturable nonlinear coupler.

(c) *Dark Soliton:* The pulse propagation in the normal dispersion region displays the existence of dark solitons with additional π phase with respect to the bright one. When a $\mathscr{PT}$-symmetric coupler is operated in the anomalous dispersion region, the switching dynamics of a bright soliton inside the coupler showed an extreme advantage over a conventional coupler. Keeping that in mind we intended to observe how $\mathscr{PT}$ symmetry affects dark soliton propagation in normal dispersion region. It is well known that as compared to the bright solitons, dark solitons are more stable in the presence of noise, they travel almost undisturbed in presence of different perturbative effects

TH-2744_166121101

inside a nonlinear directional coupler [48]. Also, for an all-optical switching device with lower critical power and shorter device length, the requirement of ultrashort pulse consequently necessitates the inclusion of third-order dispersion. Additionally, a nonlinear directional coupler, made of two fibers coupled together or a fiber with dual core, acts as a bimodal device which supports a linear combination of symmetric and antisymmetric modes, each with different propagation constants. The different group delay between these two modes during propagation along the coupler length leads to intermodal dispersion. In the coupled mode theory, this group delay between the modes is analogous to the coupling-coefficient dispersion. Previously it has been reported that both third-order dispersion and intermodal dispersion have no effect on dark soliton [48, 49, 50] but they have considerable influence on bright soliton propagation inside a conventional coupler [51, 52, 53, 54, 55, 56]. In the presence of such dispersive coupling, a new kind of dark soliton has been introduced in a dual-core coupler [57]. Intrigued by the steady nature of the dark soliton, in this thesis, we study the steering dynamics of the dark soliton in $\mathscr{PT}$-symmetric couplers and investigate if $\mathscr{PT}$ symmetry amplifies the effect of third-order and intermodal dispersions.

1.2 Outline of the Thesis

In the following, we present a more elaborate plan of the thesis by including a description of the various problems that have been addressed, in the form of different chapters of the thesis. There are a total of six chapters.

Chapter 1: already provides the introduction to the thesis, where the background and motivation for the work is outlined. It also contains the literature review and report of the recent developments in the field of $\mathscr{PT}$ symmetry in optics.

Chapter 2: This chapter is devoted to familarise the readers with relevant concepts related to research problems discussed in this thesis. Here, we discuss the concept of parity-time symmetry in the context of an optical system. This is followed by a brief discussion on solitons and physics behind soliton switching.

Chapter 3: In this chapter, we investigate the soliton steering dynamics in a $\mathscr{PT}$-

TH-2744_166121101

symmetric directional coupler in the femtosecond domain in great detail. We first explore the effects of individual higher-order perturbations (higher-order dispersions, self-steepening and intrapulse Raman scattering) on switching dynamics. Following that, we investigate the cumulative combined effects of all perturbations, which result in a significant improvement in the stability and switching of fs soliton against individual perturbations as well as unperturbed cases. With a high gain/loss, the combined effect of perturbations is found to stabilize the soliton pulse evolution in the coupler from the chaotic behavior of unperturbed evolution. This work demonstrates that it is possible to achieve efficient soliton steering, even in the femtosecond regime, at very low critical power at a relatively higher gain/loss coefficient in the $\mathscr{PT}$-symmetric directional coupler. It has been previously reported that in the context of conventional couplers intrapulse Raman scattering restabilizes the symmetric solitons at sufficiently large energies. However, in the case of a $\mathscr{PT}$-symmetric coupler, we show that a partly radiating solitons caused by high gain/loss values (although the pulse is low energy fundamental soliton) are stabilised in the presence of higher-order perturbations. This finding is new in the context of ultrafast soliton steering in a $\mathscr{PT}$-symmetric coupler, paving the way for stable and efficient fs all-optical switching at low energy than the conventional one.

Chapter 4: In connection with the all-optical switching devices, in this chapter, we concentrate on the steering dynamics in a $\mathscr{PT}$-symmetric saturable nonlinear coupler. We first obtain the exact soliton solution which can propagate through such a medium and then observe the transmission characteristics of that pulse for the $\mathscr{PT}$-symmetric coupler and solve the corresponding equation considering the device length to be half-beat length. The corresponding theoretical model along with a discussion on the numerical finding of soliton solution which can propagate in a saturating nonlinear medium has been demonstrated. The bistable solitons in the context of $\mathscr{PT}$-symmetric coupler with saturable nonlinearity has been studied. The spatiotemporal characteristics of solitons are illustrated and the phase-controlled soliton switching behavior is demonstrated.

Chapter 5: In this chapter we demonstrate steering dynamics of dark soliton in a $\mathscr{PT}$-symmetric nonlinear directional coupler in the presence of third-order dispersion and intermodal dispersions. A complete switching with an excellent efficiency at a very low critical power, even lower as compared to the bright soliton switching has been observed. The numerical results showing that both the dispersions have no effect on

TH-2744_166121101

soliton steering in $\mathscr{PT}$-symmetric couplers which makes the dark solitons to be a stable solution under dispersive effects. Additionally, we have studied the switching dynamics of the dark soliton by controlling the phase of a weaker signal in $\mathscr{PT}$ couplers with two different coupling lengths and demonstrated its advantage over the power-controlled one.

Chapter 6: This chapter concludes the thesis with a summary of the major findings of the research works carried out, and a brief outline on the scope for future studies.

TH-2744_166121101

TH-2744_166121101

CHAPTER 2

THEORETICAL BACKGROUND

This chapter is devoted to familiarize the reader with the relevant concepts discussed in this thesis.

2.1 $\mathscr{PT}$ Symmetry

In the first course on Quantum Mechanics, we are taught that the Hamiltonian, H, describing a quantum system needs to be Hermitian, i.e. $H = H^\dagger$. This is because, the eigenvalues corresponding to a Hermitian Hamiltonian is always real; and eigenvalues are directly related to physically observable quantities in experiments. While the quantum mechanics we are familiar with is still quite successful, in 1998 Carl Bender and S. Boettcher [1] put forward a completely new perspective. They said that even non-Hermitian Hamiltonians could exhibit real eigen-spectra provided they obey the parity-time symmetry, resulting in the so-called parity-time symmetric quantum mechanics. Before we understand what is meant by parity-time symmetry, it should be kept in mind that this seemingly new quantum mechanics is not in conflict with the usual quantum mechanics, rather it is an extension of the conventional quantum mechanics into the complex domain. In fact, the story began by the close investigation of the following class of $\mathscr{PT}$-symmetric Hamiltonians, having the form:

$$H = p^2 + x^2(ix)^\varepsilon \tag{2.1}$$

TH-2744_166121101

where p and x are momentum and position respectively, while ε is a real parameter and $i = \sqrt{-1}$. The Hamiltonians, H, are $\mathscr{PT}$-symmetric because, under space reflection x changes sign, while under time reversal i changes the sign in the part (ix). Hence under the combined operation of parity and time reversal, the Hamiltonian remains invariant. To put mathematically, the parity and the time-reversal operations refer to the following:

$$\mathscr{P} : \hat{x} \rightarrow -\hat{x},\ \hat{p} \rightarrow -\hat{p}$$

$$\mathscr{T} : \hat{x} \rightarrow \hat{x},\ \hat{p} \rightarrow -\hat{p},\ i \rightarrow -i$$

It should be noted that unlike Hermitian Hamiltonians, $\mathscr{PT}$-symmetric Hamiltonians exhibit phase transition in the following sense. All the eigenvalues of the Hamiltonians described by Eq.(2.1) are real for $\varepsilon \geq 0$, a regime called unbroken $\mathscr{PT}$ symmetry. On the other hand, eigenvalues cease to be real, i.e. they become complex when, $-1 < \varepsilon < 0$; this is known as the regime of broken $\mathscr{PT}$ symmetry. This is a common characteristic of parity-time symmetric Hamiltonians. There is a threshold value of the parameter, ε, say, $\varepsilon = \varepsilon_{th}$ at which the Hamiltonians enter from the broken to the unbroken $\mathscr{PT}$-regime or vice-versa.

In quantum mechanics, the so-called Schrödinger equation (with $\hbar = m = 1$) is given by $i\partial_t \psi = \hat{H}\psi$, where $\hat{H} = \hat{p}^2/2 + V(\hat{x})$ and $\hat{p} \rightarrow -i\partial_x$. The Hamiltonian H is parity-time symmetric if $[H, \mathscr{PT}] = 0$, which basically means that we must have: $V(\hat{x}) = V^*(-\hat{x})$. In other words,parity-time symmetry requires that the real part (R) of such a potential is an even function of position x whereas the imaginary part (I) is an odd function. Thus the Hamiltonian must have the form $\hat{H} = \hat{p}^2/2 + V_R(\hat{x}) + i\varepsilon V_I(\hat{x})$. Clearly if $\varepsilon = 0$, then the Hamiltonian is Hermitian. It so happens that the Hamiltonian H still exhibits real spectra as long as ε is below some threshold value, ε_{th}, as discussed earlier, referring to the so-called unbroken $\mathscr{PT}$-regime. The physicists, in particular a group at CREOL, University of Central Florida, led by Professor Demetrios Chrostodoulides, was clever enough to observe the isomorphism between the Schrödinger equation and the so-called paraxial equation of diffraction in optics,given by: $i\partial_z \phi + [(1/2k)\partial_{xx} + k_0 n]\phi = 0$, where $k_0 = 2\pi/\lambda$ and $k = k_0 n_0$. And $n = n_R(x) + i n_I(x)$ is the complex refractive index, where n_R is the real refractive index profile and n_I represents the imaginary gain/loss profile. λ is the wavelength of light in vacuum and n_0 represents the background refractive index. In general, $n_0 \gg n_{R,I}$. It was quickly evident to the CREOL group that the optical system

TH-2744_166121101

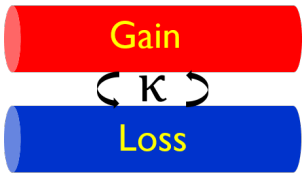

Figure 2.1: Schematic of a $\mathscr{PT}$-symmetric directional coupler. The coupling co-efficient is denoted by κ.

would be $\mathscr{PT}$-symmetric if the following conditions are satisfied: $n_R(x) = n_R(-x)$ and $n_I(x) = -n_I(-x)$. Subsequently, they came up with a proposal to connect $\mathscr{PT}$-symmetric quantum mechanics and optics [6]. Obviously, fulfilment of these conditions must have far reaching consequences! It turns out that one needs to synthesise artificial optical structures to fulfil the above-mentioned conditions. Since, physically speaking, the imaginary part of the complex refractive index n, i.e. $n_I(x)$ refers to the loss (gain) profile of the structure at position, x ,the condition $n_I(x) = -n_I(-x)$ demands that there must also have a corresponding gain (loss) profile at position, $-x$, for the structure to be parity-time symmetric. In other words, $\mathscr{PT}$ symmetry is attained through a judicious inclusion of gain-loss dipoles in such structures. This issue will be more clear to the readers in the following section when we will discuss a $\mathscr{PT}$-symmetric directional coupler. When fabricated, these man-made engineered structures exhibit astonishing characteristics which could be utilized for various novel applications. The key point is that 'loss' which is usually considered to be an 'evil' in optical systems is no longer so, rather it turns out to be a blessing in this new kind of optics! Thus, nature demands that in non-Hermitian or $\mathscr{PT}$-symmetric optics, all the so-called basic three ingredients of optics, namely: refractive index, gain and loss are equally important.

2.1.1 Understanding $\mathscr{PT}$-Optics via a directional coupler

Many features of non-Hermitian optics could be understood with a directional coupler. A directional coupler is basically a pair of two parallel optical waveguides placed close to each other so that they are coupled to one another via the so-called evanescent coupling and the final outputs are directed in two different directions. Now the structure is $\mathscr{PT}$-symmetric, therefore if one waveguide has loss, then the other one must have equal gain or vice-versa [refer to Fig. 2.1].

In optics, the propagation of the electric field envelope inside a linear waveguide

TH-2744_166121101

follows the normalized linear Schrödinger equation [the nonlinear Schrödinger equation has been discussed in detail in Sec. 2.5]. Thus, a linear directional coupler made of two waveguides placed in close proximity of each other, such system can be described by the following set of coupled Schrödinger equations:

$$i\frac{da}{dz} - iga + \kappa b = 0, i\frac{db}{dz} + igb + \kappa a = 0 \tag{2.2}$$

Here κ and g respectively are the coupling and the gain/loss parameter. On the other hand, a and b represent the optical fields in the gain and the loss waveguide respectively. It is easy to see that the Hamiltonian describing the system in (a,b) basis is given by:

$$H = \begin{pmatrix} ig & -\kappa \\ -\kappa & -ig \end{pmatrix} \tag{2.3}$$

Clearly, the Hamiltonian H in Eq.(2.3) is non-Hermitian. Also, it is parity-time symmetric, as it satisfies the commutation relation, $[H, \mathscr{PT}] = 0$, where $\mathscr{P} = \begin{pmatrix} 0 & 1 \\ 1 & 0 \end{pmatrix}$ and $\mathscr{T}$ refers to taking the complex conjugation. The eigenvalues of the Hamiltonian is given by: $E = \sqrt{\kappa^2 - g^2}$. It means, as long as $\kappa > g$, the eigenvalues are real and the system is said to be in the unbroken $\mathscr{PT}$-regime. On the other hand, when $\kappa < g$, the eigenvalues become complex, i.e., the system enters into the so-called broken $\mathscr{PT}$-regime. The transition from the unbroken to the broken $\mathscr{PT}$-regime occurs at the critical value of the coupling parameter, $g_{th} = \kappa$ (please recall ε_{th}!). This phase-transition point is also known as the EP or the $\mathscr{PT}$-threshold. At the EP, the eigenstates, also termed as *supermodes*, of the system coalesce. This is easy to see. The eigenstates of the Hamiltonian in Eq.(3) below the $\mathscr{PT}$-threshold (i.e. when $g < \kappa$) could easily be written as, with $sin\Theta = g/\kappa$, as follows:

$$|1\rangle_{belowEP} = \begin{pmatrix} 1 \\ e^{i\Theta} \end{pmatrix}, |2\rangle_{belowEP} = \begin{pmatrix} 1 \\ -ie^{-i\Theta} \end{pmatrix} \tag{2.4}$$

On the other hand, above the $\mathscr{PT}$-threshold (i.e. when $g > \kappa$), the supermodes could be written as, with $cosh\Theta = g/\kappa$, as given below:

$$|1\rangle_{aboveEP} = \begin{pmatrix} 1 \\ ie^{\Theta} \end{pmatrix}, |2\rangle_{aboveEP} = \begin{pmatrix} 1 \\ ie^{-\Theta} \end{pmatrix} \tag{2.5}$$

Quite clearly, exactly at the EP i.e. when $g = \kappa$, both the modes coalesce to $|1,2\rangle = \begin{pmatrix} 1 \\ i \end{pmatrix}$. In fact, the coalescence of eigenvectors at the EP is a typical feature of all $\mathscr{PT}$-symmetric

TH-2744_166121101

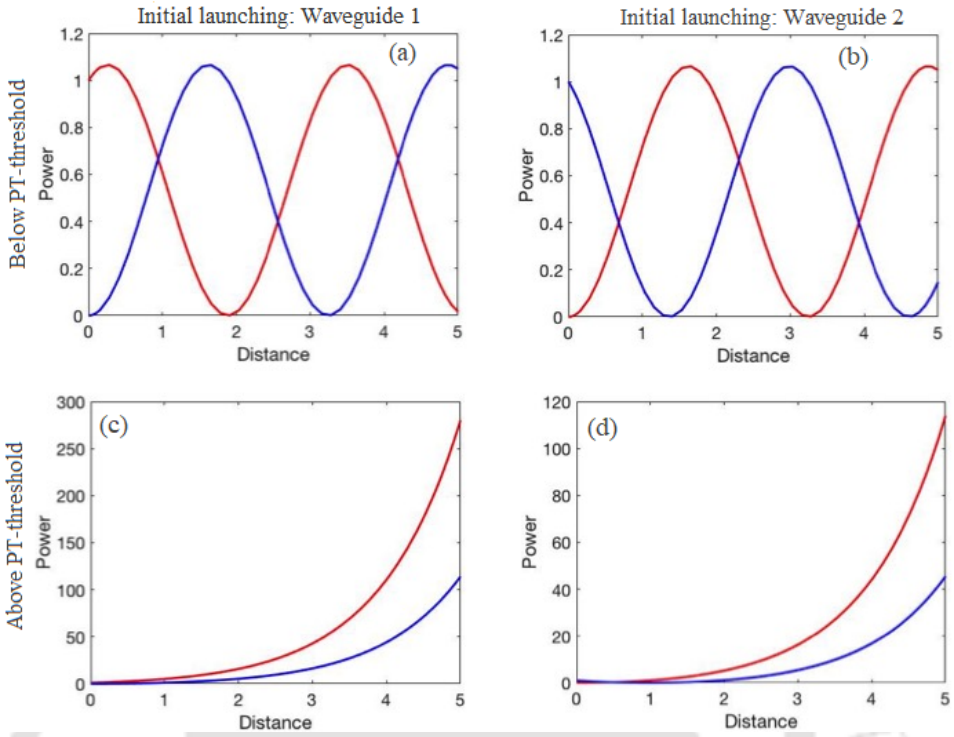

Figure 2.2: Optical wave propagation when the system is excited at either waveguide 1 [left panel: (a) and (c)] or waveguide 2 [right panel: (b) and (d)]. The launch conditions are at $z = 0$: for (a) and (c), $a = 1$ and $b = 0$; while for (c) and (d), $a = 0$ and $b = 1$. Light propagates in a non-reciprocal manner both below (upper panel) and above threshold (lower panel). The red curves correspond to the output power in the first waveguide and the blue curves correspond to the output power in the second waveguide of a $\mathscr{PT}$-symmetric coupler.

systems. This has immense physical implications in $\mathscr{PT}$-symmetric optical systems such as non-reciprocal behavior and power oscillations.

Fig. 2.2 depicts the non-reciprocal nature of wave propagation in the $\mathscr{PT}$-couplers. Below the $\mathscr{PT}$-threshold, with exchange of the input channel from first waveguide (gain) to the second waveguide (loss), we obtain an entirely different output state in the spatial evolution of the optical power [see Fig. 2.2(a) and Fig. 2.2(b)]. On the other hand, above the $\mathscr{PT}$-threshold, light always leaves the coupler from the first waveguide while experiencing an exponential amplification of power in the presence of gain in that waveguide, irrespective of the launch condition (be it in the first waveguide or in the second waveguide), albeit in a non-reciprocal manner [see Fig. 2.2(c) and Fig. 2.2(d)]. The physics behind this phenomenon could be traced back to the fact that above the $\mathscr{PT}$-threshold, eigenvalues of the Hamiltonian describing the system are complex, with

TH-2744_166121101

Figure 2.3: Non-reciprocity in $\mathcal{PT}$ synthetic structures.

the corresponding amplitudes exponentially increasing (red curves in Fig. 2.2(c) and 2.2(d)), please refer to the eigenvalue $|1\rangle_{aboveEP}$ in Eq.(2.5), where due to $\kappa \neq 0$ some finite amplitude is always in the other waveguide owing to the coupling (blue curves in Fig. 2.2(c) and 2.2(d)). Thus, only one supermode effectively survives. The unexpected non-reciprocity behavior of $\mathcal{PT}$-optical system is more clearly illustrated in Fig. 2.3.

Here the green arrows refer to a light beam that enters a synthetic $\mathcal{PT}$ structure from the left, and exits from the right. On the other hand, the red arrow on the right shows a light beam that enters the same $\mathcal{PT}$ system in exactly the opposite direction. Astonishingly, the red beam fails to retrace the path of the green beam but instead emerges from the structure (left red arrow) along a different trajectory. This occurs owing to the *parity-time* invariance. Apart from the non-reciprocal behavior, one can observe that when the coupling of the waveguides is sufficiently strong, i.e. in the regime of unbroken $\mathcal{PT}$-symmetry, the system is in equilibrium and one observes Rabi oscillations (power oscillations), where the optical power oscillates back and forth between the two waveguides. On the other hand, when the coupling becomes too weak and the system enters into the broken $\mathcal{PT}$-regime, the Rabi oscillations cease and the system can no longer remain in equilibrium; the power then grows exponentially in one waveguide and decays exponentially in the other [60].

2.2 Kerr effect

This is a nonlinear effect, and arguably the most important relevant to the thesis. It is worthwhile to note that, here we are discussing this, and other nonlinear and dispersive effects (refer to Secs. 2.4-2.6) in the context of a standard optical fiber; but the discussions are valid even for any other dielectric media. Standard optical fibers are made of fused silica which is a dielectric and, like any other dielectric, its response to light becomes nonlinear for intense electromagnetic fields. This nonlinear response

TH-2744_166121101

is expressed through nonlinear dependence of polarization on light intensity, $I = |\vec{E}|^2$, where $\vec{E}$ is the electric field vector. This dependence is usually written down as [58]:

$$\vec{P} = \varepsilon_0 [\chi^{(1)} \cdot \vec{E} + \chi^{(2)} : \vec{E}\vec{E} + \chi^{(3)} : \vec{E}\vec{E}\vec{E} + \cdots] \tag{2.6}$$

where $\chi^{(j)}(j = 1,2,3,..)$ is the j^{th} order susceptibility, which is a tensor of rank $(j+1)$ and ε_0 is the permittivity of free space. $\chi^{(j)}$ is a complex tensor and its real and imaginary parts lead to different nonlinear phenomena. The above result can be deduced using Lorentz model with anharmonicity in the motion of bound electrons. The linear susceptibility $\chi^{(1)}$ represents the dominant contribution to $\vec{P}$ and manifests itself through the refractive index $n(\omega)$ and the attenuation co-efficient $\alpha(\omega)$. $\chi^{(2)}$ is related to quadratic nonlinear effects, such as second harmonic generation and sum- and difference-frequency generation. The third-order susceptibility $\chi^{(3)}$ represents the cubic response of the medium to the incident light. The real part of $\chi^{(3)}$ is responsible for nonlinear effects such as third harmonic generation, four-wave mixing, and self-phase and cross-phase modulations. On the other hand, the imaginary part of $\chi^{(3)}$ results in the effects such as stimulated Raman scattering and stimulated Brillioun scattering. Since silica glass molecules are centro-symmetric, $\chi^{(2)} = 0$, for silica glass. Therefore, the lowest order nonlinear effects in silica glass fibers are due to $\chi^{(3)}$. $\chi^{(3)}$ leads to the nonlinear addition to the refractive index of the fiber-core via self-phase modulation.

Therefore, if we confine ourselves to cubic nonlinearity in optical fiber, or any dielectric media having centro-symmetry, the polarization vector could be written as:

$$\vec{P} = \vec{P}_L + \vec{P}_{NL} \tag{2.7}$$

where,

$$\vec{P}_L = \varepsilon_0 \int_{-\infty}^{\infty} \chi^{(1)}(t-t')\vec{E}(r,t')dt' \tag{2.8}$$

and

$$\vec{P}_{NL} = \varepsilon_0 \int_{-\infty}^{\infty}\int_{-\infty}^{\infty}\int_{-\infty}^{\infty} \chi^{(3)}(t-t_1, t-t_2, t-t_3)\vec{E}(r,t_1)\vec{E}(r,t_2)\vec{E}(r,t_3)dt_1dt_2dt_3 \tag{2.9}$$

In the frequency domain the polarization has the following simple representation,

$$\vec{P}_L = \varepsilon_0 \chi^{(1)}(\omega)\vec{E}(r,\omega) \tag{2.10}$$

$$\vec{P}_{NL} = \varepsilon_0 \chi^{(3)}(\omega_1,\omega_2,\omega_3)\vec{E}(r,\omega_1)\vec{E}(r,\omega_2)\vec{E}(r,\omega_3) \tag{2.11}$$

TH-2744_166121101

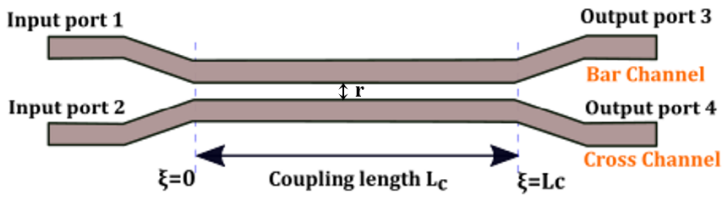

Figure 2.4: Schematic diagram of a directional coupler.

As mentioned above, the cubic nonlinearity results in an intensity dependent refractive index

$$n(\omega, |E|^2) = n_0 + n_2|E|^2, \tag{2.12}$$

where $n_0(\omega)$ is the linear part given by the following approximate formula [35]:

$$n_0^2(\omega) = 1 + \sum_{j=1}^{m} \frac{B_j \omega_j^2}{\omega_j^2 - \omega^2} \tag{2.13}$$

where ω_j are the resonance frequencies and B_j is the strength of the j-th resonance. The nonlinear refractive index co-efficient n_2 is usually called the Kerr-coefficient. If we assume the incident light to be linearly polarized, then only one component of $\chi^{(3)}(\chi^{(3)}_{xxxx})$ contributes to the nonlinear change in the refractive index. The nonlinear coefficient n_2 is then given by

$$n_2 = \frac{3}{8n_0} Re\left(\chi^{(3)}_{xxxx}\right) \tag{2.14}$$

where Re stands for the real part of the susceptibility tensor $\chi^{(3)}$. The experimentally observed value of n_2 for fused silica ranges from $2.2 \times 10^{-22} m^2/W$ to $3.4 \times 10^{-20} m^2/W$, which is small compared to most other nonlinear media by at least 2 orders of magnitude [35]. Despite this, nonlinear effects are easily observed in silica fibers even at relatively low input power levels. This is possible primarily because of a very small cross-sectional area of the core of a single-mode optical fiber which has a diameter of the order of $5\mu m$.

2.3 Nonlinear directional fiber coupler

A nonlinear directional fiber coupler is essentially based on a linear directional coupler shown in Fig. 2.4 in which r is the separation between the constituent fibers. A linear directional coupler relies on the coherent interaction between two single-mode fibers placed near each other. This interaction takes place through evanescent field overlap between fields confined within the individual cores leading to periodic exchange of energy

TH-2744_166121101

between the cores. The presence of nonlinearity detunes the waveguides and can result in intensity dependent switching between the output ports.

In the limit of weak coupling, the coupled mode equations for the nonlinear directional coupler (NLDC) with identical constituent fibers and Kerr nonlinearity are [67]:

$$i\frac{dA_1}{dz} + k_0 n_2 |A_1|^2 A_1 = -\kappa_0 A_2 \tag{2.15a}$$

$$i\frac{dA_2}{dz} + k_0 n_2 |A_2|^2 A_2 = -\kappa_0 A_1 \tag{2.15b}$$

where κ_0 is the linear coupling constant, k_0 is the free-space wave number and $|A_1|$ and $|A_2|$ represent the complex electric field envelope amplitudes in fibers 1 and 2, respectively. In the absence of nonlinearity, the solutions for A_1 and A_2 can be written as

$$A_1(z) = a_1 \cos(\kappa_0 z) + b_1 \sin(\kappa_0 z) \tag{2.16a}$$

$$A_2(z) = a_2 \cos(\kappa_0 z) + b_2 \sin(\kappa_0 z) \tag{2.16b}$$

The boundary conditions:

$$A_1(0) = A_0, A_2(0) = 0 \tag{2.17}$$

corresponding to the case when light is injected into fiber 1 with fiber 2 kept empty, yield

$$a_2 = b_1 = 0 \tag{2.18}$$

Therefore,

$$A_1(z) = A_0 \cos(\kappa_0 z) \tag{2.19a}$$

$$A_2(z) = A_0 \sin(\kappa_0 z) \tag{2.19b}$$

The output intensities at the bar and cross output ports are given by

$$I_1 = I_0 \cos^2\left(\frac{\pi L_c}{L_{coh}}\right) \tag{2.20a}$$

$$I_2 = I_0 \sin^2\left(\frac{\pi L_c}{L_{coh}}\right) \tag{2.20b}$$

where L_{coh} is the coherence length defined as

$$L_{coh} = \frac{\pi}{\kappa_0} \tag{2.21}$$

and gives the characteristics length over which the input signal is completely coupled from one fiber to the other and back. Clearly if $L_c = \frac{L_{coh}}{2}$, a signal input into the fiber

TH-2744_166121101

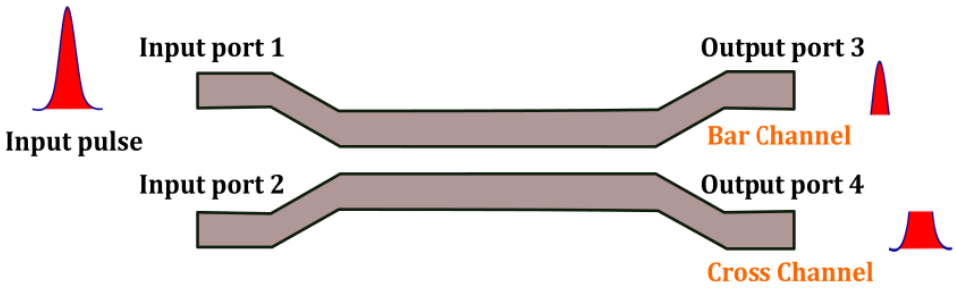

Figure 2.5: Schematic illustration of partial switching of pulse inside a fiber coupler.

1 emerges at the output from fiber 2 (cross-state). In this case the coupler is called a half-beat length coupler. If nonlinearity is taken into account one can still solve the coupled mode equations with the same boundary conditions in terms of Jacobi elliptic function cn to obtain [67]:

$$I_1 = \frac{I_0}{2}\left[1 + cn\left(\frac{2\pi L_c}{L_{coh}}, \left(\frac{I}{I_{cr}}\right)^2\right)\right] \tag{2.22a}$$

$$I_2 = \frac{I_0}{2}\left[1 - cn\left(\frac{2\pi L_c}{L_{coh}}, \left(\frac{I}{I_{cr}}\right)^2\right)\right] \tag{2.22b}$$

where the critical intensity I_{cr} is defined as

$$I_{cr} = \frac{\lambda_0}{n_2 L_{coh}} \tag{2.23}$$

and gives the intensity for which the input light is equally divided between two output ports. Here, in Eq.(2.23), λ_0 is the free space wavelength of light. For a half-beat length coupler, the critical intensity results in a π phase-shift of the input signal in fiber 1. If $I > I_{cr}$, the fraction of light existing in input fiber 1 increases towards unity. Thus, the given two-terminal device performs a switching operation by directing the input signal to emerge from one of the output ports. This kind of nonlinear directional coupler was first proposed by Jensen in 1982 [80] for switching of a continuous wave (CW) signal. When pulsed signals were used, it was observed that only the central high intensity part got switched. One could explain it as follows. Because the nonlinear phase shift is proportional to the instantaneous intensity, different portions of the pulse experience different phase shifts. Only the central portion of the high-power pulse exceeds the critical intensity and remains in fiber 1. The wings get cut-off and go into the second fiber [see Fig. 2.5]. This phenomenon was called partial switching or pulse break up and resulted in undesirable reduced integrated energy contrast.

In 1988, Trillo et al. [33] pointed out that pulse break-up could be avoided by using a

TH-2744_166121101

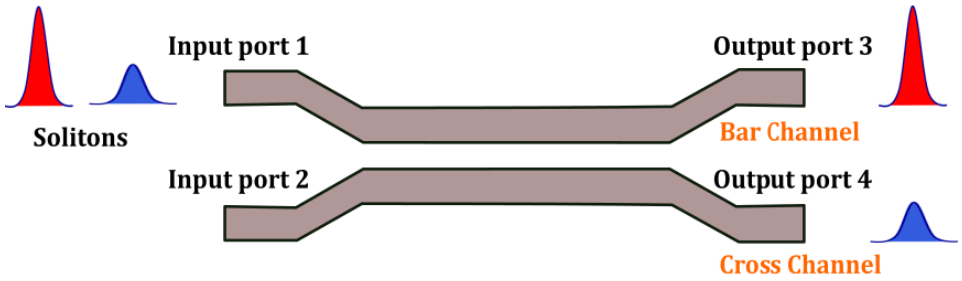

Figure 2.6: Schematic illustration of complete switching of solitons inside a fiber coupler.

soliton pulse as the input signal. Since then, soliton switching in nonlinear fiber coupler has been receiving considerable attention in Kerr as well as non-Kerr fiber systems [67]. The physics behind soliton switching can be understood from the fact that the nonlinear phase shift due to self-phase modulation is constant across the entire soliton pulse, owing to which, if the input pulse intensity exceeds I_{cr}, the pulse switches as a whole, i.e., as a single unit and no pulse break-up takes place. This mode of soliton switching is called intensity-induced switching. In order to understand the mechanism, see Fig. 2.6. One soliton with lower peak power (displayed by the blue pulse) and another one with higher peak power (displayed by the red pulse), both of them having intensities greater than I_{cr}, switch as a whole pulse in two different output channels depending on their intensities. Varying the input peak power of the soliton is not the only way to achieve soliton switching. One can also have soliton switching, as shown by Trillo and Wabnitz [78], by injecting a weak pulse in one of the input cores (say, the second core) of the coupler when a strong soliton pulse is injected into the first core. This switching can be controlled by relative phase change of the weak control pulse. The physics behind phase induced soliton switching can be understood as follows: The general requirement of switching is to attain a phase shift of the order of 2π. This can be achieved by launching a weak signal having an initial phase difference, say ϕ, into the second core along with the strong signal pulse launched in the first core. The inclusion of the weak signal drives the coupler into the domain of nonlinearly phase-mismatched condition for an appropriate value of ϕ and results in soliton switching.

2.4 Dispersive and Nonlinear Phenomena

In this section, we briefly discuss some dispersive and nonlinear phenomena relevant to the thesis work. For more detailed exposition, readers are referred to the excellent text book by Prof. G.P. Agrawal [35]. This section is based on that text book.

TH-2744_166121101

2.4.1 Group Velocity Dispersion and Third-Order Dispersion

· **(a) Group Velocity Dispersion:** Dispersion originates from the frequency dependence of the refractive index $n_0(\omega)$. An optical pulse is a wave packet containing a large number of frequency components. Due to frequency dependence of the refractive index, different frequency components of the pulse propagate at different velocities and the pulse undergoes group velocity dispersion (GVD). Quantitatively the phenomenon is characterized by the so-called GVD parameter D:

$$D = -\frac{2\pi c}{\lambda^2}\beta_2 \approx \frac{\lambda}{c}\frac{d^2 n_0(\omega)}{d\lambda^2} \tag{2.24}$$

where, $\beta_2 = \frac{d^2\beta}{d\omega}$ is the second-order dispersion co-efficient, λ is the operating wavelength and c is the speed of light.
GVD results in temporal broadening of the pulse, as it propagates along the fiber. Owing to this, one defines a characteristic length L_D

$$L_D = \frac{T_0^2}{|\beta_2|} \tag{2.25}$$

where T_0 is the initial width of the pulse. If we take an unchirped Gaussian pulse with field distribution

$$u(z=0,T) = exp\Big[-\frac{t^2}{T_0^2}\Big] \tag{2.26}$$

propagating in the z-direction along the fiber, then the pulse-width after a propagation distance z is given by

$$T(z) = T_0\Big[1+\Big(\frac{z}{L_D}\Big)^2\Big]^{\frac{1}{2}} \tag{2.27}$$

Therefore, for $z = L_D$; we obtain $T = \sqrt{2}T_0$ and the characteristic dispersion length L_D is defined as the distance over which the pulse width broadens by a factor of $\sqrt{2}$. A couple of comments are in order here. Firstly, according to Eq.(2.27), an unchirped pulse broadens identically monotonically in both the normal as well as anomalous-dispersion regime because

$$\Big(\frac{z}{L_D}\Big)^2 = \frac{z^2|\beta_2|^2}{T_0^4} \tag{2.28}$$

is insensitive to sgn(β_2). Secondly, besides causing pulse broadening, dispersion also leads to chirping of the Gaussian pulse via phase modulation. As a result, in

TH-2744_166121101

the normal dispersion regime ($\beta_2 > 0$) , the frequency is reduced in the leading edge of the pulse while it is increased in the trailing edge. This dispersive chirping of the pulse plays the key role in the formation of an optical soliton in fibers.

· **(b) Third-Order Dispersion:** Under certain situations, for instance when the operating wavelength is near the zero-dispersion wavelength λ_D or when the pulse has a pulse width less than $1ps$, it becomes necessary to take third-order dispersion (TOD) into account. TOD is characterized by the co-efficient

$$\beta_3 = \frac{1}{3!}\left(\frac{\partial^3 \beta}{\partial \omega^3}\right)_{\omega=\omega_0} \tag{2.29}$$

in the Taylor expansion of the dispersion relation $\beta = \beta(\omega)$ around the carrier frequency ω_0. It leads to asymmetric pulse broadening and generates oscillatory structures at the trailing and the leading edges of the pulse. Similar to the case of second-order dispersion, one can define a characteristic dispersion length

$$L'_D = \frac{T_0^3}{|\beta_3|} \tag{2.30}$$

Third-order dispersion becomes important if [35]

$$L'_D \leq L_D, or, T_0 \left|\frac{\beta_2}{\beta_3}\right| \tag{2.31}$$

2.4.2 Self-Phase Modulation

One of the most striking features of pulse propagation in a nonlinear medium is the nonlinearity induced phase modulation referred to as Self-Phase Modulation (SPM) [58] which, coupled with the dispersion effects, gives rise to various interesting nonlinear phenomena in a fiber. When a high-intensity short pulse is coupled to optical fiber, the refractive index of the medium is modified and, acquires an intensity dependent nonlinear part over that of the usual linear part $n_0(\omega)$, expressed by the Eq.(2.12). It is this intensity dependent refractive index that gives rise to the SPM. In optical fibers it is more convenient to express propagation in terms of modal power rather than intensity. If A_{eff} is the effective cross-sectional area of the mode, then $I + P/A_{eff}$, where P is the power carried by the optical beam. Due to the intensity dependence of the refractive index, the propagation constant of a mode can now be written as

$$\beta_{NL} = \beta + \gamma P, \quad \gamma = \frac{n_2 \omega_0}{c A_{eff}} \tag{2.32}$$

TH-2744_166121101

The phase shift suffered by an optical beam in propagating through a length L of the optical fiber is given by

$$\phi = \int_0^L \beta_{NL} dz = \beta L + \gamma P L \tag{2.33}$$

Since the propagation constant β_{NL} of the mode depends on the power carried by the mode, the phase ϕ of the emergent wave depends on its own power and hence is referred to as 'self-phase' modulation. It leads to the spectral broadening and modulation of optical pulses. In the absence of GVD, SPM induced spectral broadening occurs without change in the temporal pulse shape. One of the most useful consequences of SPM is the existence of optical solitons in the presence of the anomalous GVD.

2.4.3 Self-steepening

Self-steepening (SS) results from the intensity dependence of the group velocity, because of which the peak of the pulse moves at a lower speed than the wings as it propagates inside an optical fiber. The net result is that the pulse becomes asymmetric, with its peak shifting toward the trailing edge. The trailing edge becomes steeper and steeper with increasing propagation distance. SS eventually leads to the formation of an optical shock, analogous to the development of an acoustic shock on the leading edge of a sound wave. Due to the fact that SS is caused by intensity dependence of the group velocity which is proportional to the temporal derivative of the Kerr term, it is also called Kerr-dispersion. It leads to an asymmetry in the SPM broadened spectra of ultra-short pulses.

2.4.4 Stimulated Raman Scattering

Stimulated Raman scattering (SRS) is one of the most prominent phenomena that result due to stimulated inelastic scattering, in which the light traveling in the fiber transfers a part of its energy to the fiber medium. Usual Raman scattering involves scattering of a photon by one of the molecules of a Raman active medium to a lower frequency photon. The scattered radiation, along with the light at the incident frequency ω_0, also contains light at frequencies, $\omega_0 + \omega_m$, and $\omega_0 - \omega_m$ where ω_m is the vibrational frequency of the molecule of the medium. The down-shifted component at $\omega_0 - \omega_m$ is called the Stokes wave whereas the up-shifted component at $\omega_0 + \omega_m$ is called the anti-Stokes wave. In its essence, Raman scattering is a linear phenomenon. However, if the incident beam is intense, a nonlinear version of Raman scattering takes place in which the

TH-2744_166121101

Stokes component grows rapidly such that most of the incident energy is transferred to it. The stimulated Raman gain in silica glass fiber extends over a large frequency range with a broad peak near 13 THz. As a result, SRS can turn an optical fiber into a broadband Raman amplifier and a tunable Raman laser. However, it can also limit the performance of a multichannel lightwave communication system through cross-talk between neighbouring channels.

2.5 Nonlinear Schrödinger Equation

The pulse propagation in a nonlinear optical fiber or waveguide is typically described by the so-called Nonlinear Schrödinger Equation (NLSE). This equation can be derived from the Maxwell's equations, usually applying the so called slowly varying envelope approximation. For details, readers are again referred to [35]. The NLSE has the following well-known form:

$$i\frac{\partial A}{\partial z} - \frac{\beta_2}{2}\frac{\partial^2 A}{\partial T^2} + \gamma|A|^2 A = 0 \tag{2.34}$$

where $A(z,T)$ is the slowly varying complex amplitude of the pulse envelope. $T = t - \frac{z}{v_g}$ is the time measured in a frame of reference moving at the group velocity v_g of the pulse. The NLSE Eq.(2.34) should be modified for ultra-short optical pulses whose width is close to or $< 1ps$. For such short pulses we must take into account higher order nonlinear effects due to stimulated inelastic scattering such as SRS and dispersive effects like the TOD. Then, the NLSE takes the following form:

$$i\frac{\partial A}{\partial z} - \frac{\beta_2}{2}\frac{\partial^2 A}{\partial T^2} + \gamma|A|^2 A = i\frac{\beta_3}{6}\frac{\partial^3 A}{\partial T^3} - i\frac{\gamma}{\omega_0}\frac{\partial}{\partial T}(|A|^2 A) + \gamma T_R A\frac{\partial|A|^2}{\partial T} \tag{2.35}$$

Eq.(2.35) describes propagation of optical pulses in a single mode fiber. β_2 governs the effect of GVD. β_3 governs the effects of TOD. The first, second and the third term on the R.H.S of Eq.(2.35) take into account the effect of TOD, SS and the intrapulse Raman scattering (IRS), respectively. T_R is the Raman response time.

2.6 Optical Solitons

Solitons in general refer to a localized propagating wave solution of a nonlinear dispersive or diffractive partial differential equation which preserves its shape and velocity, under a collision with a similar localized propagating wave in a lossless medium. The collision

TH-2744_166121101

property distinguishes a soliton from the so-called solitary wave which may not fulfil these requirements of remaining undistorted after collision with each other. Existence of soliton solutions solely depends on the properties of the medium. Optical fibers, for example, can support two types of temporal solitons: Bright Solitons in anomalous GVD regime and the dark soliton in the normal GVD regime. A bright soliton is a lump of light propagating along the fiber. A dark soliton, on the other hand, is a dark hole in the CW background. Depending on the localization property and the spatial dimensions in which they exist, solitons are classified into three major categories: (i) temporal solitons, (ii) spatial solitons and (iii) spatio-temporal solitons. As our work in this thesis is mainly concentrated to the first category of solitons mentioned above, we will now discuss a little bit in detail about temporal solitons.

As we have discussed earlier, individually both GVD and SPM phenomena can create major problems in a fiber-optic communication system. But if a system is designed in such a way that the effects of dispersion and SPM perfectly cancel each other out, a pulse may propagate through a fiber without any change in shape and velocity in a lossless fiber. Such pulses also remain unchanged under a collision with a similar pulse and are called temporal solitons.

The partial differential equation that governs pulse evolution in a nonlinear and isotropic fiber with circular cross-section is given by the NLSE discussed earlier (Eq.(2.35)).

Introducing

$$\tau = \frac{T}{T_0}, \quad \xi = \frac{z}{L_D}, \quad U = \frac{A}{\sqrt{P_0}} \tag{2.36}$$

where T_0 is a measure of the pulse width, P_0 is the peak power of the pulse and L_D is the dispersion length as described in Eq.(2.25). Eq.(2.34) can be written in the following dimensionless form:

$$i\frac{\partial U}{\partial \xi} - \frac{sgn(\beta_2)}{2}\frac{\partial^2 U}{\partial \tau^2} + N^2|U|^2U = 0 \tag{2.37}$$

where $sgn(\beta_2) = +1$ or -1, depending on whether β_2 is normal GVD or anomalous GVD. The parameter N is defined as

$$N^2 = \gamma P_0 L_D = \frac{\gamma P_0 T_0^2}{|\beta_2|} \tag{2.38}$$

Now introducing $u = NU$, Eq.(2.34) can be re-written as

$$i\frac{\partial u}{\partial \xi} - \frac{sgn(\beta_2)}{2}\frac{\partial^2 u}{\partial \tau^2} + |u|^2u = 0 \tag{2.39}$$

TH-2744_166121101

where the positive sign in the second term corresponds to anomalous GVD ($\beta_2 < 0$) whereas the negative sign corresponds to the normal GVD ($\beta_2 > 0$). This is the standard nondimensional form of the NLSE. In the case of anomalous GVD, the corresponding NLSE Eq.(2.39) possesses a bright soliton solution

$$u(\xi,\tau) = \psi(\tau) exp\big(\frac{i}{2}\xi\big) \tag{2.40}$$

where $\psi(\tau)$ satisfies

$$u(0,\tau) = \psi(\tau), \quad \lim_{|z|\to\infty} \psi(\tau) = \lim_{|z|\to\infty} \frac{d\psi}{d\tau} = 0 \tag{2.41}$$

The general asymptotic solution consists of solitons and localized radiations.

2.6.1 Bright solitons

As mentioned above, in the anomalous GVD regime, an optical fiber supports bright solitons. The NLSE in this case takes the form as mentioned in Eq.(2.39) with $\beta_2 = -1$. Considering the launch of an input pulse having an initial amplitude distribution

$$u(0,\tau) = N sech(\tau) \tag{2.42}$$

into the fiber, Eq.(2.39) was solved via Inverse Scattering Theorem method (ISTM) by Satsuma and Yajima [59] who obtained soliton solutions of different orders. Thus, the stationary bright fundamental soliton (which corresponds to $N = 1$) solution of the NLSE Eq.(2.39) is given by

$$u(0,\tau) = sech(\tau)\ exp\big(\frac{i}{2}\xi\big) \tag{2.43}$$

The above solution represents a lump of light and is called a bright soliton. Soliton solutions of Eq.(2.39) corresponding to $N > 1$ are called higher order solitons. The shape of the pulse remains unchanged during propagation when $N = 1$ but follows a periodic pattern for integer values of $N > 1$, such that the input shape is recovered periodically at $\xi = \frac{m\pi}{2}$ where m is an integer. This happens because of the variations in the relative strength of dispersive and nonlinear effects which depend on the distance of propagation. Since $\xi = z/L_D$, the soliton period z_0, defined as the characteristics distance over which the higher order solitons recover their initial shape, is given by

$$z_0 = \frac{\pi}{2} L_D = \frac{\pi T_0^2}{2|\beta_2|} \tag{2.44}$$

TH-2744_166121101

The soliton period z_0 and the soliton order N play an important role in quantifying temporal solitons in an optical fiber.
In general, the ISTM rigorously predicts that the $N-th$ order soliton can be formed when the parameter N lies in the range [35]

$$N-\frac{1}{2}\leq N\leq N+\frac{1}{2} \tag{2.45}$$

This means that a fundamental soliton can be created by an input for which $N\in[0.5,1.5]$. The concrete form of the input shape is not important so long as a localized input is used with N in the above specified range. This can be understood from the concept of temporal mode of a nonlinear waveguide. Higher intensities in the central part of a localized pulse increase the refractive index there and create a temporal waveguide. The waveguide supports temporal modes just the same way as the core-cladding index difference leads to spatial modes in an optical fiber. This is why, even if the input pulse does not exactly match the temporal mode of this waveguide, the major part of the pulse energy is still coupled to the temporal mode. The residual energy spreads in the form of dispersive waves.

2.6.2 Dark solitons

In the normal GVD regime an optical fiber supports dark solitons. The NLSE in this case takes the form:

$$i\frac{\partial u}{\partial \xi}-\frac{1}{2}\frac{\partial^2 u}{\partial \tau^2}+|u|^2u=0 \tag{2.46}$$

The intensity profile of the resulting solutions of Eq.(2.46) exhibits a dip in a uniform background, and it is the dip that remains unchanged during propagation inside the fiber. Since the dip is characterized by the absence of light in it, the soliton is called a dark soliton. The dark soliton solution is given by [35]:

$$u_D(\xi,\tau)=\sqrt{(1-\sigma^2 sech^2(\tau))}exp[i(K\xi+\phi(\tau))] \tag{2.47}$$

where the time dependent phase $\phi(\tau)$ is

$$\phi(\tau)=\sin^{-1}\left(\frac{\sigma\tanh(\tau)}{\sqrt{(1-\sigma^2 sech^2(\tau))}}\right) \tag{2.48}$$

Here K is a constant and σ is called the dip parameter or blackness and varies in the range $[0,1]$. For $\sigma=1$, the intensity at the dip center, $\tau=0$, falls to zero. For other values

TH-2744_166121101

of σ, the dip does not go to zero. The solution with $\sigma = 1$ is called the fundamental dark soliton. It has been shown by numerical simulations that the dip can propagate as a dark soliton even against a non-uniform background, provided the light intensity is uniform in the vicinity of the dip.

Numerical simulations also show that they are more stable in the presence of noise and spread more slowly in the presence of fiber loss as compared to bright solitons. They are also relatively less affected by many perturbative effects such as IRS, amplifier-induced timing jitter etc. These features make dark soliton a potential candidate for applications in fiber optic communication systems.

2.6.3 Bistable solitons

Bright and dark solitons are prominently exhibited by materials exhibiting Kerr nonlinearity, i.e. media where the refractive index increases linearly with intensity. There exists, however, numerous materials, such as chalocogenide glasses, silica doped with organic dye, where the nonlinearity begins to saturate very early at low intensity or low optical power. In such media, the refractive index is effectively modelled an intensity dependent function $f(I)$ as follows:

$$n(I) = n_0 + n_2 f(I), \tag{2.49}$$

The corresponding NLSE takes the following form [88]:

$$i\frac{\partial u}{\partial \xi} + \frac{1}{2}\frac{\partial^2 u}{\partial \tau^2} + f(|u|^2)u = 0 \tag{2.50}$$

It is easy to obtain a shape preserving solution of Eq.(2.50) assuming a solution of the form: $u(\xi,\tau) = V(\tau)\exp(iK\xi)$, with the boundary condition, $V = 0$ as $|\tau| \to \infty$. Here, $V(\tau)$ is independent of ξ and determine the shape of the soliton. K is a constant parameter, and is related to the soliton energy, E_s, as follows [88]:

$$E_s(K) = \frac{1}{2}\int_0^{P_m} [K - F(P)]^{-\frac{1}{2}} dP, F(P) = \frac{1}{P}\int_0^P f(P)dP, \tag{2.51}$$

where $P = V^2$, $F(0) = 0$ and P_m is the smallest positive root of $F(P) = K$. Now, we can have many solutions depending on the saturation function $f(P)$, each having the same energy but different values of the wavenumber K and P_m. In most cases, only two solutions are

TH-2744_166121101

found to be stable, and they are known as the bistable solitons.

It is worthwhile to mention that the contents of this chapter is based on many resources [88, 108, 89, 58, 67]. In particular, the contents of Section 2.1 is reproduced, with due permission, from Ref.[108]. We believe that, having all the relevant concepts in one place would be of great help to the readers to appreciate the rest of the chapters of this thesis.

भारतीय प्रौद्योगिकी संस्थान गुवाहाटी • Indian Institute of Technology Guwahati •

TH-2744_166121101

CHAPTER 3

ULTRAFAST FEMTOSECOND SOLITON STEERING IN KERR $\mathscr{PT}$ COUPLERS

In this chapter, we carry out a detailed study on soliton steering dynamics in a $\mathscr{PT}$-symmetric NLDC in the femtosecond (fs) domain. In this regime, the practical application of any real fiber coupler requires incorporation of higher-order perturbative effects such as TOD and fourth-order dispersion (FOD), SS, and IRS. With a high gain/loss, the combination of all these effects is found to stabilize the soliton pulse evolution in the coupler from the chaotic behaviour of unperturbed evolution. This work demonstrates that efficient soliton steering can be achieved at very low critical power and a relatively higher gain/loss even in the fs regime.

3.1 Introduction

In high-speed signal processing and ultrafast communication systems, all-optical switching devices are considered to be key elements that have drawn significant attention over the past few decades [30]. In this context, a dual-core NLDC featuring power-dependent switching has been studied extensively [31, 32, 33]. After the first experimental observation of $\mathscr{PT}$-symmetric effect [6] in linear waveguide directional coupler with balanced

*The results of this chapter have been arxived as the following paper: A. Sahoo, D. K. Mahato, A. Govindarajan and A. K. Sarma, *"Ultrafast all-optical femtosecond soliton steering in $\mathscr{PT}$-symmetric fiber couplers"*. This paper is under review in Physical Review A.

TH-2744_166121101

gain/loss, an opportunity for further research [19, 60, 61] has emerged in the direction of $\mathscr{PT}$-symmetric linear/nonlinear couplers. Several studies have shown that such couplers are beneficial over a conventional one for all-optical switching when operating in the nonlinear regime [62, 63, 64]. Previously, the stability of optical solitons in $\mathscr{PT}$-symmetric fiber couplers has been investigated with semi-analytical and numerical approaches, wherein exact stable states have been found [28, 65].

Following the report of the requirement of high critical power for ps short pulse soliton switching, getting reduced sharply as a result of incorporation of $\mathscr{PT}$ symmetry in a NLDC [26], it is of particular interest to explore the idea of $\mathscr{PT}$-symmetric fiber coupler for the fs pulse switching and observe the switching dynamics under the effect of balanced gain and loss. The $\mathscr{PT}$-symmetric system mathematically described in Reference [26] shows to utilize the well-known coupled NLSE. However, in the domain of ultra-short fs solitons, ranging from few fs to 1 ps, for the purpose of practical application of any real fiber coupler, it requires incorporation of higher-order perturbative effects such as higher-order dispersions (HODs) including TOD and FOD, SS, and IRS [34, 35] in the coupled NLSE.

Thereafter, in this work, we investigate the soliton steering dynamics in a $\mathscr{PT}$-symmetric directional coupler in the fs domain in great detail. We first explore the effects of individual higher-order perturbations (IRS, SS, HODs) on steering dynamics. Following that, we investigate the cumulative combined effects of all perturbations, which result in a significant improvement in the stability and switching of fs soliton against individual perturbations as well as unperturbed cases.

In an earlier work [66], it has been reported that in the context of conventional couplers IRS restabilizes the symmetric solitons at sufficiently large energies. However, in the case of a $\mathscr{PT}$-symmetric coupler, we show that a partly radiating solitons caused by high gain/loss values (although the used pulse is a low energy fundamental soliton) are stabilized in the presence of higher-order perturbations. This finding is new in the context of ultrafast soliton steering in a $\mathscr{PT}$-symmetric coupler, paving the way for stable and efficient fs all-optical switching at low energy than the conventional one.

3.2 Model: $\mathscr{PT}$-symmetric fiber coupler

To discuss the fs pulse switching in a $\mathscr{PT}$-symmetric fiber coupler, it is important to consider the generalized NLSE with an integral form of the nonlinearities. This is

TH-2744_166121101

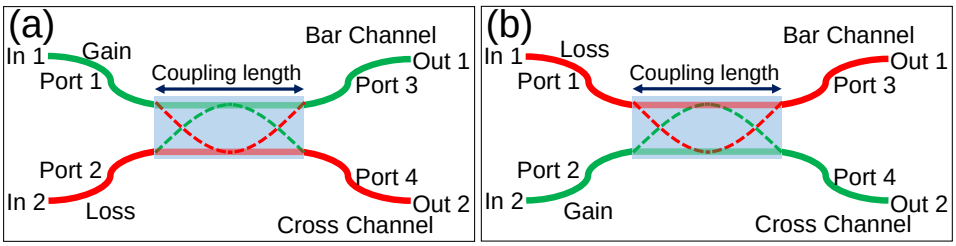

Figure 3.1: Schematic diagrams of fiber couplers with (a) type-1 and (b) type-2 $\mathscr{PT}$-symmetric configuration.

because it was experimentally observed that, for an ultrashort pulse which has a wide spectrum in the frequency domain, a continuous downshift of the center frequency takes place as an effect of the higher-order nonlinearities [35]. Therefore, the coupled-mode equations of the slowly-varying envelops $A_{1,2}(z,t)$ in the two channels of the fiber couplers can be written in normalized units of the form [26, 67]:

$$i\partial_\xi u_{1,2} + \sum_{n=2}^{\infty} \delta_n (i\partial_\tau)^n u_{1,2} \mp i\Gamma u_{1,2} + \kappa u_{2,1} + (1 + is\partial_\tau) R(\tau) \otimes |u_{1,2}|^2 u_{1,2} = 0, \tag{3.1}$$

where $u_{1,2}(\xi,\tau) = A_{1,2}/\sqrt{P_0}$, with P_0 being the peak power of the input pulse. The propagation distance (z) and time (t) variables are, respectively, normalized with new parameters as $\xi = z/L_D$ and $\tau = (t - zv_g^{-1})/t_0$, with $L_D = t_0^2/|\beta_2(\omega_0)|$, where t_0 is the input pulse width, v_g is the group-velocity of the pulse, and $\beta_2(\omega_0)$, the GVD parameter at the carrier frequency ω_0. The inter-core linear coupling (K) and balanced gain/loss (G) parameters are scaled as $\kappa = KL_D$ and $\Gamma = GL_D$. Also, the terms $\delta_n [= \beta_n/(n!|\beta_2|t_0^{n-2})]$, $s [= 1/(\omega_0 t_0)]$, and $R(\tau) = (1 - f_R)\delta(\tau) + f_R h_R(\tau)$ respectively denote the normalized parameters of HOD, SS or shock, and the nonlinear response function, which includes Kerr nonlinearity via $\delta(\tau)$ and Raman response function $[h_R(\tau)]$ that connects through the convolution integration $\otimes$ with the field envelops. Here, $h_R(\tau) = (1 - f_b)(\tau_1^{-2} + \tau_2^{-2})\tau_1 \exp(-\tau/\tau_2)\sin(\tau/\tau_1) + f_b[(2\tau_b - \tau)/\tau_b^2]\exp(-\tau/\tau_b)$ [68], with $f_R = 0.245$ being the fractional contribution of the delayed Raman response to nonlinear polarization, $\tau_1 = 12.2\,\text{fs}/t_0$, $\tau_2 = 32\,\text{fs}/t_0$, $\tau_b \approx 96\,\text{fs}/t_0$, and the relative contribution of the boson peak is included through $f_b = 0.21$.

The system described by Eq. (3.1) is $\mathscr{PT}$-symmetric due to the presence of the equal gain and loss in the two waveguides which has been written in terms of $\mp\Gamma$. As shown in Fig. 3.1 the case of fiber couplers [shown in Fig. 3.1], two types of configurations are specified based on the sign of Γ, namely type-1 (for $\Gamma > 0$) and type-2 (for $\Gamma < 0$)

TH-2744_166121101

$\mathscr{PT}$-symmetric couplers as done in [26]. Following an earlier study which has confirmed that a 2π coupler with type-1 $\mathscr{PT}$ configuration exhibits richer steering dynamics, achieving low critical steering power (P_{cr}, normalised with respect to the input power) while maintaining excellent transmission efficiency [26]. In view of this, we confine our analysis to the 'type-1 $\mathscr{PT}$-coupler' (with coupling length $L_c = 2\pi$), which we refer to as the '$\mathscr{PT}$-symmetric coupler' throughout the text. Similarly, we restrict our system to work in the unbroken regime alone by fixing a condition of $\kappa > \Gamma$ as $\kappa = 1$ and $\Gamma = 0.5$. This is due to the fact that power-controlled steering is limited within the unbroken $\mathscr{PT}$-symmetric regime as the soliton pulse exhibits severe instability in the broken $\mathscr{PT}$-symmetric regime. Note that Eq. (3.1) contains all the higher-order terms that act as perturbations in the context of ultrashort (fs) pulse dynamics [35]. When the pulse duration is large enough (ps or larger), IRS and SS can be ignored. Also, if the input pulse is launched far away from the zero-dispersion frequency, one can neglect HODs. In such a case, Eq. (3.1) resembles the unperturbed coupled-mode equation for $\mathscr{PT}$-symmetric systems for ps pulses [26].

To investigate the soliton switching dynamics, the unperturbed equation is first numerically solved by launching $u_1(0,\tau) = \sqrt{P_0}sech(\tau)$ and $u_2(0,\tau) = 0$. The numerical simulations are carried out using the split-step Fourier method (SSFM) for coupled-mode equations [26, 35] incorporating with fourth-order Runge-Kutta algorithm. Next, we numerically solve the Eq. (3.1) taking into account all of the perturbations present in the system. The numerical investigations show that HODs and higher-order nonlinear phenomena have a significant impact on the fs steering dynamics in $\mathscr{PT}$-symmetric couplers. The study further reveals that for an ultrashort pulse propagation, P_{cr} depends on $\delta_{n,n>2}$ (HOD parameters), IRS, and s (SS or shock effect), i.e., $P_{cr} \sim f(\delta_n, \mathrm{IRS}, s)$. The strength of these perturbations can be tuned by varying the input pulse duration t_0. We extensively study the pulse dynamics for a wide range of t_0 (from 5 fs to 1 ps). In order to get into the detail switching dynamics, we first systematically analyze the individual perturbation effects. Then, the combined effects of all the higher-order perturbations are discussed in some details.

3.3 Impact of higher-order nonlinear effects

Higher-order perturbations on ultrashort pulses have been studied in various optical waveguides, and the effects on pulse dynamics are significant. It is known that a fs soliton

TH-2744_166121101

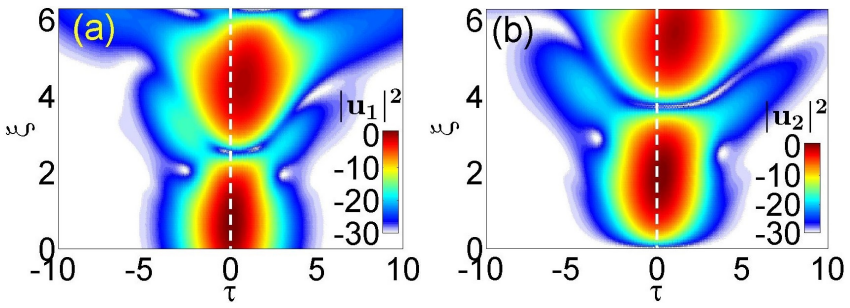

Figure 3.2: The evolution of a 10 fs pulse in the two channels of a type-1 2π $\mathscr{PT}$-symmetric fiber coupler with the normalized input pump power $P_0 = 1$ under the effect of IRS are depicted in (a) and (b) in dB scale.

with ultrashort pulse width t_0 and intense peak power can excite higher-order nonlinear effects like IRS and SS in fiber. Under the influence of IRS, the central frequency of the soliton is known to experience a redshift [69]. IRS also influences the temporal dynamics of the soliton by imposing a temporal deceleration. In a single soliton case, the effect of IRS leads to Raman amplification and lasing. SS, on the other hand, creates an optical shock on the leading edge of the pulse, resulting in asymmetric spectral broadening [35].

In order to investigate the effect of IRS and SS on the soliton steering dynamics in a 2π $\mathscr{PT}$-symmetric fiber coupler, we first numerically solve Eq.(3.1) for a 10 fs input *sech* pulse in the presence of IRS only. The temporal evolutions are plotted in Figs. 3.2(a) and 3.2(b) for the two channels of the coupler. As it is observed, here the power of a fs soliton launched into the first channel steers back and forth between the two channels and eventually exits from the second one. We observe that there is no temporal acceleration or deceleration for the conventional counterpart; this is represented by the white vertical dashed lines at the center $\tau = 0$ in Figs. 3.2(a) and 3.2(b). Whereas, for the $\mathscr{PT}$-symmetric coupler case as shown in the same figures, the IRS-induced characteristic temporal decelerations are evident. For a short optical pulse, in the absence of any perturbation, inclusion of $\mathscr{PT}$ symmetry revealed a critical switching power to be $P_{cr} = 1.37$ with a sharp transmission efficiency [dotted curve in Fig. 3.3(a)]. However, for a pulse with $t_0 = 10$ fs, the IRS perturbation present in the system increases the critical switching power to $P_{cr} = 1.75$ while maintaining the transmission efficiency at nearly 99% (blue solid curve). As a result, above the critical switching power, almost all of the output energy will be shared by the first channel, with a negligible amount by the second channel (red solid curve) [see Fig. 3.3(b)]. The transmission characteristics for the 2π conventional case with IRS perturbation are also

TH-2744_166121101

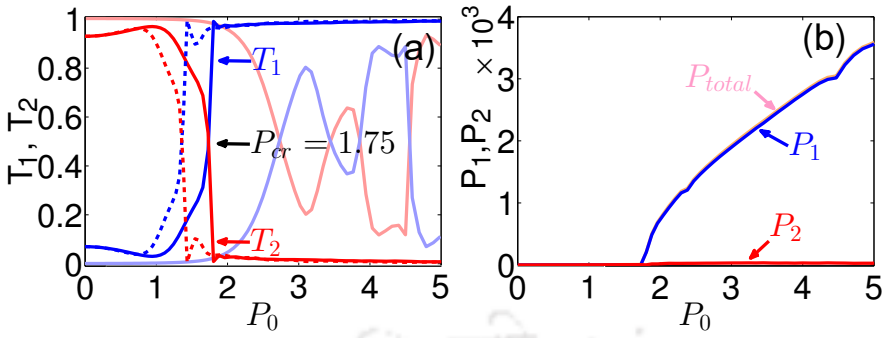

Figure 3.3: The corresponding switching dynamics of 10 fs pulse are depicted in (a) and (b) for $\kappa = 1$ and $\Gamma = 0.5$. The dashed curves in (a) illustrate the unperturbed case and light-solid lines represent the conventional coupler with the IRS.

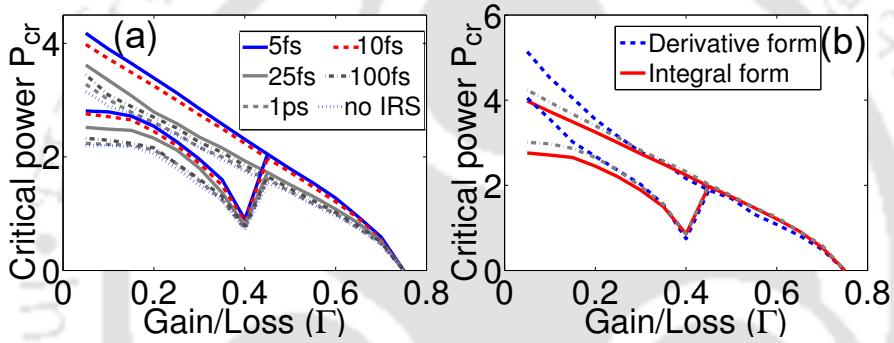

Figure 3.4: (a) Relation between the critical switching power P_{cr} with Γ as a function of t_0 and (b) relative comparison between the integral NLSE model and the derivative model for IRS perturbation with $t_0 = 10$ fs. The effect of SS on P_{cr} vs Γ is also shown in (b) by gray dot-dashed curve.

depicted in Fig. 3.3(a) by the light-solid curves for comparison, which shows significantly less efficient multiple steering of soliton switching compared to the $\mathscr{PT}$ counterpart.

Additionally, we explore the role of the input pulse width in order to demonstrate the relationship between critical switching power and the gain/loss parameter in a 2π coupler. With the increase in the pulse width from $t_0 = 5$fs to $t_0 = 1$ ps, the value of the critical switching power decreases significantly as shown in Fig. 3.4(a). For a lower value of gain/loss ($\Gamma < 0.45$), in this figure, two threshold power indicates dual steering inside the $\mathscr{PT}$-symmetric coupler. For sufficiently high gain/loss ($\Gamma > 0.7$), Fig. 3.4(a) shows ultralow critical switching power P_{cr}. From the output power plot as shown in Fig. 3.4(b), we observe that above the critical power of switching P_{cr}, the total energy exits from the first channel as the power amplification is 10^3 times more as compared to the power below the critical power.

TH-2744_166121101

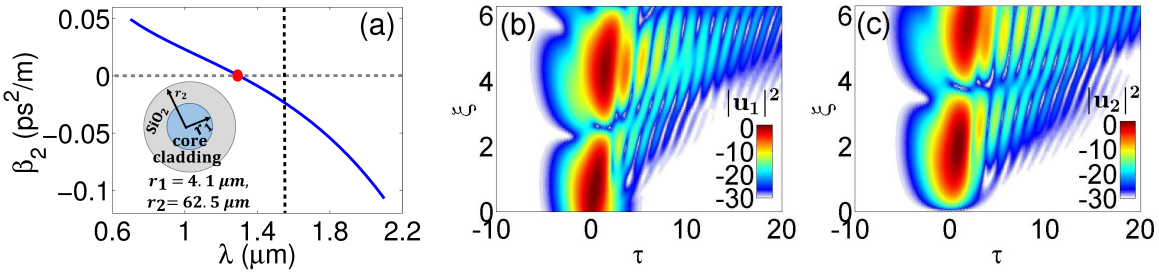

Figure 3.5: (a) GVD profile of a single-mode fiber. Here, the vertical dotted line indicates the launching wavelength, and the red-circle represents the location of the zero-GVD wavelength. The cross-sectional geometry of the fiber is also shown in the inset [72]. (b) and (c) soliton evolution in the two channels of 2π type-1 $\mathscr{PT}$-symmetric coupler under the effect of TOD for $t_0 = 5$ fs.

For further verification of how accurate this integral form of the IRS model of Eq. (3.1) with respect to the derivative form of the IRS [35], we plot the critical switching power as a function of gain/loss parameter in Fig. 3.4(b). For $\Gamma < 0.45$, it can be noticed that the integral model (red solid curves) works better for an ultrashort pulse as compared to the derivative model (blue dashed curves). However, both of these models appear to be equivalent once $\Gamma > 0.45$. The soliton switching dynamics is further modified by the influence of SS. For a 10fs pulse, we find that the critical switching power increases at lower values of Γ as illustrated by the gray dot-dashed curve in Fig. 3.3(b). However, at higher values of Γ the values of P_{cr} are same for both IRS and SS.

3.4 Impact of higher-order dispersions

In soliton propagation, HODs are of particular importance, and they could be considered as perturbations. For a given waveguide geometry, dispersion profile may vary rapidly with frequency, making HOD more pronounced. While the interplay between Kerr-nonlinearity and GVD produces stable solitonic structure in time and frequency domains, HODs lead to significant temporal and spectral distortion. More specifically, the soliton sheds energy in the form of dispersive waves (DWs) that produce isolated spectral peaks [35, 70, 71]. In this process, the temporal distribution of the soliton is affected by the generation of asymmetric (for TOD) and symmetric (for FOD) side-lobes.

Here, we consider a 2π $\mathscr{PT}$-symmetric single-mode fiber coupler whose cross-sectional geometry and the GVD profile are shown in Fig. 3.5(a). For this GVD profile, the values of the second-order GVD, TOD and FOD at the launching wavelength

TH-2744_166121101

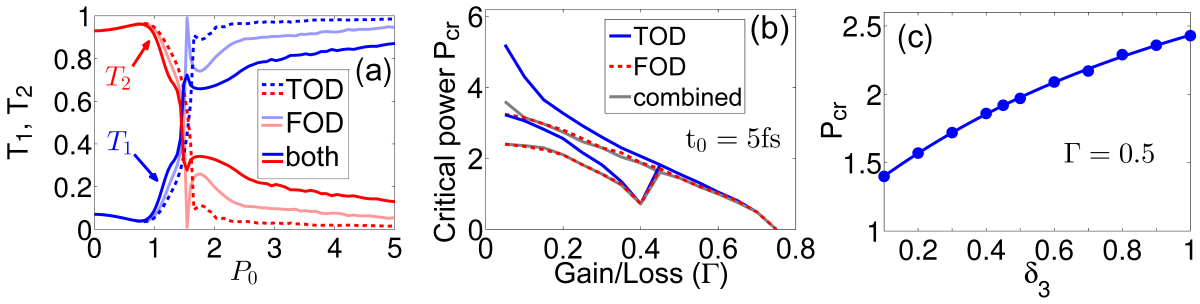

Figure 3.6: (a) Switching dynamics and (b) critical switching power P_{cr} as a function of gain/loss parameter Γ in the presence of TOD only, FOD only, and combined effects for $t_0 = 5$ fs. (c) P_cr vs TOD parameter δ_3. Here the normalized gain/loss parameter is taken as $\Gamma = 0.5$. Here, dashed lines represent unperturbed case, and solid lines represent the effect of all perturbations.

$\lambda_0 = 1.55\,\mu$m are calculated as, $\beta_2 \approx -23.391\,\text{ps}^2/\text{km}$, $\beta_3 \approx 0.13472\,\text{ps}^3/\text{km}$, and $\beta_4 \approx -4.1128 \times 10^4\,\text{ps}^4/\text{km}$, respectively. The back and forth temporal evolution of a fundamental soliton between two channels are illustrated in Figs. 3.5(b) and 3.5(c) in the presence of TOD by solving Eq. (3.1) for a 5 fs input sech pulse. In both the figures, the presence of side-wings indicates the presence of DWs. Here the HOD is dominated by the TOD term, which results in asymmetric one-sided lobes.

Moving to the switching dynamics, like IRS perturbation, the critical switching power is also modified in the presence of HOD terms. Fig. 3.6(a) shows that the critical switching power (P_{cr}) increases from that of the unperturbed case [see Fig. 3.3(a)]. It is also observed that FOD degrades the overall switching efficiency of the $\mathscr{PT}$-symmetric coupler. Next, we plot the critical switching power as a function of gain/loss coefficient in Fig. 3.6(b), where the β_3 produces the larger switching power than that of the β_4. Also, one can observe from Figs. 3.4(a) and 3.6(b) that considering a $t_0 = 5$ fs pulse, the critical switching power is significantly increased for lower gain/loss values in the presence of HOD as compared to the higher-order nonlinearity. For further verification of how the strength of δ_3 (this can be obtained for different waveguide geometry with different GVD profile or for a fixed GVD structure with varying t_0) affects the P_{cr}, we plot P_{cr} as a function of δ_3 in Fig. 3.6(c) for $\Gamma = 0.5$ and $\kappa = 1$. These figures suggest that for a fixed Γ and κ, the TOD and FOD parameters significantly affect the critical switching power and the transmission efficiency.

TH-2744_166121101

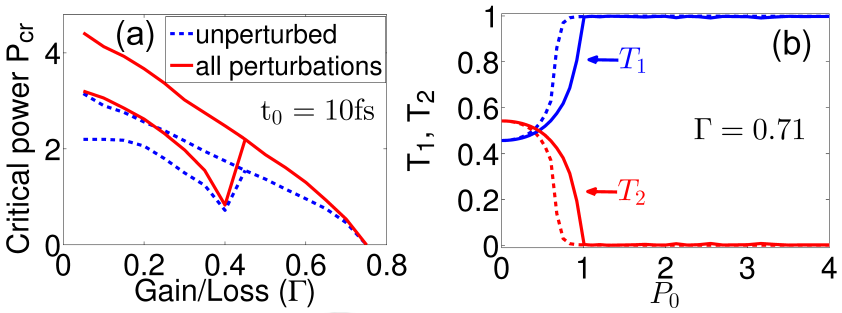

Figure 3.7: (a) P_{cr} as a function of Γ under the combined influence of higher-order nonlinearity and HOD effects. (b) Switching dynamics inside the two channels of a type-1 2π $\mathscr{PT}$-symmetric fiber coupler.

3.5 Combined effect of higher-order perturbations

So far, we have discussed in detail the individual perturbative effects of both higher-order nonlinearities and HODs on the switching dynamics of a 10 fs ultrashort pulse. Here, we analyze the combined effects of the above-stated higher-order perturbations on the switching dynamics. For this purpose, we plot the variation of critical switching power as a function of gain/loss parameter as shown in Fig. 3.7(a). It exhibits a similar trend as observed in the cases of the individual perturbations [Figs. 3.4(a) and 3.6(b)]. However, the combined effects of all the perturbations (which is the practical case for fs soliton in fibers) enhances the critical switching power for lower gain/loss value more than that of the individual perturbation. However, for higher gain/loss values, $\Gamma > 0.7$, the difference between both critical switching powers is minimum.

Next, we plot the transmission energy over a range of input pump power at $\Gamma = 0.71$ in Fig. 3.7(b). We observe that although the critical power remains the same ($P_{cr} \approx 0.38$) for both unperturbed and combined perturbations in $\mathscr{PT}$-symmetric couplers with the transmission efficiency improves considerably ($\sim 99\%$) from that of the individual perturbations. So, in the context of fs soliton steering in a $\mathscr{PT}$-symmetric fiber coupler, we can achieve very low critical power with almost full energy transfer at a relatively higher gain/loss coefficient.

To validate the fact, we plot the temporal evolution of a fundamental soliton between two channels, as shown in Figs. 3.8[(a),(b)] (without perturbations) and Figs. 3.8[(c),(d)] (combination of all perturbations). Also, we plot the same evolution for a conventional coupler considering all higher-order perturbations in Figs. 3.8[(e),(f)] for comparison. These plots demonstrate that, with a high gain/loss, the combined effects of perturbations

TH-2744_166121101

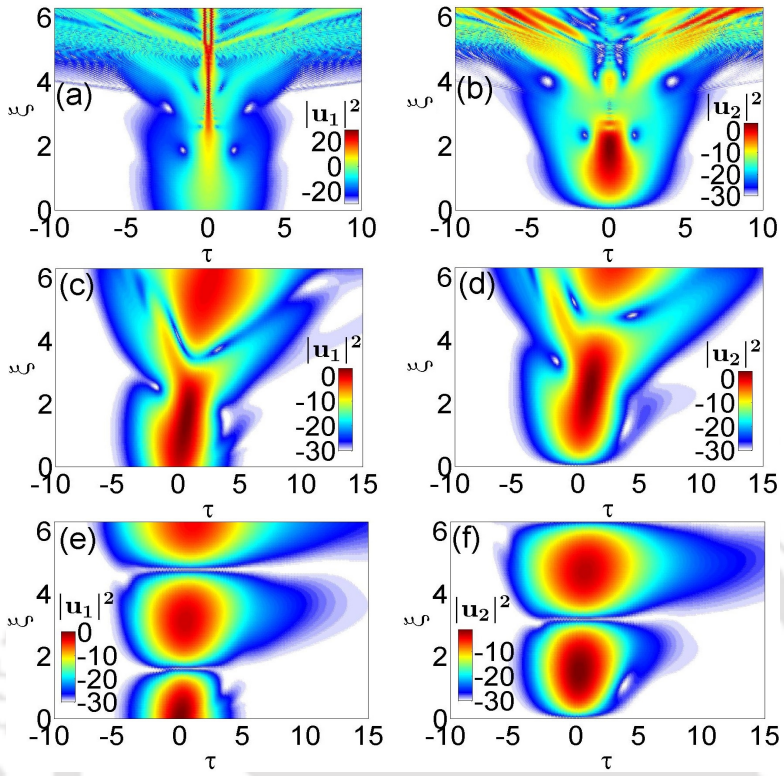

Figure 3.8: Soliton evolution in the two channels of 2π type-1 $\mathscr{PT}$-symmetric coupler without perturbations (a), (b), and with all perturbations (c), (d) for $\kappa = 1$, $\Gamma = 0.65$, and $t_0 = 10$ fs. (e), (f) Represent soliton evolution in a conventional coupler with all perturbations present for $\kappa = 1$ and $t_0 = 10$ fs.

stabilize the pulse evolution from the chaotic behavior of unperturbed evolutions. This could be attributed to the fact that IRS and HOD have opposite phenomena on spectral power (IRS tries to redshift the spectrum and HOD, in this case, tries to blueshift the spectrum in the form of DWs) that try to self-organize the power flow to have more stable pulse evolution.

3.6 Summary

In summary, we have demonstrated theoretically that while in conventional fiber coupler fs soliton steering is hard to realize as it takes higher critical pump power to switch the pulse due to various perturbative effects, in a $\mathscr{PT}$-symmetric fiber coupler, these perturbations, in particular, IRS rather assists in efficient soliton steering, in the presence of high gain/loss. This work may open up plethora of applications and studies related to ultrafast soliton steering and switching using $\mathscr{PT}$-symmetric fiber coupler in high

TH-2744_166121101

gain/loss regime.

TH-2744_166121101

TH-2744_166121101

CHAPTER 4

BISTABLE SOLITON SWITCHING IN SATURABLE NONLINEAR $\mathscr{PT}$ COUPLER

This chapter provides a comprehensive study of all-optical switching dynamics in a $\mathscr{PT}$-symmetric fiber coupler composed of a saturable nonlinear material as a core. In such a saturable nonlinear medium, bistable solitons may evolve due to the balance between dispersion and saturable nonlinearity, which we extend in the context of $\mathscr{PT}$-symmetric coupler. Our investigations of power-controlled and phase-sensitive switching show richer soliton switching dynamics than the currently existing conventional counterparts, which may lead to ultrafast and efficient all-optical switching dynamics at very low power owing to the combined effects of $\mathscr{PT}$ symmetry and saturable nonlinearity. In addition to the input power, the relative phase of the input solitons and saturable coefficient are additional controlling parameters that efficiently tailor the switching dynamics. Also, we provide a suitable range of system and pulse parameters that would be helpful for the practical realization of the coupler to use in all-optical switching devices and photonic circuits.

*The results presented in this chapter have been published in the following paper: A. Sahoo, D. K. Mahato, A. Govindarajan and A. K. Sarma, *"Bistable soliton switching dynamics in a $\mathscr{PT}$-symmetric coupler with saturable nonlinearity"*, Phys. Rev. A **105**, 063503 (2022).

TH-2744_166121101

4.1 Introduction

In the previous chapter ultrashort soliton steering dynamics in a $\mathscr{PT}$-symmetric Kerr nonlinear coupler have been discussed. For couplers with Kerr nonlinear material, the refractive index varies with the input pulse intensity as $n(I) = n_0 + n_2 I$. When used in any practical application, the nonlinear response of all materials tend to saturate at higher input intensities. For silica with low nonlinear coefficient value, the Kerr nonlinearity saturates at high input intensity. As a consequence, most of the conventional coupler made with silica with lower nonlinear coefficient n_2, also requires higher input power for switching. To overcome this hindrance in switching, non-Kerr nonlinear medium such as semiconductor doped glass and organic polymers, have been employed owing to their higher n_2 values as compared to pure silica [36] and their relatively low saturable intensities [37, 74]. These non-Kerr materials show nonlinearities getting saturated at essentially much lower input intensities which is convenient to achieve in experiments. Saturable nonlinearity (SN) is introduced, one can expect to achieve advantageous transmission characteristics over the Kerr one. In most of the practically used materials to compose a fiber coupler, the nonlinearity saturates at a certain finite value of input power. When one needs to deal with such materials, the mathematical model of NLSE needs to incorporate the saturating form of the nonlinearity rather than the very usual Kerr nonlinearity. In such a saturable nonlinear medium, usual bright solitons does not exist, instead bistable solitons may evolve due to the balance between dispersion and saturable nonlinearity, which we extend in the context of $\mathscr{PT}$-symmetric coupler. Our investigations of power-controlled and phase-sensitive switching show richer soliton switching dynamics than the currently existing conventional counterparts, which may lead to ultrafast and efficient all-optical switching dynamics at very low power owing to the combined effects of $\mathscr{PT}$ symmetry and saturable nonlinearity. In addition to the input power, the relative phase of the input solitons and saturable coefficient are additional controlling parameters that efficiently tailor the switching dynamics. Also, we provide a suitable range of system and pulse parameters that would be helpful for the practical realization of the coupler to use in all-optical switching devices and photonic circuits.

In the context of couplers, which are mostly utilized as all-optical switching devices, when nonlinearity is introduced under the effect of $\mathscr{PT}$ symmetry, several authors reported the existence of the bright, dark, gap, and Bragg solitons, as well as many other

TH-2744_166121101

interesting phenomena [19, 20, 22, 23, 24, 25, 73]. The operation of $\mathscr{PT}$-symmetric couplers, especially with the Kerr nonlinearity, showed improvement as the critical power of switching reduces drastically while maintaining high-efficiency [26]. However, a conventional coupler with Kerr nonlinear medium has a low nonlinear coefficient n_2, which requires high input power for switching. To overcome this hindrance, non-Kerr saturable nonlinear media, such as semiconductor doped glass and organic polymers, have been employed due to their higher n_2 values compared to pure silica [36] and their relatively low saturable intensities [37, 74]. Therefore, for the $\mathscr{PT}$-symmetric couplers, if SN is introduced, one can expect to achieve advantageous transmission characteristics over the Kerr one.

Now, one needs to be clear that such media do not support Kerr solitons; instead, there exist bistable solitons, which are basically two solitons having the same pulse width, but different energies and shapes [39]. The switching dynamics inside conventional saturable nonlinear couplers (SNCs) by utilizing the bistable solitons have been reported previously [40, 41, 42], which had been found to be better alternatives for all-optical switching devices [43]. Furthermore, while there have been several studies demonstrating the existence of stable fundamental soliton, gap soliton, and higher-order solitons in different $\mathscr{PT}$-symmetric potentials [44, 45, 46, 47], there has not been any study on the existence of bistable solitons inside a $\mathscr{PT}$-symmetric SNC and their switching dynamics.

Therefore, in connection with the all-optical switching devices, in this work, we concentrate on the steering dynamics in a $\mathscr{PT}$-symmetric $\pi/2$ SNC. We first obtain the exact soliton solution which can propagate through such a medium and then observe the transmission characteristics of that pulse for the $\mathscr{PT}$-symmetric coupler and solve the corresponding equation considering the device length to be half-beat length. The corresponding theoretical model has been described in Sec. 4.2, along with a discussion on the numerical finding of soliton solution, which can propagate in a saturable nonlinear medium. In Sec. 4.3, we discuss bistable solitons in the context of $\mathscr{PT}$-symmetric coupler with SN followed by its power-controlled switching dynamics in Sec. 4.4. The spatiotemporal characteristics of solitons are illustrated in Sec. 4.5. Finally, in Sec. 4.6, we discuss the phase-controlled dynamics of the solitons. The paper is concluded by Sec. 4.7.

TH-2744_166121101

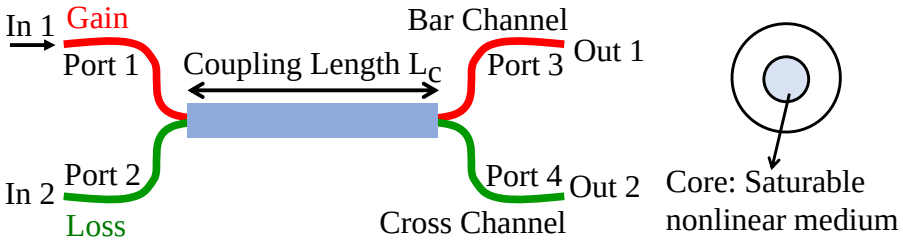

Figure 4.1: Schematic diagram of a $\mathscr{PT}$-symmetric directional fiber coupler whose core is made up of a saturable nonlinear medium.

4.2 Model and Theory

We consider a $\mathscr{PT}$-symmetric nonlinear directional coupler with SN [shown in Fig. 4.1] in which the medium's nonlinear response saturates beyond a threshold power. The optical pulse propagation in such a coupler can be modelled by a set of coupled-mode NLSEs of the slowly-varying complex-valued electric field envelops $A_1(z,t)$ and $A_2(z,t)$ in the two channels [26, 67, 75], which can be written in dimensionless form as:

$$i\frac{\partial u}{\partial \xi} + \frac{1}{2}\frac{\partial^2 u}{\partial \tau^2} + f(|u|^2)u + \kappa v = i\Gamma u, \tag{4.1a}$$

$$i\frac{\partial v}{\partial \xi} + \frac{1}{2}\frac{\partial^2 v}{\partial \tau^2} + f(|v|^2)v + \kappa u = -i\Gamma v, \tag{4.1b}$$

where $u(\xi,\tau) = A_1/\sqrt{P_0}$ and $v(\xi,\tau) = A_2/\sqrt{P_0}$, with P_0 being the peak input power; $\xi = z/L_D$ and $\tau = (t - z/v_g)/t_0$ are respectively the normalized distance and time, with $L_D = t_0^2/|\beta_2(\omega_0)|$, and t_0, v_g and β_2 are the input pulse duration, group-velocity of the pulse and the GVD parameter at the carrier frequency ω_0. The linear coupling coefficient (K) and the balanced linear gain/loss coefficient (G) are rescaled as: $\kappa = KL_D$ and $\Gamma = GL_D$. Also, in our model, we adopt the mostly used mathematical model of the saturable nonlinear response [41, 76], the dimensionless form of which is represented as

$$f(|u|^2) = \frac{|u|^2}{1 + s|u|^2}, \tag{4.2}$$

where $s = P_0/I_{sat}$ is the dimensionless refractive index saturation parameter (also known as the strength of saturation), with I_{sat} being the characteristic saturable intensity of the medium. Note that, when $s = 0$, Eqs. (4.1a) and (4.1a) reduce to the well-known Kerr nonlinearity, and when one increases s, the saturation effect of the refractive index increases accordingly. The system described by Eq. (4.2) is a $\mathscr{PT}$-symmetric system, whose operational domains are categorized into three regions: unbroken regime ($\kappa > \Gamma$),

TH-2744_166121101

broken regime ($\kappa < \Gamma$) and an EP ($\kappa = \Gamma$). In the unbroken $\mathscr{PT}$-symmetric regime, it has been observed in previous works [26, 77] that the poor transmission efficiency and unstable soliton evolution make a half-beat length ($\xi = \pi/2\kappa$) $\mathscr{PT}$-symmetric Kerr coupler an inappropriate choice as compared to one-beat length ($\xi = 2\pi/\kappa$) $\mathscr{PT}$-symmetric Kerr coupler that shows enhanced switching efficiency. In the case of a $\mathscr{PT}$-symmetric SNC, however, we consider the device to be operated in the unbroken $\mathscr{PT}$ regime with the coupler length equal to the half-beat length, which provides better switching dynamics with a lower critical power than the Kerr counterpart.

4.2.1 Soliton evolution and switching dynamics

It is well known that the coupled NLSEs described by Eqs.(4.1a) and (4.1b) are not integrable by the ISTM. Thus, in order to obtain the fundamental solutions corresponding to the coupled NLSE with saturating nonlinearity, we need to exploit numerical techniques. Considering the case of a lossless medium with $\kappa \to 0$, first we obtain two independent NLSEs representing pulse propagation in each core. Then we consider the solution of such decoupled NLSE system in the following form:

$$u_s(\xi,\tau) = [\psi(\tau)]^{1/2} e^{i\beta\xi} \tag{4.3}$$

where β is the nonlinear propagation constant shift. By substituting u_s and Eq. (4.3) in Eq. (4.1) we get,

$$\frac{1}{8}\frac{d}{d\psi}\left(\frac{d\psi}{d\tau}\frac{1}{\sqrt{\psi}}\right)^2 + \frac{\psi}{1+s\psi} - \beta = 0 \tag{4.4}$$

Here, it is to be noted that for certain values of β, one can obtain stationary pulse profile by solving this differential equation numerically. For any other arbitrary β values, there exists no stationary solutions. Now integrating the above equation, we obtain:

$$\frac{1}{8}\left(\frac{d\psi}{d\tau}\frac{1}{\sqrt{\psi}}\right)^2 + \frac{1}{s}\left[\psi - \frac{\ln(1+s\psi)}{s}\right] - \beta\psi = 0 \tag{4.5}$$

In order to get a localized bright soliton solution, we require $\frac{d\psi}{d\tau} = 0$ at the peak of the soliton where the maximum amplitude is $\psi|_{\tau=0} = \psi_0$. Using this condition we obtain the β values as,

$$\beta = \frac{1}{s}\left[1 - \frac{\ln(1+s\psi_0)}{s\psi_0}\right] \tag{4.6}$$

TH-2744_166121101

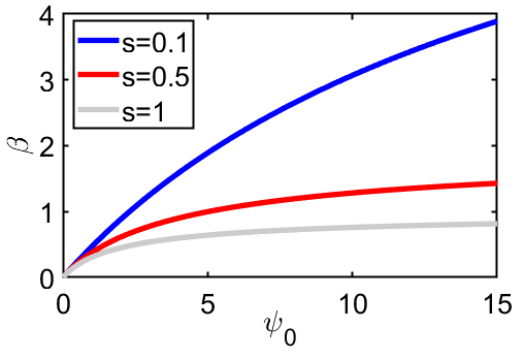

Figure 4.2: Variation of β with ψ_0 for different s value.

Substituting Eq.(4.6) into Eq.(4.5), we obtain the following differential equation:

$$\frac{d\psi}{d\tau} = -2\sqrt{(2)}\frac{\psi}{s}\left[\frac{\ln(1+s\psi)}{\psi} - \frac{\ln(1+s\psi_0)}{\psi_0}\right]^{1/2} \tag{4.7}$$

Thereafter, for a given value of ψ_0 and s, the solution of the differential Eq. (4.7) can be obtained numerically by the most widely used SSFM. We have shown the variation of β with ψ_0 for three different values of s parameter in Fig. 4.2. It shows that for higher value of s, the shifting of the propagation constant saturates over a wide range of input peak power. In our work, we have considered $s = 1$, i.e., the input pulse has been launched at the saturating power at which the nonlinear response of the medium saturates. Also, the bright soliton solution corresponding to Eq.(4.7) for saturable nonlinear medium depicted by the F-model has been illustrated in Fig. [4.3(a)].

We then consider this soliton solution as the seed solution and solve the set of Eqs. (4.1a) and (4.1b) numerically by applying the symmetrized split-step Fourier method complemented with the fourth-order Runge-Kutta algorithm. Next, to investigate the switching dynamics, we calculate the transmission coefficient T_j, which represents the fractional output power in the j-th channel after propagation of critical coupling length L_c being equal to the half-beat length of the coupler as:

$$T_j = \frac{\int_{-\infty}^{\infty}|u(L_c,\tau)|^2 d\tau}{\int_{-\infty}^{\infty}(|u(L_c,\tau)|^2 + |v(L_c,\tau)|^2)d\tau} = \frac{P_j}{P_1+P_2}, \tag{4.8}$$

where $P_1 = \int_{-\infty}^{\infty}|u(L_c,\tau)|^2 d\tau$ and $P_2 = \int_{-\infty}^{\infty}|v(L_c,\tau)|^2 d\tau$ are the output powers of the transmitted pulse in the output ports of the two channels. In order to investigate the switching dynamics, we plot the transmission coefficient T_1 [evaluating Eq.(4.4)] in the first channel of a conventional (blue dashed curve) and a $\mathscr{PT}$-symmetric (red solid curve)

TH-2744_166121101

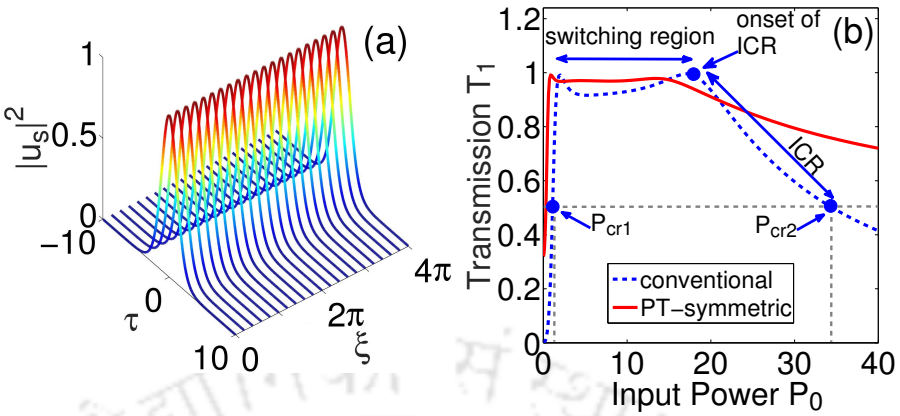

Figure 4.3: (a) Soliton solution inside a saturable nonlinear medium, obtained for $s = 1$ considering the single NLSE. (b) Transmission in the first channel of the conventional ($\Gamma = 0$) and $\mathscr{PT}$-symmetric $\pi/2$ ($\Gamma = 0.06$) SNCs with $\kappa = 0.1$ and $s = 1$, where different operational regions are identified.

SNCs for coupling coefficient $\kappa = 0.1$ and coupling length $L_c = \pi/2\kappa = 5\pi$ in Fig. 4.3(b). The various regions of operation for all-optical switching for the conventional coupler are illustrated in the same figure, which can also be translated to the $\mathscr{PT}$-symmetric one. Here, the switching curve shows four basic regimes: the coupling region (below the lower-branch critical power P_{cr1}); the switching region [between P_{cr1} and the onset of the intermediate coupling region (ICR)]; the ICR; and another coupling region above the higher-branch critical power P_{cr2}, after which the power remains in the second channel for any further increase in the input power P_0. Thus, for efficient switching, one must concentrate solely on the range of input power corresponding to the switching region. Furthermore, we find that the higher branch of critical power P_{cr2} appears to be too high to be useful for any optical switching. Therefore, we focus on the lower-branch critical power P_{cr1} and term it as P_{cr} for the rest of our work in order to operate the SNC as an efficient all-optical switching device. Now, with the introduction of balanced gain/loss, the critical power P_{cr} is reduced considerably, and both the switching steepness and transmission efficiency are enhanced. For further investigation of how the gain/loss parameter Γ affects the switching dynamics, we plot the P_{cr} as a function of Γ for specific values of $\kappa = 0.1$ and $s = 1$ in Fig. 4.4(a). This plot indicates that when Γ approaches the singularity (i.e., $\Gamma = \kappa = 0.1$ in this particular case), no switching occurs, implying that regardless of the input power, all of the power remains in the launching channel. The corresponding transmission is shown in Fig. 4.4(b) for four different values of

TH-2744_166121101

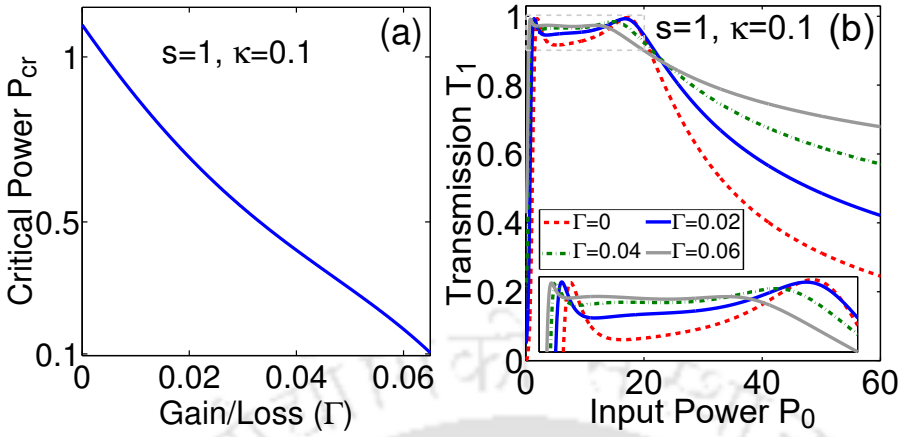

Figure 4.4: (a) Relation between critical power P_{cr} and gain/loss parameter Γ. (b) Effect of gain/loss on the switching dynamics of both conventional ($\Gamma = 0$) and $\mathscr{PT}$-symmetric ($\Gamma \neq 0$) SNCs.

$\Gamma = 0$, 0.02, 0.04, and 0.06. As we gradually increase Γ from 0 to 0.06, we observe a lower critical power with better transmission efficiency [see inset of Fig. 4.4(b)]. Hence, based on these results, we fix the gain/loss value of the $\mathscr{PT}$-symmetric SNC to be $\Gamma = 0.05$ for further investigations on the switching dynamics.

4.3 Bistable Soliton dynamics in $\mathscr{PT}$-symmetric saturable coupler

Before going deeper into the details of soliton switching dynamics in $\mathscr{PT}$-symmetric SNCs, we first investigate the properties of bistable solitons and their dynamics, which occur inherently in saturable nonlinear systems. Previous researches have looked into the fundamental properties of bistable solitons in saturable nonlinear media, where there exist two solitons with the same pulse width but different shapes and energies [39, 41]. In our work, it is interesting to investigate how the seed soliton [Eq. (4.3)], which is inherently bistable in nature for a specific range of ansatz parameters, evolves in the couplers and retain their properties as well as individual switching characteristics. To investigate the properties of bistable solitons, we first define the dimensionless soliton energy ε as

$$\varepsilon = \int_{-\infty}^{\infty} |u(\tau)|^2 d\tau. \tag{4.9}$$

TH-2744_166121101

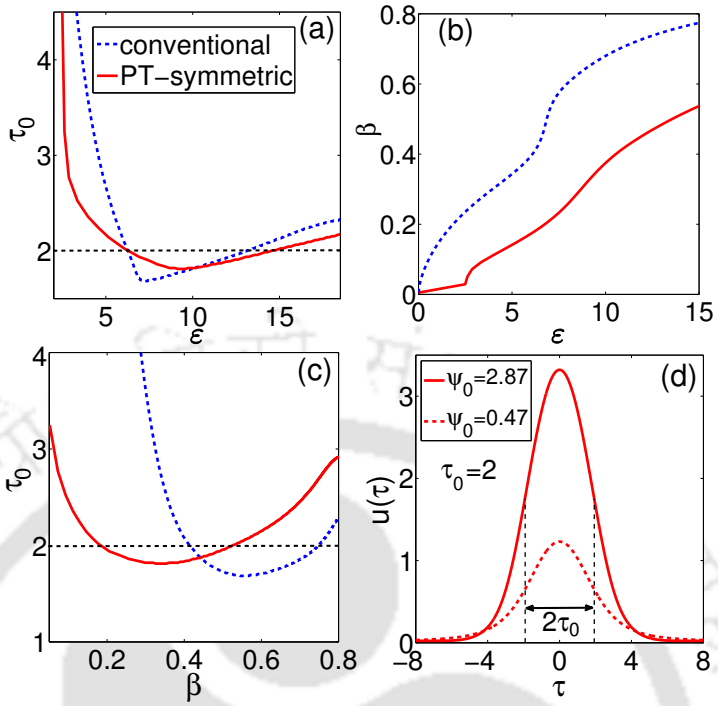

Figure 4.5: Variation of output pulse energy ε of the coupler as a function of (a) output pulse width τ_0 and (b) propagation constant shift β of the input seed soliton [Eq.(4.3)]. (c) The variation of τ_0 as a function of β. Solid red curves in (a-c) represent the case with $\mathscr{PT}$ symmetry, whereas dashed blue curves represent the conventional one. (d) Amplitude $u(\tau)$ of the bistable solitons at the output of the $\mathscr{PT}$-symmetric SNC corresponding to $\tau_0 = 2$ for two energies $\varepsilon = 6.22$ and $\varepsilon = 14.65$, respectively. The horizontal dashed lines in (a), (c), and vertical dashed lines in (d) indicate that $\tau_0 = 2$.

Next, for a given value of soliton peak amplitude $\psi(\tau = 0) = \psi_0$, we compute the output pulse width τ_0 and the propagation constant shift β [presented in Eq.(4.3)]. In Fig. 4.5(a), we plot the variation of pulse energy ε [Eq.(4.9)] at the first output port of the $\pi/2$ coupler as a function of the output pulse width τ_0 by varying the peak amplitude ψ_0 of input seed soliton. Similarly, we plot the variation of ε as a function of β [see Fig. 4.5(b)] and the τ_0 vs β [see Fig. 4.5(c)] for the system parameters $\kappa = 0.1$, $\Gamma = 0.05$, and $s = 1$. The bistability nature is clearly evident in both the conventional (dashed blue curves) and $\mathscr{PT}$-symmetric (solid red curves) SNCs [there exist two values of ε and β at the same $\tau_0 = 2$, as shown by the horizontal dashed line in Figs. 4.5(a) and 4.5(c)]. Furthermore, these plots indicate that the addition of a $\mathscr{PT}$-symmetric potential modifies the parameter space of the soliton in comparison to the conventional SNC. The bistable solitons inside the $\mathscr{PT}$-symmetric SNC with two different energies $\varepsilon = 6.22$

TH-2744_166121101

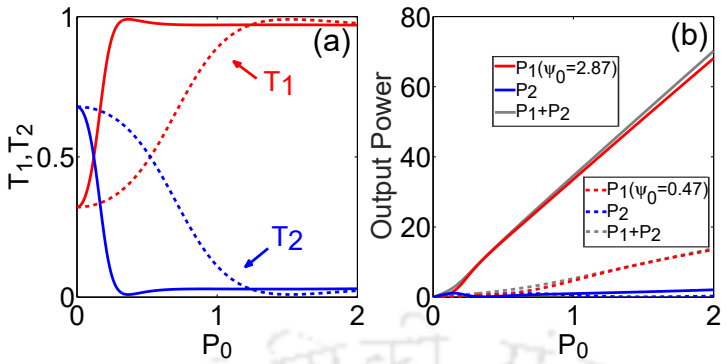

Figure 4.6: (a),(b) Switching dynamics of bistable solitons in the $\mathscr{PT}$-symmetric SNC corresponding to the pulse width $\tau_0 = 2$ and two input peak amplitude $\psi_0 = 0.47$ (dashed curves) and $\psi_0 = 2.87$ (solid curves).

and $\varepsilon = 14.65$ corresponding to the pulse width $\tau_0 = 2$ are shown in Fig. 4.5(d). Here, the higher amplitude soliton (solid red curve) corresponds to the higher input peak amplitude $\psi_0 = 2.87$, while the lower amplitude soliton (dashed red curve) corresponds to the lower input peak amplitude $\psi_0 = 0.47$. Thus, by examining Figs. 4.5(a)-4.5(d), we can conclude that the bistable solitons exist in the unbroken regime of a $\pi/2$ $\mathscr{PT}$-symmetric SNC in the weak coupling regime.

Next, the switching dynamics of the individual bistable solitons obtained in Fig. 4.5(d) are investigated in Figs. 4.6(a) and 4.6(b). Here, we observe two independent steering dynamics for two solitons depending on the soliton amplitude. The critical power of switching corresponding to the pulse with $\psi_0 = 2.87$ is lower than that of the pulse with $\psi_0 = 0.47$. This is because the nonlinear response of the medium becomes saturated earlier in the case of pulse with high input peak amplitude, causing the switching to occur faster than in the case of pulse with low input peak amplitude. In the following sections, our investigations mainly focus on the switching dynamics of a single soliton case for a given pulse width, which have applications in all-optical switching devices and photonic circuits.

4.4 Power-controlled switching dynamics

To discuss the power-controlled switching dynamics, we assume that in the presence of coupling coefficient ($\kappa \neq 0$), the soliton is always launched into the input port (port 1) of

TH-2744_166121101

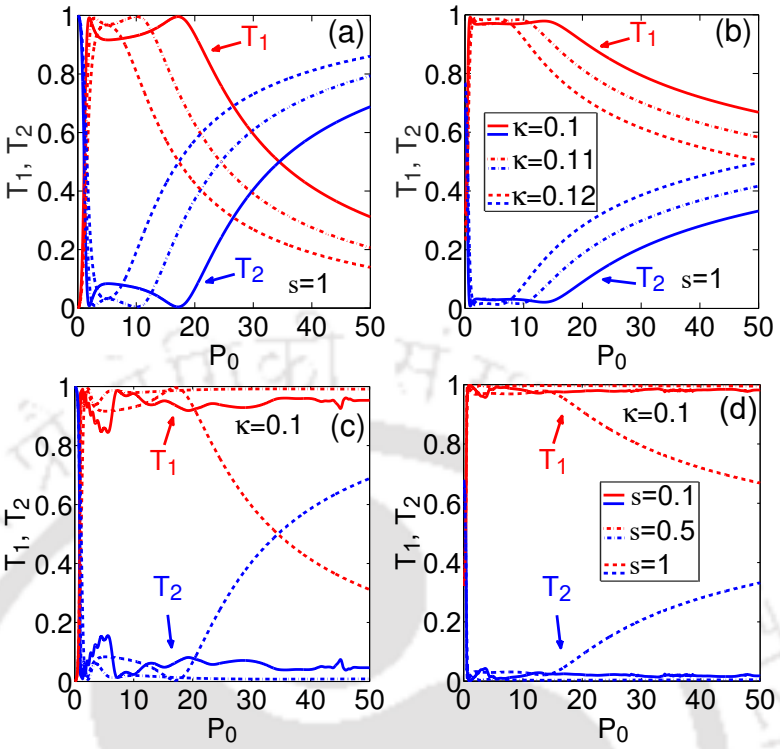

Figure 4.7: Switching dynamics of (a) conventional and (b) $\mathscr{PT}$-symmetric ($\Gamma = 0.05$) SNCs for different κ with fixed $s = 1$. (c) and (d) represent the same for different s with fixed $\kappa = 0.1$.

the first channel, and the second channel is kept empty so that

$$u(\xi = 0, \tau) = u_s(\xi = 0, \tau)v(\xi = 0, \tau) = 0. \tag{4.10}$$

With the initial conditions above in Eq.(4.10), we discuss the effect of coupling coefficient κ on the switching dynamics for a conventional ($\Gamma = 0$) and a $\mathscr{PT}$-symmetric ($\Gamma = 0.05$) SNCs by setting the saturation to be maximum, $s = 1$, shown in Figs. 4.7(a) and 4.7(b). For both the SNCs, the lower value of κ shows lower critical power and better transmission efficiency across a wider input power range.

Next, we study the role of the strength of SN, s for the same two couplers in the weaker coupling regime by setting $\kappa = 0.1$, shown in Figs. 4.7(c) and 4.7(d). In both the conventional and the $\mathscr{PT}$-symmetric SNCs, we observe a Kerr coupler-like behavior for lower saturation strengths, $s = 0.1$ and $s = 0.5$. In contrast, the typical effect of SN in the high input power domain is observed once the couplers are operated with maximum saturation $s = 1$. In Table I, we provide a list of the normalized values of critical powers for the two types of SNCs, showing the variations of κ and s. We observe that, when the strength of SN increases gradually, unlike a conventional SNC, the critical power

TH-2744_166121101

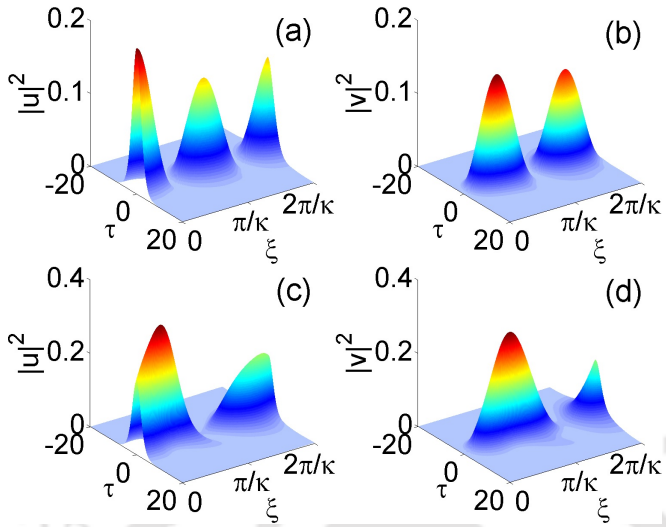

Figure 4.8: Spatiotemporal evolution of solitons in (a),(b) conventional SNC ($\Gamma = 0$), and (c),(d) $\mathscr{PT}$-symmetric SNC ($\Gamma = 0.05$) with input power $P_0 = 0.2$. The system parameters are taken to be: $\kappa = 0.1$ and $s = 1$.

Table 4.1: Normalized values of critical power P_{cr} for different strength of saturation and coupling coefficients.

Fixed parameter	Varying parameter	$P_{cr,conventional}$ ($\Gamma = 0$)	$P_{cr,\mathscr{PT}}$ ($\Gamma = 0.05$)
	$\kappa = 0.1$	1.10	0.30
$s = 1$	$\kappa = 0.11$	1.30	0.38
	$\kappa = 0.12$	1.59	0.47
	$s = 0.1$	0.82	0.37
$\kappa = 0.1$	$s = 0.5$	0.86	0.32
	$s = 1$	1.10	0.30

of switching tends to decrease for a $\mathscr{PT}$-symmetric one. Thus, based on the values of critical powers P_{cr} given in Table 4.1, we can conclude that for weaker coupling region ($\kappa = 0.1$) and maximum saturation strength ($s = 1$), a $\mathscr{PT}$-symmetric coupler is more efficient as compared to the conventional one.

TH-2744_166121101

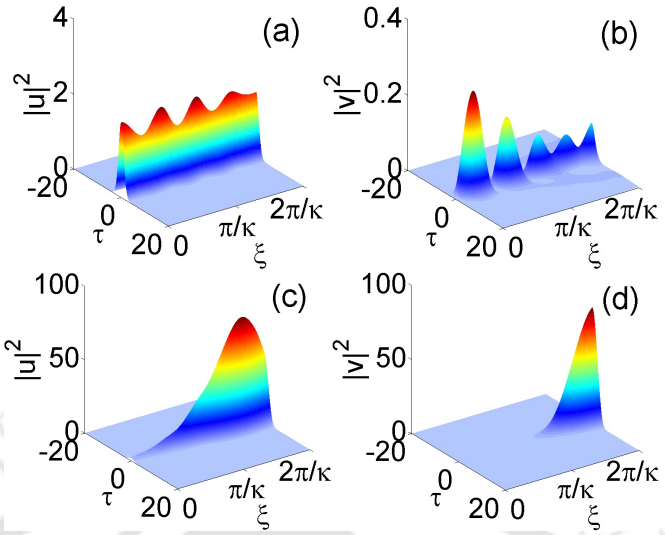

Figure 4.9: Spatiotemporal evolution of solitons in (a),(b) conventional SNC, and (c),(d) $\mathscr{PT}$-symmetric SNC with input power $P_0 = 2$. All the other parameters are the same as in Fig. 4.8.

4.5 Spatiotemporal Soliton Dynamics

In this section, we illustrate the spatiotemporal evolution dynamics of a soliton inside the two cores of the two SNCs. In Figs. 4.8(a)-4.8(d), with the previously chosen values of $\kappa = 0.1$, $s = 1$ and $\Gamma = 0.05$, we plot the corresponding evolution dynamics inside the couplers in the linear regime where the input power is chosen to be $P_0 = 0.2$, lower than the critical power $P_{cr} = 0.3$. One can predict these evolution trends inside the conventional and $\mathscr{PT}$-symmetric SNCs by following the switching curves in Fig. 4.3(b). In this linear regime, the soliton couples back and forth inside the two channels and eventually exists from the output port of the first channel. On the other hand, if a soliton is launched in the nonlinear regime, where the input power is set to be $P_0 = 2$, higher than P_{cr}, we observe that the soliton switches back to the launching core and remains in there in the case of a conventional SNC [see Figs. 4.9(a) and 4.9(b)]. However, for the case of a $\mathscr{PT}$-symmetric SNC, we observe that the soliton power comes out of the second channel as shown in Figs. 4.9(c) and 4.9(d)]. Thus, with the inclusion of gain/loss in the SNC, the nonlinear switching takes a different route than the conventional one.

TH-2744_166121101

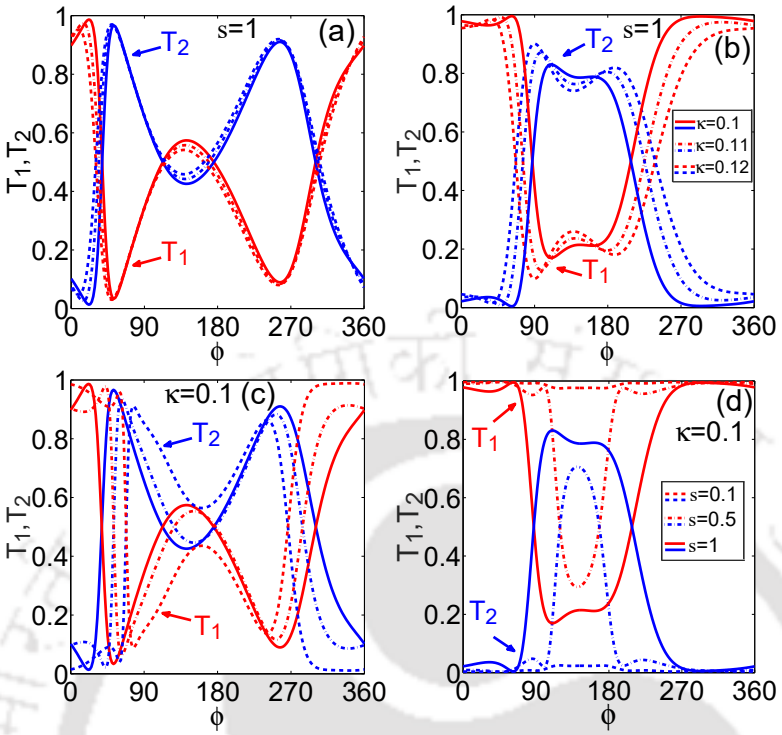

Figure 4.10: Phase-controlled switching dynamics of (a) conventional and (b) $\mathscr{PT}$-symmetric ($\Gamma = 0.05$) SNCs for different κ with fixed $s = 1$. (c), (d) represent the same for different s with fixed $\kappa = 0.1$.

4.6 Switching dynamics by controlling the relative phase

In addition to the power-controlled switching, for the completeness of the study, we investigate phase-sensitive switching dynamics as another type of all-optical switching device in this section. The basic idea of a phase-sensitive switching is that by adjusting the input power and the relative phase of a weaker pulse in the second channel, one can control the steering dynamics of the stronger pulse which is launched into the first channel [78, 79]. Therefore, we consider two soliton pulses launched into the input ports (port 1 and port 2) of the two channels as

$$u(\xi = 0, \tau) = u_s, \quad \text{and,} \quad v(\xi = 0, \tau) = \frac{u_s}{\sqrt{r}} e^{i\phi}, \tag{4.11}$$

where r is the power ratio factor and ϕ is the relative phase between the two soliton pulses. For a typical value $r = 4$, and considering Eq. (4.11) as inputs, we show the effect of coupling coefficient for both conventional and $\mathscr{PT}$-symmetric SNCs considering the

TH-2744_166121101

same set of κ as discussed in the power-controlled case. The $\mathscr{PT}$-symmetric SNC displays considerably better sharp phase-sensitive switching as compared to the conventional one, with more than 90% transmittance over certain ranges of ϕ [see Figs. 4.10(a) and 4.10(b)]. We observe that the lower the coupling coefficient, the higher the transmission efficiency for a certain range of ϕ. We also plot the effect of the strength of SN on the phase-controlled switching dynamics while considering the previous set of s values as in the power-controlled case. Here, we observe that for the conventional SNC, the lower s value ($s = 0.1$) displays higher transmission efficiency over certain range of ϕ [see Fig. 4.10(c)]. Whereas in the $\mathscr{PT}$-symmetric SNC, for the lower strength of saturation, the transmittance in the first channel is more than 97% for any ϕ value [dashed red curve Fig. 4.10(d)]. Thus, by controlling the phase of the weaker pulse, we can steer the stronger pulse to come out from the desired channel. By observing these results, we can conclude again that a $\mathscr{PT}$-symmetric SNC is better than a conventional SNC to be used as a phase-controlled switching device as well.

4.7 Summary

To conclude, we have investigated the steering and switching dynamics of bistable solitons in a $\mathscr{PT}$-symmetric coupler with saturable nonlinearity. One of the objectives of the work was to investigate if the scheme of optical $\mathscr{PT}$ symmetry enhances the transmission characteristics of the saturable coupler compared to the one with Kerr nonlinearity as well as the conventional counterparts. We find the answer is affirmative. The soliton is found to be stable while propagating through the coupler. It turns out that both the power and the phase-controlled mode of switching works well in the $\mathscr{PT}$-symmetric saturable nonlinear coupler. It is anticipated that owing to the huge reduction in the peak power and rich transmission characteristics, the proposed $\mathscr{PT}$-symmetric coupler with saturation nonlinearity would be of great utility for many signal processing applications. Apart from that, there could be a resurgence of research works in this area considering the promising results reported in this work.

TH-2744_166121101

TH-2744_166121101

CHAPTER 5

DARK SOLITON STEERING IN KERR $\mathscr{PT}$ COUPLER WITH DISPERSIVE PERTURBATION

In this chapter, we study steering dynamics of dark soliton in a $\mathscr{PT}$-symmetric NLDC in the presence of TOD and intermodal dispersion (IMD). A complete switch with an excellent efficiency at a very low critical power, even lower as compared to the bright soliton switching has been observed. The numerical results show that both TOD and IMD have no effect on soliton steering in $\mathscr{PT}$-symmetric couplers with coupling length $\pi/2$. But as we increase the coupling length to 2π, IMD shows marginal effects for dark soliton steering in $\mathscr{PT}$-symmetric couplers while TOD shows no impact. Additionally, we have also studied the phase-controlled switching in $\mathscr{PT}$ couplers with two different coupling lengths and demonstrated its advantage over the power-controlled one.

5.1 Introduction

In the context of all-optical switching, the nonlinear effects of conventional directional coupler have been exploited utilizing mostly its power-dependent switching [80] and the phase-dependent switching characteristics [78, 79, 81, 82]. In previous chapters, we

*The results of this chapter have been published in the following paper: D. K. Mahato, A. Govindarajan and A. K. Sarma, *"Dark soliton steering in $\mathscr{PT}$-symmetric couplers with third-order and intermodal dispersions"*, J. Opt. Soc. Am. B **37**, 3443-3452 (2020).

TH-2744_166121101

discussed and mentioned that, in power-dependent switching, when low power CW is launched in a NLDC, the two cores periodically exchange power due to the evanescent coupling, and eventually the pulse stays in the cross channel. On the other hand, for high power CW, the total power remains in the launching core due to the intensity induced phase mismatch. A detailed report on NLDC with different gain and loss distributions has revealed that the critical power for CW switching decreases as equal amount of gain and loss are introduced to the system [83]. However, as CW and pulse tend to break during nonlinear switching, soliton switching was introduced as another possible choice to enhance NLDC operation [33, 84, 85, 86]. It was found that the advantages of soliton switching are mainly the stable propagation without pulse breaking and the peak-power dependent switching characteristic which enables complete switching from one core to another within a coupling length. The soliton switching with conventional coupler has been studied quite extensively in the past, since mid-eighties. However research in this area was primarily dominated by theoretical exploration. In fact the whole research area was put in dormant due to the lack of experimental progress. This happened due to the requirement of extremely high critical power of switching, say, the order of 10 kW or more [67]. Fortunately, the introduction of the idea of $\mathscr{PT}$ symmetry and its subsequent experimental validation brought new hopes. Very recently, it has been observed that the requirement of high critical power for bright soliton switching reduces remarkably [26] by introducing $\mathscr{PT}$ symmetry through the combination of equal amount of gain and loss in the two waveguides of an NLDC. In passing it should be noted that, while soliton switching in $\mathscr{PT}$-symmetric couplers has been explored just recently, stability solitons in such systems have already been studied by Malomed and his collaborators [20, 28, 29].

However, it is well known that as compared to the bright solitons, dark solitons are more stable in the presence of noise, they travel almost undisturbed in presence of different perturbative effects inside an NLDC [87]. Also, for an all-optical switching device with lower critical power and shorter device length, the input soliton is required to be ultrashort pulse. This requirement of ultrashort pulse consequently necessitates the inclusion of TOD, in particular, when the pulse is operated near the zero dispersion regime [88]. In general, the effect of TOD in an optical fiber is to tend the intensity profile of a pulse asymmetric with an oscillatory tail near one of its edges [88]. Further, an NLDC, made of two fibers coupled together or a fiber with dual core, acts as a bimodal device which supports a linear combination of symmetric and antisymmetric modes,

TH-2744_166121101

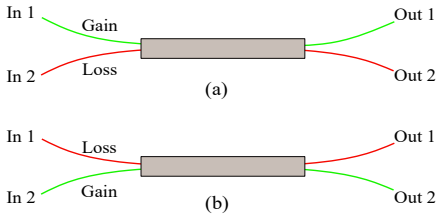

Figure 5.1: Schematic illustrations of two different configurations of $\mathscr{PT}$-symmetric coupler: (a) Type-1 and (b) Type-2 $\mathscr{PT}$-symmetric coupler.

each with different propagation constants. When optical power is launched into one of the two cores, both the modes inside NLDC are equally excited. Thus, different group delay between these two modes during propagation along the coupler length leads to a phenomenon called the IMD. In the coupled mode theory, this group delay between the modes is analogous to the coupling-coefficient dispersion. Previously it has been reported that both TOD and IMD have no effect on dark soliton [87, 90, 91] but they have considerable influence on bright soliton propagation inside a conventional coupler [92, 93, 94, 95, 96, 97]. Recently a new kind of dark soliton has been introduced in a dual-core coupler [98] in the presence of such dispersive coupling. Also, it needs to be mentioned here that an optical system combined with IMD is known to be invariant under $\mathscr{CPT}$ symmetry, where $\mathscr{C}$ symbolizes transverse spatial inversion related to the swapping of the two waveguides inside a coupler [99, 100, 101, 102].

In this work, intrigued by the steady nature of the dark soliton, the steering dynamics of dark soliton in $\mathscr{PT}$-symmetric couplers has been explored.

5.2 Theoretical Model

In general, soliton propagation inside an NLDC can be represented by a pair of coupled NLSEs. Thus, the soliton dynamics inside a $\mathscr{PT}$-symmetric coupler with balanced gain and loss can be expressed mathematically as [26]:

$$i\frac{\partial\Psi_1}{\partial\xi}-\frac{1}{2}\frac{\partial^2\Psi_1}{\partial\tau^2}-i\delta_3\frac{\partial^3\Psi_1}{\partial\tau^3}+|\Psi_1|^2\Psi_1+\kappa\Psi_2+i\kappa_1\frac{\partial\Psi_2}{\partial\tau}=i\Gamma\Psi_1 \tag{5.1}$$

$$i\frac{\partial\Psi_2}{\partial\xi}-\frac{1}{2}\frac{\partial^2\Psi_2}{\partial\tau^2}-i\delta_3\frac{\partial^3\Psi_2}{\partial\tau^3}+|\Psi_2|^2\Psi_2+\kappa\Psi_1+i\kappa_1\frac{\partial\Psi_1}{\partial\tau}=-i\Gamma\Psi_2 \tag{5.2}$$

where, ψ_1 and ψ_2 denote the slowly varying complex-valued envelopes in the bar (core 1) and the cross channel (core 2) of the $\mathscr{PT}$-symmetric coupler. The second and the third

TH-2744_166121101

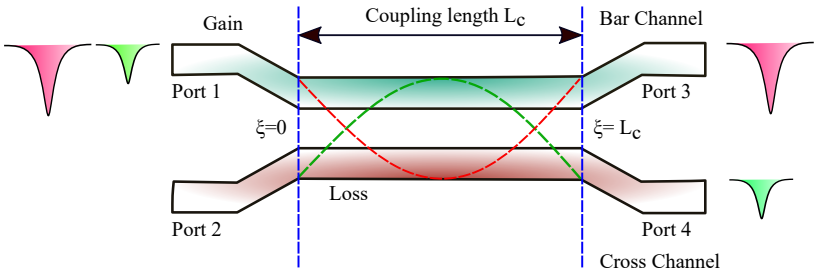

Figure 5.2: Schematic diagram portraying steering dynamics of dark solitons inside $\mathscr{PT}$-symmetric couplers.

term of Eqs. (5.1) and (5.2) represent the GVD and the TOD, respectively. The fourth term is the SPM term, where its coefficient is scaled to be one. κ , κ_1, δ_3 are, respectively, the normalized linear coupling coefficient, IMD and TOD. Also, Γ represents balanced gain (Γ>0) and loss (Γ<0) inside two channels making the system to be $\mathscr{PT}$-symmetric. It should be noted that the considered model is not applicable to coupler made of non-Kerr media such as organic, photorefractive and semiconductor materials. Again, the waveguides consisting of the coupler are assumed to be single-moded. If one has to consider coupler with multimoded waveguides, a different model needs to be considered. In fact, this is a new and emerging field of research. However, in the current work we are primarily concerned with silica-based optical fiber or coupler made with materials exhibiting Kerr nonlinearity.

In the following, we illustrate the effect of inclusion of gain and loss by two different configurations. When Γ>0 in Eqs.(5.1) and (5.2), the system is termed as type-1 $\mathscr{PT}$-symmetric coupler, having gain in the first waveguide and loss in the second Fig. 5.1(a). The other structure is termed as type-2 $\mathscr{PT}$-symmetric coupler with Γ<0 in the coupled equations, having loss in the first waveguide and gain in the second Fig. 5.1(b). These two configurations bearing the same notion of $\mathscr{PT}$ symmetry are introduced in order to highlight which model among these two (gain/loss and loss/gain) exhibits rich steering dynamics, as transmission property may differ since gain and loss have been swapped inside the waveguides [26]. It is worthwhile to stress again that the first observation of $\mathscr{PT}$ symmetry in optics was accomplished via a judicious design of a coupled waveguide which involved two-wave mixing process in order to provide gain and doping of transition metal ions to provide loss [6]. It could be possible to adopt the similar scheme to realize the present model for fiber coupler. Specifically, at 1550 nm, the gain can be provided by doping rare earth element like erbium in one channel and the loss by another dopant in

TH-2744_166121101

the second channel which shows absorption in the same wavelength regime. But as we are dealing with the dark soliton, a dispersion-shifted fiber or a dispersion-compensated fiber having normal dispersion at 1550 nm can be optically pumped and utilized as the gain channel.

As the NLDC can serve a potential candidate for all-optical switching, we mainly aim our attention to power-controlled steering dynamics of dark soliton inside $\mathscr{PT}$-symmetric couplers following with the phase-controlled one. In general, any $\mathscr{PT}$-symmetric system exhibits two parametric regions, a region of unbroken $\mathscr{PT}$ symmetry where all eigenvalues are real and a region of broken symmetry where some of the eigenvalues are real and the rest are complex. Following the notion, $\mathscr{PT}$-symmetric couplers are said to be operating in unbroken $\mathscr{PT}$-symmetric regime when κ>Γ and in broken $\mathscr{PT}$-symmetric regime when κ<Γ [6]. If the value of coupling coefficient equals to the value of gain/loss parameter, i.e., κ=Γ, the system is in singularity condition. In this paper, we limit our system to work in the unbroken $\mathscr{PT}$-symmetric regime (κ>Γ) and scale the linear coupling coefficient κ and the gain/loss parameter, Γ, to be 1 and 0.5, respectively. As shown in Fig. 5.2, we also assume that the second waveguide has been kept empty ($\Psi_2(\xi=0,\tau)=0$) and the input soliton pulse is always launched at port 1 of first waveguide, i.e.,

$$\Psi_1(\xi=0,\tau)=q\ \tanh(q\tau) \tag{5.3}$$

where, $q^2=P_0$ represents the input peak power, depending on which the dark soliton switches to any of the two output ports. To illustrate the effects of TOD and IMD on the dark soliton propagation in $\mathscr{PT}$-symmetric couplers, Eqs.(5.1) and (5.2) are then numerically solved by the split-step Fourier method [90]. Here we calculate the fractional output power in the j-th core ($j=1,2$) by the transmission coefficient which is represented as,

$$T_j=\frac{\int_{\infty}^{\infty}|\Psi_j(L_c,\tau)|^2d\tau}{\int_{-\infty}^{\infty}(|\Psi_1(L_c,\tau)|^2+|\Psi_2(L_c,\tau)|^2)d\tau}=\frac{P_j}{P_1+P_2} \tag{5.4}$$

where, $P_1=\int_{-\infty}^{\infty}|\Psi_1(L_c,\tau)|^2d\tau$ and $P_2=\int_{-\infty}^{\infty}|\Psi_2(L_c,\tau)|^2d\tau$ are the output powers of the transmitted pulse in the ports 3 and 4 of the coupler. The parameter L_c refers to the total coupling length of the system.

TH-2744_166121101

5.3 Results and Discussions

In this section, dark soliton steering dynamics in the above two configurations of a $\mathscr{PT}$-symmetric coupler having one-beat coupling length, defined as $L_c = 2\pi$ with $\kappa = 1$, are demonstrated. To understand the steering dynamics of dark soliton in $\mathscr{PT}$-symmetric couplers, we first consider the case of a conventional NLDC with coupling length 2π as illustrated in Fig. 5.3(a). It can be seen that the switching dynamics of the dark soliton inside conventional coupler exhibit periodic steering which consumes significant amount of pump power in order to achieve unit transmission efficiency. Now, to study the effect of equal amount of gain and loss in the two channels, the input pulse with peak power P_0 is launched at port 1 and the outputs are measured at ports 3 and 4. From Fig. 5.3(c), it can be clearly seen that the critical power gets reduced to $P_{cr} = 1.25$ with an excellent transmission efficiency for a type-1 $\mathscr{PT}$-symmetric coupler as compared to the unwanted oscillation in the conventional one [see Fig. 5.3(a)]. Here, the steering dynamic shown in Fig. 5.3(d) reveals that above the critical power, the total energy is completely transferred to the bar channel unlike the conventional coupler where the sharing of power is observed to be oscillating in between the cores [see Fig.5.3(b)].

For the alternative configuration of $\mathscr{PT}$-symmetric coupler, as it has been illustrated in Fig. 5.3(e), the switching power gets reduced to a much lower value as, $P_{cr} = 0.7$ when compared to the type-1 coupler. In the linear regime, when input pulse power is low, Fig. 5.3(e) depicts that there is 60:40 energy sharing between the bar and cross channels. On the other hand, in the nonlinear regime, when the input pulse power is above the critical power, almost complete energy transfer has been achieved in the cross channel. Note that even though the type-2 $\mathscr{PT}$-symmetric coupler shows lower critical power, the switching steepness degrades considerably as compared to type-1 $\mathscr{PT}$-symmetric coupler. Also, for the type-1 $\mathscr{PT}$-symmetric coupler, the amplification of the output pulse intensity above the critical power is more than a factor of 5 times the output pulse in the type-2 coupler [Figs. 5.3(d) and 5.3(f)]. Thus, we observe enhanced steering dynamics for dark solitons inside both type-1 and type-2 $\mathscr{PT}$-symmetric couplers as compared to the conventional one.

Additionally, the role of the critical power for the type-1 and type-2 $\mathscr{PT}$-symmetric couplers with one-beat coupling length has been illustrated in Figs. 5.3(g) and 5.3(h). It can be observed that for the type-1 coupler, the inclusion of different gain/loss (Γ) values results in two threshold intensities, namely as $P_{cr}(I)$ and $P_{cr}(II)$ for $\Gamma < 0.33$. It

TH-2744_166121101

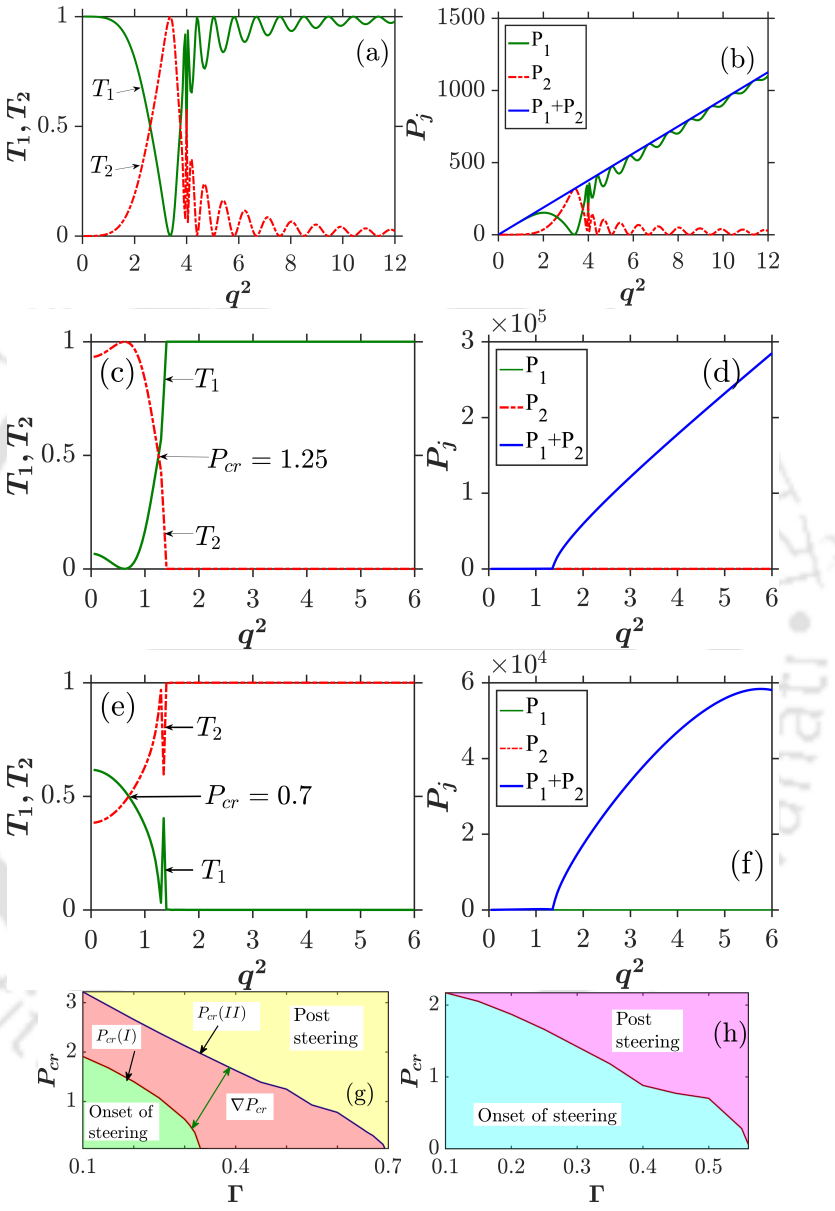

Figure 5.3: Steering dynamics of dark solitons for 2π coupler: (a) and (b) conventional coupler, (c) and (d) Type-1 $\mathscr{PT}$-symmetric couplers, (e) and (f) Type-2 $\mathscr{PT}$-symmetric couplers. The variation of critical power against the gain/loss is depicted in (g) type-1 $\mathscr{PT}$ and (h) type-2 $\mathscr{PT}$-symmetric couplers.

TH-2744_166121101

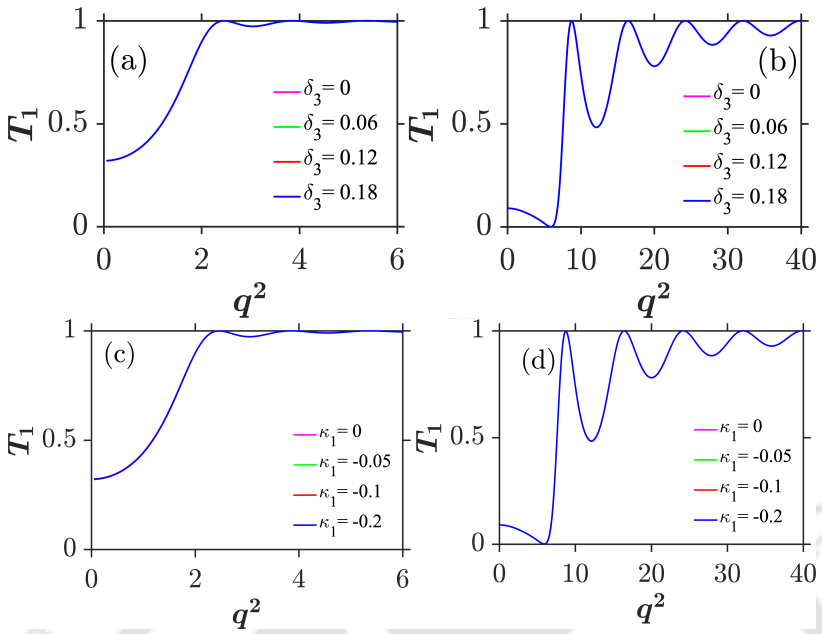

Figure 5.4: Steering dynamics of dark solitons for $\pi/2$ coupler: (a) and (b) represent the effect of TOD for type-1 and type-2 $\mathscr{PT}$-symmetric couplers respectively. (c) and (d) represent the effect of IMD for type-1 and type-2 $\mathscr{PT}$-symmetric couplers.

is to be noted that the curve corresponding to $P_{cr}(I)$ drops to the value 0.05 at $\Gamma = 0.33$, indicating that there will be only one critical power of switching which corresponds to $P_{cr}(II)$. As Γ increases beyond $\Gamma > 0.33$, the critical power for switching corresponding to $P_{cr}(II)$ reduces. However, for a type-2 coupler we observe different dynamics where the critical power linearly decreases with an increase in the gain/loss parameter up to the value $\Gamma = 0.4$. On further increment of Γ, in the region $0.4 < \Gamma < 0.5$, the rate of change in critical power shows gradual slowdown and for $\Gamma > 0.5$ the critical power decreases sharply indicating that one can achieve ultralow critical power of switching as Γ approaches the singularity condition Γ=1. Now, we move on to study the influences of TOD and IMD on such dark soliton switching in $\mathscr{PT}$-symmetric couplers by varying TOD parameter δ_3 and IMD κ_1 in the coupled equations (Eqs.(5.1) and (5.2)). As mentioned earlier, it has been previously reported that both TOD and IMD have no effects on transmission characteristics of dark soliton in the conventional half-beat length coupler [87]. Nevertheless, we have observed that $\mathscr{PT}$-symmetric couplers function efficiently with one-beat coupling length, contrary to the conventional couplers performing better at half-beat length. Thus, by incorporating gain and loss parameters in the conventional coupler, effects of TOD and IMD have been observed in the above $\mathscr{PT}$-symmetric coupler

TH-2744_166121101

configurations with both the half-beat ($L_c = \pi/2$) and one-beat coupling length ($L_c = 2\pi$). To study TOD and IMD effects, we choose different values of $\delta_3 = 0, 0.06, 0.12, 0.18$, and $\kappa_1 = 0, -0.05, -0.1, -0.2$ based on the previous works [87, 55] and plot transmission coefficients against the input pump intensity. It can be observed from Fig. 5.4 that both TOD and IMD have no effects on the dark soliton inside type-1 and type-2 $\mathscr{PT}$-symmetric couplers. For type-1 $\mathscr{PT}$-symmetric coupler, in the linear domain below the critical power, the bar channel shares 32% of total energy and attains 99.99% energy above $P_{cr} = 1.2$ [Figs. 5.4(a) and 5.4(c)]. Whereas for type-2 $\mathscr{PT}$-symmetric coupler, in the linear domain the bar channel shares 8% of the total energy and shows multiple periodic oscillation above the critical power $P_{cr} = 7.6$ where most of the energy is transferred to the bar channel [Figs. 5.4(b) and 5.4(d)]. At low pump intensity, this coupler acts as a linear coupler where evanescent coupling steers the input pulse into the cross channel. Whereas, at high pump intensity as a consequence of nonlinearity, the input pulse steers back to the lossy bar channel itself. Therefore, more pump power is required for dark soliton switching inside the type-2 $\pi/2$ coupler. However, as $\mathscr{PT}$-symmetric couplers function efficiently with 2π coupling length, next we will observe the effects of TOD and IMD in the above $\mathscr{PT}$-symmetric coupler configurations with coupling length $L_c = 2\pi$.

5.3.1 Effect of TOD

To study the TOD effect for 2π $\mathscr{PT}$-symmetric couplers we consider the same set of TOD parameters used in the case of $\pi/2$ coupler as $\delta_3 = 0, 0.06, 0.12$, and 0.18. We notice that TOD has no influence on dark soliton switching inside both type-1 and type-2 $\mathscr{PT}$-symmetric couplers even with 2π coupling length [Figs. 5.5(a) and 5.5(b)]. Here, it is to be observed that for type-1 coupler, an increase in the coupling length hikes the switching steepness inside the bar channel [Figs. 5.4(a) and 5.5(a)].

While, in the alternative configuration of $\mathscr{PT}$-symmetric coupler, as the input pulse is launched at port 1 where loss is incorporated, we observe that the switching steepness gets reduced while improving the transmission efficiency to almost unity as compared to the $\pi/2$ coupler [Figs. 5.5(b) and 5.4(b)]. Here, for the type-2 $\mathscr{PT}$-symmetric coupler a significant difference in the transmission characteristics is observed for $L_c = \pi/2$ and 2π. Unlike $\pi/2$ coupler, most of the energy is transferred to the cross channel above the critical power $P_{cr} = 0.7$ and maintains unit transmission efficiency.

TH-2744_166121101

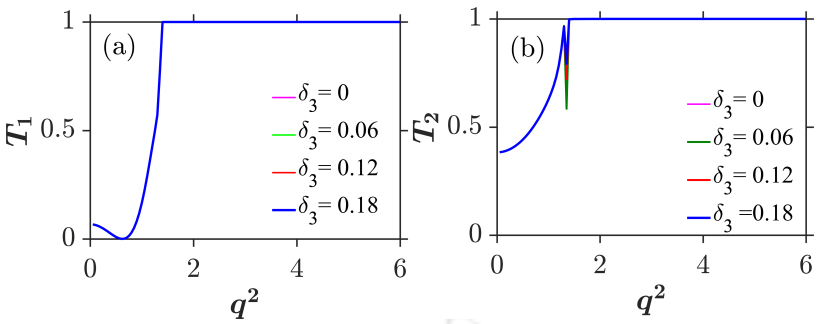

Figure 5.5: Effect of TOD on steering dynamics of dark soliton in $\mathscr{PT}$-symmetric couplers of length 2π. (a) and (b) represent the transmission characteristics in type-1 and type-2 coupler respectively.

5.3.2 Effect of IMD

Next, we discuss the effect of IMD on 2π $\mathscr{PT}$-symmetric couplers by choosing the same set of κ_1 values used for the case of $\pi/2$ as shown in Figs. 5.4(c) and 5.4(d). As we design two configurations by simply swapping gain and loss parameters, the effect of IMD reveals that for 2π $\mathscr{PT}$-symmetric couplers dark soliton switching is hardly influenced by IMD. For type-1 coupler as κ_1 decreases, the switching threshold power marginally decreases while maintaining almost same transmission efficiency [Fig. 5.6(a)]. When $\kappa_1 = -0.2$, the figure reveals that the IMD has significant influence on the linear regime of the transmission characteristics in type-1 coupler.

However, for type-2 $\mathscr{PT}$-symmetric coupler with loss in the first waveguide, it has been shown in Fig. 5.6(b) that IMD has no effect on the critical power for dark soliton switching, though it shows minor influence in the nonlinear regime above the critical power. This could be explained as follows. IMD is predominantly a linear effect. When the input power is low, the dispersion mismatch between the modes dominates over that of nonlinearity resulting in exhibition of IMD effect. In presence of IMD, as the input power is incident in one of the waveguides of the NLDC, both the modes in two waveguides are been equally exited. The modes having different propagation constants will have different group velocities which will eventually tend to cause oscillations at the wings of the dark soliton. In the conventional coupler the critical power of switching is very high, while in the case of $\mathscr{PT}$-symmetric coupler the switching threshold is significantly low resulting in early dominance of nonlinearity, reducing the effect of IMD. In passing, we note that the transmission curves in Figs. 5.5 and 5.6 exhibit almost similar sharp variation with TOD and IMD for the type-1 and type-2 $\mathscr{PT}$-symmetric

TH-2744_166121101

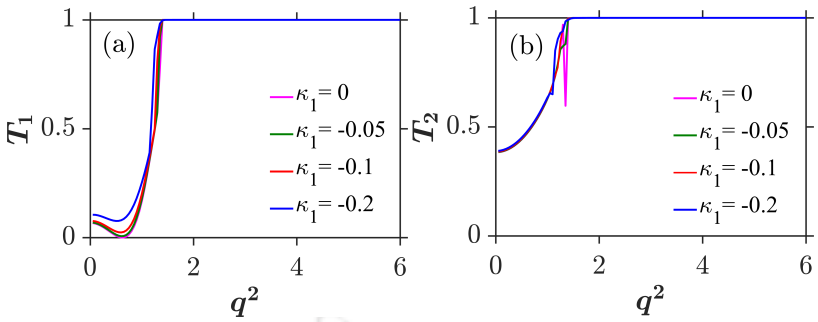

Figure 5.6: Effect of IMD on steering dynamics of dark soliton in $\mathscr{PT}$-symmetric couplers of length 2π. (a) and (b) represent the transmission characteristics in type-1 and type-2 coupler respectively.

couplers. This may be occurring owing to the almost similar phase-shift introduced by TOD and IMD. Steering of solitons between the cores of the coupler occurs subject to the fulfilment of appropriate phase-matching condition. For small coupling length ($\pi/2$ coupler) the phase-shift between the cores of the coupler, introduced by TOD and IMD is negligibly small compared to the one introduced by nonlinearity. On the other hand, due to long coupler length, in the case of 2π coupler, TOD and IMD introduces non-negligible phase-shift. However, if the peak power of the input pulse is increased further, even here the nonlinearity induced phase-shift become dominant.

5.3.3 Phase-controlled switching

In general, all-optical switching in NLDCs is mostly characterized by the power-controlled transmission at the output port. As an alternative approach to the power-controlled switching, there has been several reports on phase-controlled soliton switching where it has been analysed how a weak control pulse can steer a strong data pulse in an NLDC [78, 79, 81, 82, 86, 103]. In this work now we will show how a weak pulse injected in the second waveguide controls the switching of the strong data pulse in the first waveguide of $\mathscr{PT}$-symmetric couplers. As analysed in a previous report, a bright soliton switching can be controlled by both the intensity and the relative phase of a weak pulse [78]. Here, the steering dynamics of dark solitons have been obtained by considering normalized coupling coefficient $\kappa = 1$ and the initial conditions of the two input pulses are taken to

TH-2744_166121101

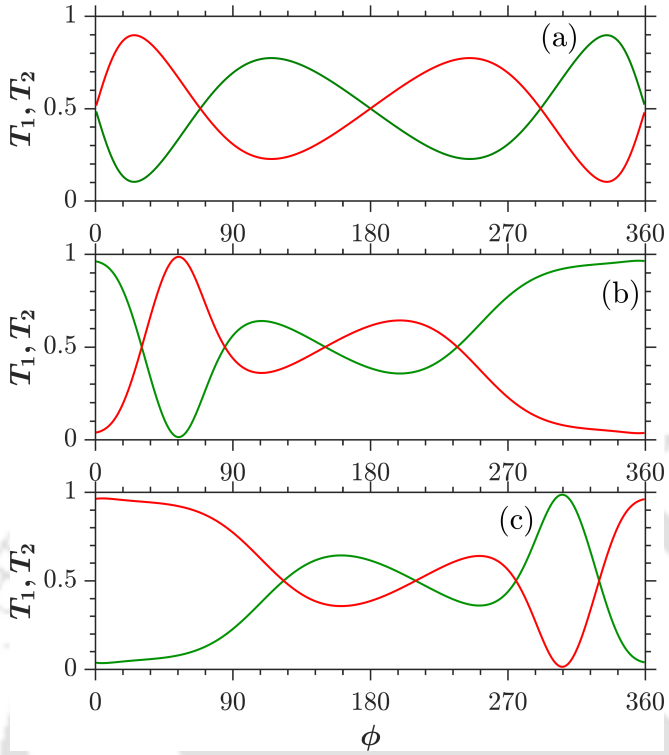

Figure 5.7: Dark soliton transmissions T_1 (green solid curve) and T_2 (red solid curve) in the bar and cross channels of $\pi/2$ couplers as a function of relative phase of the weak control pulse with power ratio $r = 1$. (a) Conventional coupler, (b) type-1 $\mathscr{PT}$-symmetric coupler and (c) type-2 $\mathscr{PT}$-symmetric coupler.

be as,

$$\Psi_1(\xi = 0, \tau) = q\tanh(q\tau), \quad \text{and,} \quad \Psi_2(\xi = 0, \tau) = \frac{q}{\sqrt{r}}\tanh(q\tau)e^{i\phi} \tag{5.5}$$

where, r is the power ratio between Ψ_1 and Ψ_2 and ϕ represents the relative phase. In order to understand the effects of phase and intensity of the weak pulse in $\mathscr{PT}$-symmetric couplers, we first calculate the transmission energy for both the conventional and $\mathscr{PT}$-symmetric couplers as a function of phase ϕ, keeping $r = 1$ fixed. It is to be noted that we have considered couplers with two different coupling lengths $L_c = \pi/2$ and $3\pi/2$ (three half-beat length). Also, TOD and IMD have zero effects which we have verified through a series of numerical experiments and so we did not show their impacts.

As shown in Fig. 5.7(a), for a conventional coupler of $\pi/2$ length, when $\phi = 0°$ the output exits port 4 (cross state). After three back and forth switching in between the two channels, finally at $\phi = 360°$ the output switches to the bar state with 52% transmission efficiency. The type-1 $\mathscr{PT}$-symmetric coupler shows that for both $\phi = 0°$ and $\phi = 360°$, the

TH-2744_166121101

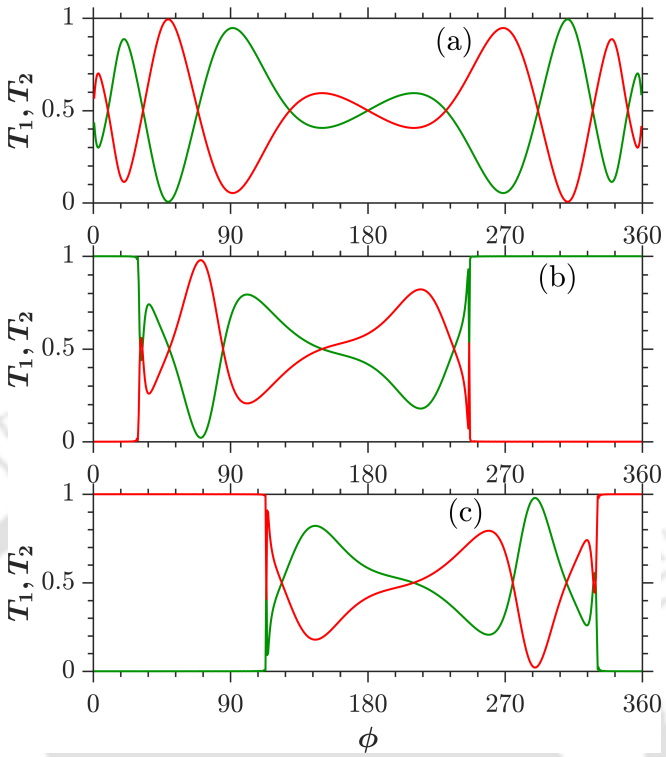

Figure 5.8: Dark soliton transmissions T_1 (green solid line) and T_2 (red solid line) in the bar and cross channels of $3\pi/2$ couplers as a function of relative phase of the weak control pulse with power ratio $r = 1$. (a) Conventional coupler, (b) type-1 $\mathscr{PT}$-symmetric coupler and (c) type-2 $\mathscr{PT}$-symmetric coupler.

output power switches to the bar state with 96% transmission efficiency [see Fig. 5.7(b)]. In contrast, the type-2 $\mathscr{PT}$-symmetric coupler reveals the output power to be switching to the cross state with the same 96% efficiency for $\phi = 0°$ and $\phi = 360°$ [Fig. 5.7(c)]. Now, as we consider $3\pi/2$ couplers, we observe that the output energy in the conventional coupler transmits at port 4 when there is no relative phase between the input pulses, i.e., when $\phi = 0°$ [Fig. 5.8(a)]. By changing ϕ we further observe that the output power switches to the bar state with 58% transmission efficiency at $\phi = 360°$. On the other hand, for type-1 $\mathscr{PT}$-symmetric coupler as shown in the Fig. 5.8(b), an excellent transmission efficiency of almost 99.99% has been observed in the range $\phi \approx 0° - 25°$ and $\phi \approx 247° - 360°$. Here we observe that the increase in the coupling length results in an extreme sharp switching to the bar state for a wide range of ϕ. Now, in the type-2 coupler containing loss in the first channel and gain in the second channel where the control pulse is launched, the output power switches to the second channel. Thus, we obtain 99.99% transmission efficiency for a type-2 $\mathscr{PT}$-symmetric coupler where the output power sharply switches

TH-2744_166121101

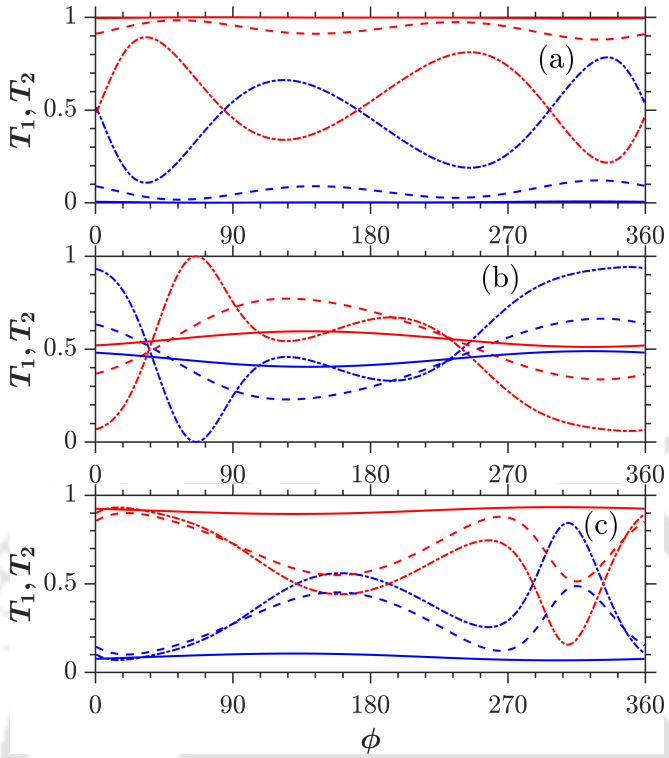

Figure 5.9: Soliton power transmissions T_1 (blue) and T_2 (red) in the $\pi/2$ coupler as a function of relative phase ϕ of the control pulse with power ratios $r = 1.5$ (dotted-dashed curves), $r = 20$ (dashed curves) and $r = 600$ (solid curves) for (a) conventional coupler and (b) type-1 $\mathscr{PT}$-symmetric coupler. A different set of values: $r = 1.5$ (dotted-dashed curves), $r = 2.6$ (dashed curves) and $r = 600$ (solid curves) for (c) type-2 $\mathscr{PT}$-symmetric coupler.

to the cross state in the range $\phi \approxeq 0° - 112°$ and $\phi \approxeq 333° - 360°$ [see Fig. 5.8(c)]. Therefore, depending on type-1 and type-2 coupler, if a control pulse with equal power and a relative phase specified by a range of ϕ can be injected in the second waveguide, almost all the output powers will be transmitted to the output ports of the gain channel.

Next, in addition to the phase-sensitive switching, the switching of a strong pulse may also be obtained by varying the input peak power of the weak control pulse. Considering the same set of coupling lengths, now we observe the transmissions in the two channels as a function of relative phase ϕ for three different values of the input peak power ratio r. As it can be clearly seen from Figs. 5.9 and 5.10, the variation of input peak power ratio r displays extremely unique transmission characteristics for both the conventional and $\mathscr{PT}$-symmetric couplers. In a conventional $\pi/2$ coupler [see Fig. 5.9(a)], for low value of $r = 1.5$ (dotted-dashed curves), the output energy exits from port 3 when the relative phase between the strong pulse and the control pulse is $\phi = 0°$ and $\phi = 360°$.

TH-2744_166121101

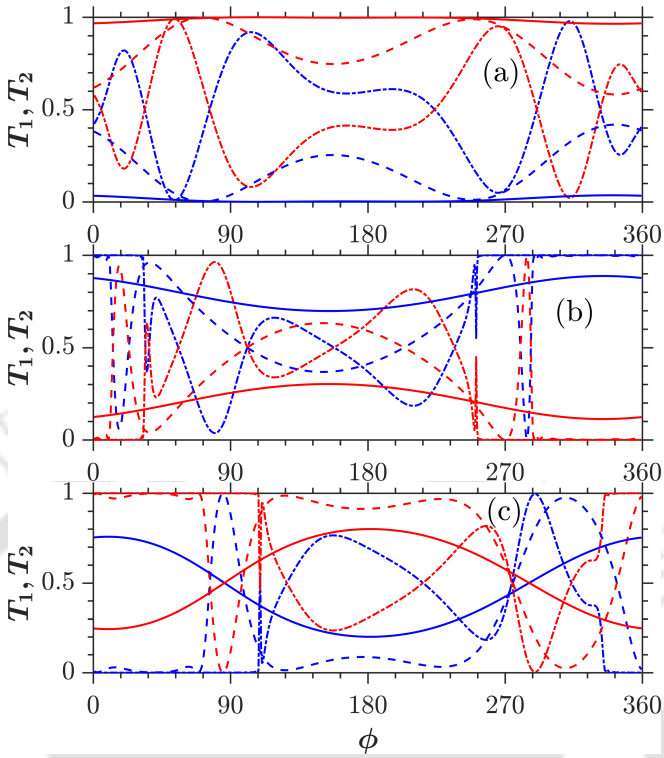

Figure 5.10: Soliton power transmissions T_1 (blue) and T_2 (red) in the $3\pi/2$ coupler as a function of relative phase ϕ of the control pulse with power ratios $r = 1.5$ (dotted-dashed curves), $r = 20$ (dashed curves) and $r = 600$ (solid curves) for (a) conventional coupler, (b) type-1 $\mathscr{PT}$-symmetric coupler and (c) type-2 $\mathscr{PT}$-symmetric coupler.

For some high values, $r = 50$ (dashed curves) and $r = 600$ (solid curves), as the control pulse becomes weak, almost the total output power switches to the cross state with efficiencies 90.89% and 99.48% respectively at $\phi = 360°$ as shown in the Fig. 5.9(a). For a type-1 $\mathscr{PT}$-symmetric coupler, it has been observed that the soliton switches to the bar state and exits port 3 for the values of $r = 1.5$ (dotted-dashed curves) and $r = 20$ (dashed curves). But the transmission curves corresponding to $r = 600$ (solid curves) show that there is no switching between the two channels as a function of ϕ and the output pulse exits port 4 with 52% transmission efficiency at $\phi = 360°$ [Fig. 5.9(b)]. The reason behind such ϕ independent transmission is that the control pulse now becomes too weak to control the strong data pulse as $r = 600$. In contrast to the type-1 coupler, type-2 $\mathscr{PT}$-symmetric coupler displays such 'no switching of channel for any ϕ' curves for much lower value $r = 2.6$ where the output gets transmitted at port 4 with a better transmission efficiency of 92% when $\phi = 360°$. As we increase the power ratio to be $r = 600$ (solid curves in Fig. 5.9(c)], it is expected that we observe the transmission to be

TH-2744_166121101

ϕ independent.

Now, for conventional couplers with $3\pi/2$ coupling length, we observe in Fig. 5.10(a) that, as the value of r is increased to $r = 20$ (dashed curves) there is no switching of soliton energy between the channels. The corresponding output exits port 4 with 62% of total power at $\phi = 0^\circ$ and achieves 99.81% and 98.89% transmission efficiencies at $\phi \approxeq 72^\circ$ and $\phi \approxeq 247^\circ$, respectively. For $r = 600$ (solid curves), the output energy transmits at the port 4 with more than 96% efficiency. We also observe that like $\pi/2$ coupler the phase ϕ has almost no effect on the transmission characteristics of the strong pulse switching for $r = 600$ [Fig. 5.10(a)]. For the type-1 $\mathscr{PT}$-symmetric coupler, as shown in Fig. 5.10(b), an increase in intensity ratio r results in a decrease in the transmission efficiency at the output port 3 when $\phi = 360^\circ$. As shown in that figure, the transmission curve corresponding to $r = 600$ (solid curves) shows no switching of channel occurring in the device for any ϕ value. Nevertheless, it shows considerable transmission efficiency while the strong pulse transmits at port 3 for any value of ϕ. Thus, if one can launch a weak pulse with high power ratio and an arbitrary phase in a type-1 $\mathscr{PT}$-symmetric coupler, the strong pulse will always switch to the bar state and exit port 3. Next, for a type-2 $\mathscr{PT}$-symmetric coupler as shown in Fig. 5.10(c), when $r = 1.5$ (dotted-dashed curves) and $r = 20$ (dashed curves), we observe that at $\phi = 0^\circ$ the output power exits at port 4 transferring 99.99% of the total power to the cross state. As we set $r = 600$ (solid curves), at $\phi = 0^\circ$ and $\phi = 360^\circ$, we observe 75% of the total power switches to the bar state. Also, following the same solid curves, we notice that 80% of the total output power switches to the cross state at $\phi = 180^\circ$. Thus, knowing that the first channel contains loss in the type-2 $\mathscr{PT}$-symmetric coupler, one can switch a desirable fraction of the total power to any channel if the weak pulse has high r value and a specific range of phase.

In this section, we investigate the effects of TOD and IMD on soliton propagation dynamics in the $\mathscr{PT}$-symmetric couplers of length 2π. To understand their effects properly, first we plot the spatiotemporal evolutions of dark soliton in both the bar and cross channels of a conventional 2π coupler. When there is no perturbative effects present ($\delta_3 = 0$, $\kappa_1 = 0$), as illustrated in Figs. 5.11(a) and 5.11(b), fundamental solitons launched at input port of bar channel (port 1) steer back and forth between two channels and finally exit at the output port of the same channel (port 3). When $\delta_3 = 0.18$, we observe that TOD has no effect on dark soliton evolution [Figs. 5.11(c) and 5.11(d)]. Also, when $\kappa_1 = -0.2$, because of different group velocities of the modes, we notice a slight twist

TH-2744_166121101

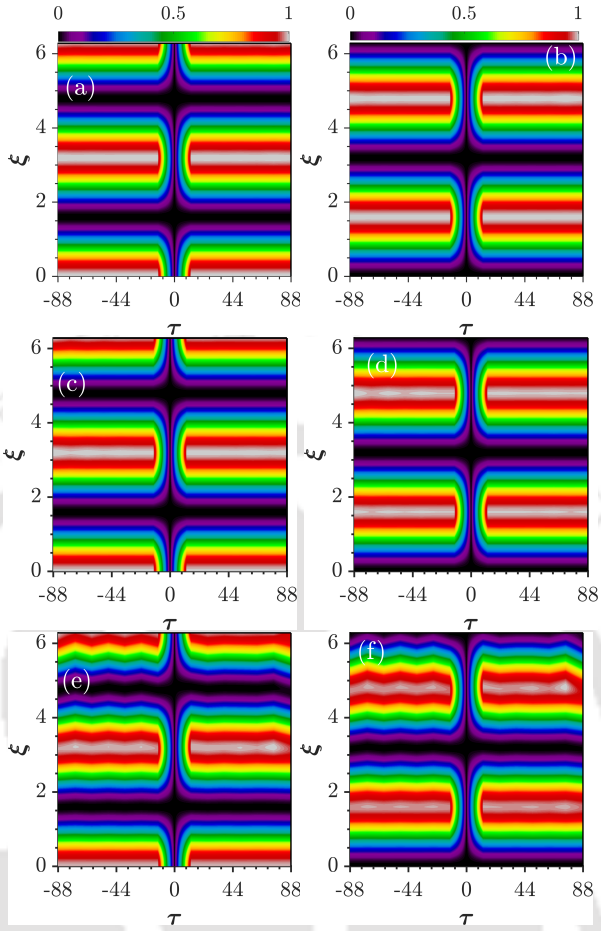

Figure 5.11: Spatio-temporal evolution of dark soliton inside a conventional 2π coupler with (a-b) $\delta_3 = 0$, $\kappa_1 = 0$; (c-d) $\delta_3 = 0.18$, $\kappa_1 = 0$; (e-f) $\delta_3 = 0$, $\kappa_1 = -0.2$. Here and in all other figures, left panels indicate the evolution in first core while the propagation in second core is portrayed in right panels.

around $\tau = 0$ [Figs. 5.11(e) and 5.11(f)]. It is to be noted that the oscillations at the wings of the dark solitons are due to the mismatch in the group velocities of the modes, resulting from the effect of IMD which originates from the dispersion mismatch between the symmetric and asymmetric modes of an NLDC.

We now display the spatiotemporal evolution of dark soliton inside the $\mathscr{PT}$-symmetric couplers. As depicted by the left two panels in Fig. 5.12(a), dark soliton is launched at port 1 and after periodic steering between the two channels, the soliton gets transmitted from the output port of the second core [see Fig. 5.12(b)]. Thus, we can conclude that a different route for switching can be established by a type-1 $\mathscr{PT}$-symmetric coupler [see

TH-2744_166121101

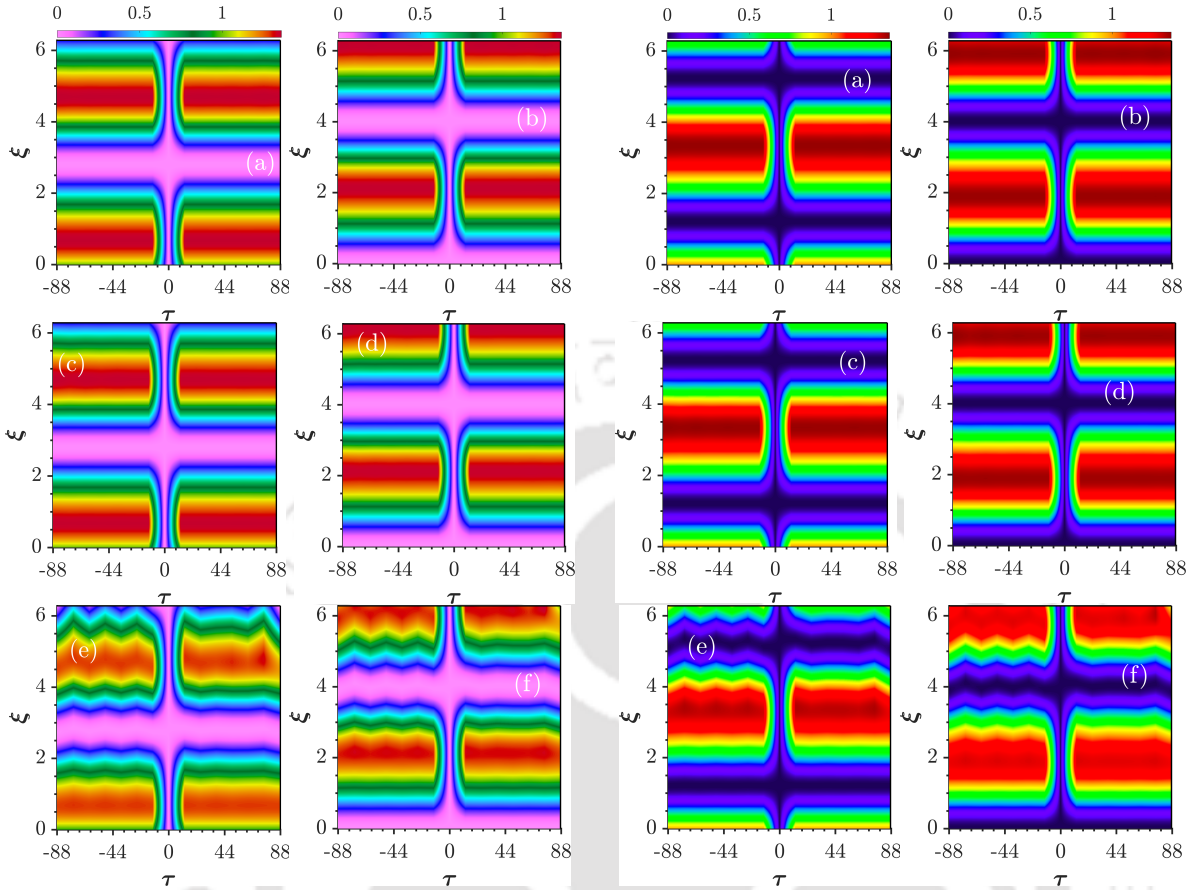

Figure 5.12: Spatio-temporal evolution of dark soliton inside a type-1 (left two panels) and type-2 (right two panels) $\mathscr{PT}$-symmetric coupler of coupling length 2π with (a) and (b) $\delta_3 = 0$, $\kappa_1 = 0$; (c) and (d) $\delta_3 = 0.18$, $\kappa_1 = 0$; (e) and (f) $\delta_3 = 0$, $\kappa_1 = -0.2$.

Fig. 5.12(a)] as compared to the conventional coupler [Fig. 5.11(a)].

For a type-2 $\mathscr{PT}$-symmetric coupler as illustrated in the right two panels, Fig. 5.12(a), the input soliton is launched at port 1. After back and forth steering through the coupling length, we observe that similar to the type-1 $\mathscr{PT}$-symmetric coupler, the dark soliton exits from the output port of the second core [see Fig. 5.12(b)]. Furthermore, we observe that TOD has no effect on dark soliton evolution for both type-1 and type-2 $\mathscr{PT}$-symmetric couplers [see left side Figs. 5.12(c), 5.12(d)] and [right side Figs. 5.12(c), 5.12(d)]. Whereas IMD influences in a similar way for both the $\mathscr{PT}$-symmetric couplers by slightly oscillating the pulse on their wings around $\tau = 0$ [see left-side Figs. 5.12(e)], 5.12(f) and right-side Figs. 5.12(e), 5.12(f)].

TH-2744_166121101

5.4 Summary

In this work, we have first presented the numerical study of dark soliton steering inside $\mathscr{PT}$-symmetric couplers for two different configurations, type-1 and type-2, with 2π coupling length. We found that the inclusion of equal amount of gain and loss results in reduction of critical power for both the $\mathscr{PT}$-symmetric couplers. We also demonstrated the effects of TOD and IMD on soliton propagation inside $\mathscr{PT}$-symmetric couplers of two coupling lengths $L_c = \pi/2$ and 2π. Based on the numerical results, we report that TOD has no effect on dark soliton steering in both $\pi/2$ and 2π $\mathscr{PT}$-symmetric couplers. Whereas, IMD shows no influence on dark soliton in $\mathscr{PT}$-symmetric couplers of coupling length $\pi/2$. But, for type-1 $\mathscr{PT}$-symmetric coupler with 2π coupling length, lower IMD value shows effect on dark soliton having low input peak power and for type-2 $\mathscr{PT}$-symmetric coupler, IMD shows influence on soliton with high input peak power. It is observed that the gain/loss parameter plays crucial role in deciding the critical power of switching. For example, in a type-1 one-beat $\mathscr{PT}$-symmetric coupler, the onset of steering occurs at $P_{cr} = 0.05$ for $\Gamma = 0.33$. It may be useful get an idea about the parameter values in real units [33, 104, 105]. For an input pulse width $T_0 = 100$ fs with GVD parameter $\beta_2 = 20 ps^2/km$ and nonlinear parameter $\gamma = 10 W^{-1} km^{-1}$, the beat length of the coupler could be estimated as 1.57 m [33]. The normalized TOD parameter, $\delta_3 = 0.12$ and the IMD parameter, $\kappa_1 = -0.2$ corresponds respectively to $1.44 ps^3/km$ and $-40 ps/km$ in real units. The critical power of switching is found to be 20 W. The loss or gain parameter one needs to maintain is $0.66 m^{-1}$ in real units. It is possible to reduce the beat length of the coupler further by reducing the pulse-width. Additionally, we have studied the phase-controlled switching for $\mathscr{PT}$-symmetric couplers with $\pi/2$ and $3\pi/2$ coupling lengths showing that the dark soliton switching in $\mathscr{PT}$-symmetric couplers can be controlled by regulating the phase and intensity of a weaker control pulse. It has been found that as the intensity of the weak control pulse decreases, the effect of relative phase on the transmission characteristics also decreases. Also, each case of the $\mathscr{PT}$-symmetric couplers with two different coupling lengths has displayed specific advantages for three different weak pulse intensities and thus can be used for switching device characterizations.

TH-2744_166121101

TH-2744_166121101

CHAPTER 6

CONCLUSION

In this thesis, we have carried out a comprehensive study of the phenomena of soliton steering and switching in $\mathscr{PT}$-symmetric NLDC. In chapter 1, we presented a brief introduction and motivation of the research problems considered in the thesis, along with the recent developments pertinent to these problems. In chapter 2, we discussed, in details, the relevant concepts and phenomena related to the research problems addressed in this thesis.

In chapter 3, we reported our study on the soliton steering dynamics in a $\mathscr{PT}$-symmetric directional coupler in the fs domain in great detail. The individual effects of HODs, SS and IRS on switching dynamics was studied. Following that, we investigated the cumulative combined effects of all perturbations, which result in a significant improvement in the stability and switching of fs soliton against individual perturbations as well as unperturbed cases. It turned out that the combined effect of perturbations, with a high gain/loss, stabilizes the soliton pulse evolution in the coupler from the chaotic behavior of unperturbed evolution. This work demonstrates that it is possible to achieve efficient soliton steering, even in the fs regime, at very low critical power at a relatively higher gain/loss coefficient in the $\mathscr{PT}$ -symmetric directional coupler. This finding is new in the context of ultrafast soliton steering in a $\mathscr{PT}$-symmetric coupler, paving the way for stable and efficient fs all-optical switching at low energy than the conventional one.

In Chapter 4, the steering dynamics in a $\mathscr{PT}$-symmetric saturable nonlinear coupler

TH-2744_166121101

is investigated. The exact soliton solution was first obtained, which could propagate through such a medium, and then we observed the transmission characteristics of that pulse for the $\mathscr{PT}$-symmetric coupler. We solved the corresponding equation considering a half-beat device length. The corresponding theoretical model along with a discussion on the numerical finding of soliton solution which can propagate in a saturating nonlinear medium has been demonstrated. The bistable solitons in the context of $\mathscr{PT}$-symmetric coupler with saturable nonlinearity has been studied. The spatiotemporal characteristics of solitons are illustrated and the phase-controlled soliton switching behavior is demonstrated.

In chapter 5, we demonstrated theoretically the steering dynamics of dark soliton in a $\mathscr{PT}$-symmetric NLDC in the presence of TOD and IMD. A complete switching with an excellent efficiency at a very low critical power, even lower as compared to the bright soliton switching was observed. It was found through numerical analysis that both the dispersions have no effect on soliton steering in $\mathscr{PT}$-symmetric couplers. This makes the dark solitons to be a stable solution under dispersive effects. Moreover, we studied the switching dynamics of the dark soliton by controlling the phase of a weaker signal in $\mathscr{PT}$ couplers with two different coupling lengths and illustrated its advantage over the power-controlled one.

Scopes of Future Work:

In this thesis we have explored the soliton steering and switching dynamics in $\mathscr{PT}$-symmetric couplers using mainly numerical methods. As a potential future work, one could look for developing some analytical methods, particularly the so-called variational methods in the context of $\mathscr{PT}$-symmetric coupled systems. This will enable more insights into the workings of various solitonic parameters in the system.

In the present thesis, we confined ourselves to exceptional points of second order (EP2s) only. EPs are widely referred as the branch point singularities at which both the eigenspectra and the associated eigenvectors corresponding to a non-conservative physical system coalesce. As the system undergoes a phase transition manifested by the sudden change in its behavioral dynamics around the critical points, systems exhibiting $\mathscr{PT}$ symmetry have drawn huge interest in recent years. The mathematical feature of an EP of order N, commonly symbolised as EPN, suggests that by varying $(N-1)$ parameters one can control the exact points at which the N number of eigenvalues and eigenvectors coalesce in parameter-space. In optics and photonics, considering a wide range of optical systems, there have been several researches on the $EP2$ [106]. However, recently there

TH-2744_166121101

have been theoretical developments around even a higher-order EP (third-order exceptional point EP3) which have provided some light on the condition one need to set in different optical structure in order to observe EP3. The first experimental investigation of EP3 in a ternary $\mathscr{PT}$-symmetric resonators has been demonstrated by observing the cubic-root dependency of the frequency splitting on the applied external perturbation in the refractive index of the system [107]. The idea of introducing a neutral resonator in between the gain and the loss resonators has paved the way to utilize such coupled system in other optical systems such as atomic physics, optomechanics and photonic crystals. One of the extremely fruitful research endeavours would be to carry out an investigation of soliton dynamics in a three-core $\mathscr{PT}$-symmetric NLDC.

TH-2744_166121101

TH-2744_166121101

BIBLIOGRAPHY

[1] C. M. Bender and S. Boettcher, "Real spectra in non-Hermitian Hamiltonians having $\mathscr{PT}$ symmetry," Phys. Rev. Lett. **80**, 5243 (1998).

[2] R. El Ganainy, K. G. Makris, D. N. Christodoulides, and Z. H. Musslimani, "Theory of coupled optical $\mathscr{PT}$-structures," Opt. Lett. **32**, 2632–2634 (2007).

[3] K. G. Makris, R. El Ganainy, D. N. Christodoulides, and Z. H. Musslimani. "Beam dynamics in PT symmetric optical lattices," Phys. Rev. Lett. **100**, 103904 (2008).

[4] Z. H. Musslimani, K. G. Makris, R. El Ganainy, and D. N. Christodoulides, "Optical solitons in PT periodic potentials," Phys. Rev. Lett. **100**, 030402 (2008).

[5] A. Guo, G. J. Salamo, D. Duchesne, R. Morandotti, M. Volatier-Ravat, V. Aimez, G. A. Siviloglou, and D. N. Christodoulides, "Observation of PT-symmetry breaking in complex optical potentials," Phys. Rev. Lett. **103**, 093902 (2009).

[6] C. E. Rüter, K. G. Makris, R. El-Ganainy, D. N. Christodoulides, M. Segev, and D. Kip, "Observation of parity–time symmetry in optics," Nat. Phys. **6**, 192-195 (2010).

[7] A. Regensburger, C. Bersch, M. A. Miri, G. Onishchukov, D. N. Christodoulides, and U. Peschel, "Parity–time synthetic photonic lattices," Nature **488**, 167-171 (2012).

[8] L. Chang, X. Jiang, S. Hua, C. Yang, J. Wen, L. Jiang, G. Li, G. Wang, and M. Xiao, "Parity–time symmetry and variable optical isolation in active–passive-coupled microresonators," Nat. Photonics **8**, 524-529 (2014).

[9] A. Cerjan, A. Raman, and S. Fan, "Exceptional contours and band structure design in parity-time symmetric photonic crystals," Phys. Rev. Lett. **116**, 203902 (2016).

TH-2744_166121101

[10] C.Hang, G. Huang, and V. V. Konotop, "PT-symmetry with a system of three-level atoms," Phys. Rev. Lett. **110**, 083604 (2013).

[11] Z. Zhang, Y. Zhang, J. Sheng, L. Yang, M.A. Miri, D. N. Christodoulides, B. He, Y. Zhang, and M. Xiao, "Observation of parity-time symmetry in optically induced atomic lattices," Phys. Rev. Lett. **117**, 123601 (2016).

[12] Y. L. Xu, W. S. Fegadolli, L. Gan, M. H. Lu, X. P. Liu, Z. Y. Li, A. Scherer, and Y. F. Chen, "Experimental realization of Bloch oscillations in a parity-time synthetic silicon photonic lattice," Nat. Comm. **7**, 1-6 (2016).

[13] H. Xu, D. Mason, L. Jiang, and J. G. E. Harris, "Topological energy transfer in an optomechanical system with exceptional points," Nature **537**, 80-83 (2016).

[14] H. Jing, Ş.K. Özdemir, H. Lü, and F. Nori, "High-order exceptional points in optomechanics," Sci. Rep. **7**, 1-10 (2017).

[15] V. V. Konotop, J. Yang, and D. A. Zezyulin, "Nonlinear waves in $\mathscr{PT}$- systems," Rev. Mod. Phys. **88**, 035002 (2016).

[16] R. Fleury, D. Sounas, and A. Alu, "An invisible acoustic sensor based on parity-time symmetry," Nat. Comm. **6**, 1-7 (2015).

[17] F. K. Abdullaev, Y. V. Kartashov, V. V. Konotop, and D. A. Zezyulin, "Solitons in $\mathscr{PT}$- nonlinear lattices," Phys. Rev. A **83**, 041805 (2011).

[18] Y. Kominis, "Dynamic power balance for nonlinear waves in unbalanced gain and loss landscapes," Phys. Rev. A **92**, 063849 (2015).

[19] S. V. Suchkov, A. A. Sukhorukov, J. Huang, S. V. Dmitriev, C. Lee, and Y. S. Kivshar, "Nonlinear switching and solitons in PT-symmetric photonic systems," Laser Photon. Rev. **10**, 177-213 (2016).

[20] Yu. V. Bludov, V.V. Konotop, and B. A. Malomed, "Stable dark solitons in $\mathscr{PT}$-dual-core waveguides," Phys. Rev. A **87**, 013816 (2013).

[21] T. P. Suneera, and P. A. Subha, "Nonlocal gap solitons in parity-time symmetric coupler with transverse real potential." J. Opt. **20**, 095504 (2018).

TH-2744_166121101

[22] A. E. Miroshnichenko, B. A. Malomed, and Y. S. Kivshar, "Nonlinearly PT-symmetric systems: Spontaneous symmetry breaking and transmission resonances," Phys. Rev. A **84**, 012123 (2011).

[23] G. Burlak and B. A. Malomed, "Stability boundary and collisions of two-dimensional solitons in $\mathscr{PT}$- couplers with the cubic-quintic nonlinearity," Phys. Rev. E **88**, 062904 (2013).

[24] I. V. Barashenkov, L. Baker, and N. V. Alexeeva, "PT-symmetry breaking in a necklace of coupled optical waveguides," Phys. Rev. A **87**, 033819 (2013).

[25] Yu V. Bludov, R. Driben, V. V. Konotop, and B. A. Malomed, "Instabilities, solitons and rogue waves in PT-coupled nonlinear waveguides," J. Opt. **15**, 064010 (2013).

[26] A. Govindarajan, A. K. Sarma, and M. Lakshmanan, "Tailoring $\mathscr{PT}$-symmetric soliton switch," Opt. Lett., **44**, 663 (2019).

[27] A. Sahoo, D. K. Mahato, A. Govindarajan, and Amarendra K. Sarma, "Ultrafast all-optical femtosecond soliton steering in $\mathscr{PT}$-symmetric fiber couplers," arXiv preprint arXiv:2111.10878 (2021).

[28] R. Driben, and B. A. Malomed, "Stability of solitons in parity-time-symmetric couplers," Opt. Lett. **36**, 4323-4325 (2011).

[29] R. Driben, and B. A. Malomed, "Stabilization of solitons in $\mathscr{PT}$ models with supersymmetry by periodic management," Eur. Phys. Lett. **96**, 51001 (2011).

[30] V. Sasikala and K. Chitra, "All optical switching and associated technologies: a review," J. Opt. **47**, 307–317 (2018).

[31] S. R. Friberg, Y. Silberberg, M. K. Oliver, et al., "Ultrafast all-optical switching in a dual-core fiber nonlinear coupler," Appl. Phys. Lett. **51**, 1135 (1987).

[32] S. R. Friberg, A. M. Weiner, Y. Silberberg, B. G. Sfez, and P. S. Smith, "Femtosecond switching in a dual-core-fiber nonlinear coupler," Opt. Lett. **13**, 904-906 (1988).

[33] S. Trillo, S. Wabnitz, E. M. Wright, and G. I. Stegeman, "Soliton switching in fiber nonlinear directional couplers," Opt. Lett. **13**, 672-674 (1988).

TH-2744_166121101

[34] N. J. Doran and David Wood, "Nonlinear-optical loop mirror," Opt. Lett. **13**, 56-58 (1988).

[35] G. P. Agrawal, "Nonlinear Fiber Optics," 5th ed. (Academic, New York, 2013).

[36] G.R. Olbright, and N. Peyghambarian. "Interferometric measurement of the nonlinear index of refraction, n 2, of CdS x Se1- x-doped glasses." Appl. Phys. Lett. **48**, 1184-1186 (1986).

[37] J. L. Coutaz, and M. Kull, " Saturation of the nonlinear index of refraction in semiconductor-doped glass," J. Opt. Soc. Am. B, **8**, 95-98 (1991).

[38] P. Roussignol, D. Ricard, J. Lukasik, and C. Flytzanis, "New results on optical phase conjugation in semiconductor-doped glasses," J. Opt. Soc. Am. B **4**, 5-13 (1987).

[39] A. E. Kaplan, "Bistable Solitons," Phys. Rev. Lett. **55**, 1291 (1985).

[40] W. Krolikowski, and B. L. Davies, "Analytic solution for soliton propagation in a nonlinear saturable medium," Opt. Lett. **17**, 1414-1416 (1992).

[41] S. Gatz, and J. Herrmann, "Soliton propagation in materials with saturable nonlinearity," J. Opt. Soc. Am. B **8**, 2296-2302 (1991).

[42] A. Kumar, T. Kurz, and W. Lauterborn,"Two-state bright solitons in doped fibers with saturating nonlinearity," Phys. Rev. E **53**, 1166 (1996).

[43] A. Kumar, and A. Kumar, "A comparative numerical study of soliton switching in a nonlinear directional coupler with saturating nonlinearity," Opt. Comm. **150**, 91-96 (1998).

[44] P. Cao, X. Zhu, Y. He, and H. Li, "Gap solitons supported by parity-time-symmetric optical lattices with defocusing saturable nonlinearity," Opt. Comm., **316**, 190 (2014).

[45] K. Zhan, H. Tian, X. Li, X. Xu, Z. Jiao, and Y. Jia, "Solitons in PT-symmetric periodic systems with the logarithmically saturable nonlinearity," Scientific reports **6**, 1-9 (2016).

TH-2744_166121101

[46] X. Zhu, and H. Li, "Multihump solitons in two-dimensional parity-time-symmetric optical lattices with focusing saturable nonlinearity," The European Physical Journal D **70**, 1-5 (2016).

[47] P. Li, D. Mihalache, and B. A. Malomed. "Optical solitons in media with focusing and defocusing saturable nonlinearity and a parity-time-symmetric external potential," Philosophical Transactions of the Royal Society A: Mathematical, Physical and Engineering Sciences **376**, 20170378 (2018).

[48] A. K. Sarma. "Dark soliton switching in an NLDC in the presence of higher-order perturbative effects," Opt. Laser Technol. **41**, 247-250 (2009).

[49] A. Govindaraji, A. Mahalingam, and A. Uthayakumar, "Numerical investigation of dark soliton switching in asymmetric nonlinear fiber couplers," Appl. Phys. B **120**, 341-348 (2015).

[50] A Govindaraji, A Mahalingam, and A Uthayakumar, "Dark soliton switching in nonlinear fiber couplers with gain," Opt. Laser Technol. **234**, 427-432 (2004).

[51] K. S. Chiang, "Intermodal dispersion in two-core optical fibers," Opt. Lett. **20**, 997-999 (1995).

[52] P. M. Ramos, and C. R. Paiva, "All-optical pulse switching in twin-core fiber couplers with intermodal dispersion," IEEE J. Quantum Electron. **35**, 983-989 (1999).

[53] S. Droulias, M. Manousakis, and K. Hizanidis, "Switching dynamics in nonlinear directional fiber couplers with intermodal dispersion," Opt. Commun. **240**, 209-219 (2004).

[54] G. L. Diankov, I. M. Uzunov, and F. Lederer, "Effect of third-order dispersion on pulse dynamics in nonlinear directional coupler," Electron. Lett. **30**, 155-156 (1994).

[55] A. Govindaraji, A. Mahalingam, and A. Uthayakumar, "Femtosecond pulse switching in a fiber coupler with third order dispersion and self-steepening effects," Optik **125**, 4135-4139 (2014).

[56] A. Kumar, and A. K. Sarma, "Soliton switching in a Kerr coupler with coupling constant dispersion: a variational analysis," Opt. Commun. **234**, 427-432 (2004).

TH-2744_166121101

[57] Y. V. Kartashov, V. V. Konotop, and B. A. Malomed, "Dark solitons in dual-core waveguides with dispersive coupling,"Opt. Lett. **40**, 4126-4129 (2015).

[58] R. W. Boyd, *Nonlinear Optics*, 4th ed. (Academic, New York, 2020).

[59] J. Satsuma and N. Yajima. "B. Initial value problems of one-dimensional self-modulation of nonlinear waves in dispersive media," Progress of Theoretical Physics Supplement **55** 284-306 (1974).

[60] R. El-Ganainy, K. G. Makris, M. Khajavikhan, Z. H. Musslimani, S. Rotter, and D. N. Christodoulides, "Non-Hermitian physics and PT symmetry," Nat. Phys. **14**, 11-19 (2018).

[61] T. P. Suneera and P. A. Subha, "Switching dynamics in parity-time symmetric coupler with nonlocal nonlinearity having transverse potentials," J. Modern Opt. **66**, 1528-1533 (2019).

[62] A. A. Sukhorukov, Z. Xu, and Y. S. Kivshar, "Nonlinear suppression of time reversals in $\mathscr{PT}$-symmetric optical couplers," Phys. Rev. A **82**, 043818 (2010).

[63] H. Ramezani, T. Kottos, R. El-Ganainy, and D. N. Christodoulides, "Unidirectional nonlinear $\mathscr{PT}$-symmetric optical structures," Phys. Rev. A **82**, 043803 (2010).

[64] S. V. Dmitriev, S. V. Suchkov, A. A. Sukhorukov, and Y. S. Kivshar, "Scattering of linear and nonlinear waves in a waveguide array with a PT-symmetric defect," Phys. Rev. A **84**, 013833 (2011).

[65] N. V. Alexeeva, I. V. Barashenkov, A. A. Sukhorukov, and Y. S. Kivshar, "Optical solitons in $\mathscr{PT}$-symmetric nonlinear couplers with gain and loss," Phys. Rev. A **85**, 063837 (2012).

[66] B. A. Malomed, I. M. Skinner, and R. S. Tasgal, "Solitons in a nonlinear optical coupler in the presence of the Raman effect," Opt. Comm. **139**, 247-251 (1997).

[67] G. P. Agrawal, "Application of Nonlinear Fiber Optics", 2nd ed. (Academic Press, 2008).

[68] Q. Lin and G. P. Agrawal, "Raman response function for silica fibers," Opt. Lett. **31**, 3086-3088 (2006).

TH-2744_166121101

[69] J. P. Gordon, "Theory of the soliton self-frequency shift," Opt. Lett. **11**, 662-664 (1986).

[70] N. Akhmediev and M. Karlsson, "Cherenkov radiation emitted by solitons in optical fibers," Phys. Rev. A **51**, 2602 (1995).

[71] D. V. Skryabin and A. V. Gorbach, "Colloquium: Looking at a soliton through the prism of optical supercontinuum," Rev. Mod. Phys. **82**, 1287 (2010).

[72] The silica core is doped with 6.3% GeO_2 and the refractive index data is adopted from A. Ghatak and K. Thyagarajan, An Introduction to Fiber Optics (Cambridge University Press, Cambridge, 1998).

[73] Y. Zhiyenbayev, Y. Kominis, C. Valagiannopoulos, V. Kovanis, and A. Bountis, "Enhanced stability, bistability, and exceptional points in saturable active photonic couplers," Phys. Rev. A **100**, 043834 (2019).

[74] P. Roussignol, D. Ricard, J. Lukasik, and C. Flytzanis, "New results on optical phase conjugation in semiconductor-doped glasses," J. Opt. Soc. Am. B **4**, 5-13 (1987).

[75] K. Nithyanandan, R. V. J. Raja, and K. Porsezian,"Modulational instability in a twin-core fiber with the effect of saturable nonlinear response and coupling coefficient dispersion," Phys. Rev. A **87**, 043805 (2013).

[76] J. M. Hickmann, S. B. Cavalcanti, N. M. Borges, E. A. Gouveia, and A. S. Gouveia-Neto,"Modulational instability in semiconductor-doped glass fibers with saturable nonlinearity," Opt. Lett. **18**, 182-184 (1993).

[77] A. Sahoo, D. K. Mahato, A. Govindarajan, and A. K. Sarma, "Ultrafast all-optical femtosecond soliton steering in PT-symmetric fiber couplers," arXiv:2111.10878 [physics.optics] (2021).

[78] S. Trillo, and S. Wabnitz, "Weak-pulse-activated coherent soliton switching in nonlinear couplers," Opt. Lett. **16**, 1-3 (1991).

[79] M. Romagnoli, S. Trillo, and S. Wabnitz, "Soliton switching in nonlinear couplers," Opt. Quant. Electron. **24**, S1237–S1267 (1992).

TH-2744_166121101

[80] S. Jensen, "The nonlinear coherent coupler," IEEE J. Quantum Electron. **18**, 1580-1583 (1982).

[81] J. M. Soto-Crespo, and E. M. Wright, "All-optical switching of solitons in two-and three-core nonlinear fiber couplers," J. Appl. Phys. **70**, 7240-7243 (1991).

[82] P. M. Ramos, and C. R. Paiva, "Optimization and characterization of phase-controlled all-optical switching with fiber solitons," IEEE J. Select. Topics Quantum Electron. **3**, 1224-1231 (1997).

[83] Y. Chen, A. W. Snyder, and D. N. Payne, "Twin core nonlinear couplers with gain and loss," IEEE J. Quantum Electron. **28**, 239-245 (1992).

[84] N. J. Doran, and D. Wood, "Soliton processing element for all-optical switching and logic," J. Opt. Soc. Am. B **4**, 1843-1846 (1987).

[85] P. Shum, K. S. Chiang, and W. A. Gambling, "Switching dynamics of short optical pulses in a nonlinear directional coupler," IEEE J. Quantum Electron. **35**, 79-83 (1999).

[86] A. K. Sarma, and A. Kumar, "Phase-induced soliton switching in fiber nonlinear directional couplers," Optical Engineering **46**, 115005 (2007).

[87] A. K. Sarma, "Dark soliton switching in an NLDC in the presence of higher-order perturbative effects," Opt. Laser Technol **41**, 247-250 (2009).

[88] G.P. Agrawal, "Nonlinear Fiber Optics, 6th Ed," Academic Press (2019).

[89] A. K. Sarma, Ph.D. Thesis, (2006).

[90] A. Govindaraji, A. Mahalingam, and A. Uthayakumar, "Numerical investigation of dark soliton switching in asymmetric nonlinear fiber couplers," Appl. Phys. B **120**, 341-348 (2015).

[91] A Govindaraji, A Mahalingam, and A Uthayakumar, "Dark soliton switching in nonlinear fiber couplers with gain," Opt. Laser Technol. **234**, 427-432 (2004).

[92] K. S. Chiang, "Intermodal dispersion in two-core optical fibers," Opt. Lett. **20**, 997-999 (1995).

TH-2744_166121101

[93] P. M. Ramos, and C. R. Paiva, "All-optical pulse switching in twin-core fiber couplers with intermodal dispersion," IEEE J. Quantum Electron. **35**, 983-989 (1999).

[94] S. Droulias, M. Manousakis, and K. Hizanidis, "Switching dynamics in nonlinear directional fiber couplers with intermodal dispersion," Opt. Commun. **240**, 209-219 (2004).

[95] G. L. Diankov, I. M. Uzunov, and F. Lederer, "Effect of third-order dispersion on pulse dynamics in nonlinear directional coupler," Electron. Lett. **30**, 155-156 (1994).

[96] A. Govindaraji, A. Mahalingam, and A. Uthayakumar, "Femtosecond pulse switching in a fiber coupler with third order dispersion and self-steepening effects," Optik **125**, 4135-4139 (2014).

[97] A. Kumar, and A. K. Sarma, "Soliton switching in a Kerr coupler with coupling constant dispersion: a variational analysis," Opt. Commun. **234**, 427-432 (2004).

[98] Y. V. Kartashov, V. V. Konotop, and B. A. Malomed, "Dark solitons in dual-core waveguides with dispersive coupling," Opt. Lett. **40**, 4126-4129 (2015).

[99] D. A. Zezyulin, Y. V. Kartashov, and V. V. Konotop, "$\mathscr{CPT}$ -symmetric coupler with intermodal dispersion," Opt. Lett. **42**, 1273-1276 (2017).

[100] Y. V. Kartashov, V. V. Konotop, and F. K. Abdullaev, "Gap solitons in a spin-orbit-coupled Bose-Einstein condensate," Phys. Rev. Lett. **111**, 060402 (2013).

[101] Y. V. Kartashov, V. V. Konotop, and D. A. Zezyulin, "$\mathscr{CPT}$ -symmetric spin-orbit-coupled condensate," Eur. Phys. Lett. **107**, 50002 (2014).

[102] B. Dana, A. Bahabad, and B. A. Malomed, "$\mathscr{CP}$ -symmetry in optical systems," Phys. Rev. A **91**, 043808 (2015).

[103] I. M. Uzunov, R. Muschall, M. Gölles, Y. S. Kivshar, B. A. Malomed, and F. Lederer, "Pulse switching in nonlinear fiber directional couplers," Phys. Rev. E **51**, 2527 (1995).

[104] A. W. Snyder and J. D. Love, "Optical Waveguide Theory," Chapman and Hall, London (1983).

TH-2744_166121101

[105] A.K. Sarma and A. Kumar, "Perturbative effects on ultra-short soliton self-switching," Pramana. **69**, 575-587 (2007).

[106] M-A. Miri and Andrea Alu, "Exceptional points in optics and photonics,"" Science **363** eaar7709 (2019).

[107] H. Hodaei, Absar U. Hassan, Steffen Wittek, Hipolito Garcia-Gracia, Ramy El-Ganainy, Demetrios N. Christodoulides, and Mercedeh Khajavikhan, "Enhanced sensitivity at higher-order exceptional points," Nature **548**, 187-191 (2017).

[108] A. K. Sarma, "Non-Hermitian Optics," arXiv:1810.10516 (2018).

TH-2744_166121101

VITA

Dipti Kanika Mahato was born on 25th April, 1992 in Purulia, West Bengal, India. She received her degree of Bachelor of Science (B.Sc.) with Physics as major and Chemistry and Mathematics as minors from University of Calcutta in 2012, and Master of Science (M.Sc.) in Physics in 2014 from West Bengal State University. She joined CSIR-Central Glass & Ceramic Research Institute (CSIR-CGCRI) in 2016 as a Junior Research Fellow. She qualified Graduate Aptitude Test In Engineering (GATE) in 2016. Subsequently, she was awarded the Junior Research Fellowship and enrolled into the Ph.D. program at the Indian Institute of Technology (IIT) Guwahati in December, 2016. She was awarded Senior Research Fellowship in 2018 by the Ministry of Human Resource and Development, Government of India.

TH-2744_166121101